

**Development and Application of Single
Pollen Nucleus Genotyping and Virus
Tools for Meiotic Gene and
Recombination Studies in Barley
(*Hordeum vulgare* L.)**

Dissertation

zur Erlangung des

Doktorgrades der Agrarwissenschaften (Dr. agr.)

der

Naturwissenschaftlichen Fakultät III

Agrar- und Ernährungswissenschaften,

Geowissenschaften und Informatik

Martin-Luther-Universität Halle-Wittenberg

vorgelegt von

Herrn Suriya Tamilselvan Nattar Amutha

Gutachter:

1. Prof. Dr. Andreas Houben
2. Prof. Dr. Charles J. Underwood

Tag der öffentlichen Verteidigung: 26. Januar 2026, Halle (Saale)

Acknowledgements

I sincerely express my gratitude to my supervisor, Dr. Stefan Heckmann, for allowing me to work on this project and for mentoring me throughout my Ph.D. work. You have always been an inspiration to me in science. I have learned so much from you, and I would not have come this far in my academic journey without your guidance and support.

I thank my mentor, Dr. Joerg Fuchs, for your scientific guidance in the dPCR project and your mental support during my time at IPK. You are one of the funniest and kindest people I have ever met. I also thank the thesis reviewers, Dr. Andreas Houben and Dr. Charles Underwood.

A big thanks to Jana Lorenz, Franziska Hartmann and Marius Dölling for your kindness and invaluable help with my research. I also thank my (former) lab members: Yun-Jae Ahn, Steven Dreissig, Maria Cuacos, Mohammad Ayoub, Riddhi Dabhi, Ana Galvan, Mijael Mendoza, Stefan Steckenborn, Chao Feng, Premanda Karidass, Baicui Wang and Ewa Piskorz. I would also like to thank all my collaborators: Jianyong Chen, Dr. Jochen Kumlehn, Stefan Hiekel and Martin Becker (Stilla Technologies), as well as the IPK gardeners and technical staff. I thank Bianka Jacobi for your support throughout my stay at IPK and also Dr. Britt Leps.

No thanks to you - but heartfelt thanks to my buddy, Dr. Saravanakumar Somu, for your support. A special thanks to Manikandan Kaaalidas and Dr. Murukarthik Jayakodi for your help with my thesis. I am also grateful to my other buddies: Gautham Fraud, Anto Fraud, Jyothi AK, Swathi VJ, Prasath Paalbuti, Nithya Nagu, Chetta and Banu Prakash. I thank also Zelal Beski and Vikky for your support. I thank my brothers and sisters for your support: Pandiyan-sheela, Shobi-siva-Seyona, Sathya-Suriya, Jhay-Naga, Sakthi-co, Gallus gang, Dhaa-co, all other Frankfurt Tamil sangham leute, Mahir, Luis, Abhay, Linkon and MisFit gang.

Finally. I thank my family members and Patty Lolito for their unwavering love and support. I dedicate this thesis to my Mom and Dad - without you, I would not be here or have come this far in life. Thank you, ammu and appa.

Table of Contents

List of Abbreviations.....	i
List of Figures and Tables.....	ii
1. Introduction.....	1
1.1. Meiosis.....	1
1.1.1. Meiotic Recombination Distribution and Regulation in Plants.....	4
1.1.2. Engineering Meiosis for Crop Breeding.....	5
1.2. Methods to Detect Meiotic Recombination Events in Plants.....	6
1.2.1. Cytology Techniques.....	6
1.2.2. Genotyping and Sequencing Platforms.....	6
1.2.3. Fluorescence-tagged Lines.....	7
1.2.4. Crystal digital (d)PCR for CO Rate Measurement.....	7
1.3. Functional Gene Study Tools for Barley (Meiotic) Research.....	9
1.3.1. Virus-Induced Genome Editing and Gene Silencing.....	10
2. Aims of this Thesis.....	12
3. Materials and Methods.....	13
3.1. Horticultural Work.....	13
3.1.1. Plant Materials Used.....	13
3.1.2. Cross-pollination in Barley.....	13
3.1.3. Plant Growth and Cultivation.....	13
3.1.4. Anther Collection for Pollen Nucleus Isolation.....	14
3.2. Molecular Work.....	14
3.2.1. Nuclei Acid Extraction.....	14
3.2.1.1. DNA.....	14
3.2.1.2. RNA and cDNA synthesis.....	15
3.2.2. Genotyping.....	15
3.2.3. PCR.....	15

3.2.3.1.	Reverse Transcriptase PCR	15
3.2.3.2.	Touch-down PCR	15
3.3.	Molecular Cloning.....	16
3.3.1.	Plasmid DNA Transformation, Screening and Verification	16
3.3.2.	Generation of BSMV- γ -sg Plasmid for Expression of sgRNA.....	16
3.3.3.	Cloning of sgRNA into BSMV- γ -sg Plasmid	16
3.3.4.	Cloning of gene fragment BSMV- γ bCDS Plasmid.....	17
3.4.	Cytology – Male Meiotic Chromosome/Nuclei Preparations	17
3.5.	<i>In silico</i> Methods.....	18
3.5.1.	Oligonucleotide Design.....	18
3.5.2.	SgRNA Design.....	18
3.5.3.	Mutation Analysis	19
3.5.4.	Statistical Analysis	19
3.5.5.	RNAi-target design	19
3.5.6.	Plot Generation.....	19
3.6.	Multiplex Crystal digital (d)PCR-based single pollen nucleus genotyping (SPNG).....	19
3.6.1.	Pollen Nuclei Isolation	19
3.6.2.	Flow Sorting of Pollen Nuclei.....	20
3.6.3.	Loading and Scanning of Naica™ Sapphire Chips.....	20
3.6.4.	Recombination Rate Analysis	21
3.7.	BSMV Infection Methods	23
3.7.1.	Agrobacterium-Mediated Infection of <i>N. benthamiana</i> with BSMV	23
3.7.2.	<i>In vitro</i> -BSMV Transcript Preparation	23
3.8.	BSMV Inoculation in Barley.....	24
4.	Results.....	25
4.1.	Multiplex Crystal Digital (d)PCR-based Single Pollen Nucleus Genotyping (Multiplex SPNG) in Barley: Male Meiotic Recombination Measurements.....	25
4.1.1.	Storage of Barley Anthers for Multiplex SPNG	25

4.1.2.	Marker Selection and Validation for Multiplex SPNG	27
4.1.3.	Six-color Crystal dPCR: Multiplex Male Meiotic Recombination Rate Assessment	28
4.1.4.	Optimizing the novel Crystal dPCR Setup for Enhanced SPNG in Barley	30
4.1.5.	Assessing Male Meiotic Recombination Rates Using Multiplex SPNG in Barley Hybrid Pollen Nuclei	34
4.1.6.	Validating Male Meiotic Recombination Rate Measurements	35
4.1.7.	CO Interference Strength within Selected Genetic Intervals in Barley Pollen Nuclei.....	37
4.1.8.	Multiplex SPNG Enables Measurement of Altered Meiotic Recombination Rates.....	37
4.1.9.	Meiotic Recombination Rates in Pollen Nuclei at Different Developmental Stages.....	39
4.2.	Barley Stripe Mosaic Virus-Induced Genome Editing (BSMVIGE) in barley.....	40
4.2.1.	Generation of <i>SpCas9</i> Expressing Barley Plants	40
4.2.2.	BSMVIGE Targeted Somatic Gene Editing at the <i>ALBOSTRIANS</i> locus in Barley.....	40
4.2.3.	Heritable Editing at the <i>ALBOSTRIANS</i> Locus in Barley	42
4.2.4.	Isolation of Virus-free <i>cmf7</i> Mutants	43
4.3.	Modification of the Meiotic Recombination Landscape Using BSMV	44
4.3.1.	Identification of Putative Meiosis-related Genes	45
4.3.2.	BSMVIGE-Directed Targeting of Identified Meiosis-related Genes	46
4.3.2.1.	Singleplex BSMVIGE.....	47
4.3.2.2.	Multiplex BSMVIGE	48
4.3.3.	Isolation of Putative Chromosome Axis and SC Mutants.....	51
4.3.4.	In barley, SC formation is required for CO formation.....	52
4.3.5.	BSMV-mediated Virus-Induced Gene Silencing (BSMVIGS) in barley	55
5.	Discussion	57

5.1.	Multiplex Crystal Digital PCR-based Single Pollen Nucleus Genotyping (Multiplex SPNG) for Male Meiotic Recombination Measurements in Barley	57
5.1.1.	Barley Anther Storage Enables High-Throughput SPNG.....	57
5.1.2.	Multiplex SPNG: CO rate in Two Linked Genetic Intervals.....	57
5.1.3.	CO Interference Strength in Barley Pollen Nuclei.....	58
5.1.4.	Multiplex SPNG Approach Detects Significant Increases in CO Rates	59
5.1.5.	Consistent Male CO Rates in Anthers Developed Across Barley Tillers	59
5.1.6.	Improving the Efficiency of Multiplex SPNG.....	60
5.2.	Barley Stripe Mosaic Virus-Induced Gene Editing (BSMVIGE) in barley.....	60
5.2.1.	Utilizing BSMV for Targeted Genome Modifications in Crop Plants.....	60
5.2.2.	Successful Implementation of BSMVIGE in Barley	61
5.2.3.	Heritable Editing and BSMV Transmission in Progeny	62
5.2.4.	Rapid Isolation of Barley Mutants Using BSMVIGE.....	62
5.2.5.	Insufficient BSMVIGE-Mediated Multiplexed Gene Editing Using MEA Strategy.....	63
5.2.6.	BSMVIGE: A Reliable Gene Editing Platform for Barley	64
5.2.7.	Enhancing the BSMVIGE Strategy in Barley and Other Crops: Further Insights.....	65
5.3.	Impaired Meiosis in SC Mutants.....	66
5.4.	BSMV-mediated Virus-Induced Gene Silencing (BSMVIGS) in Barley.....	67
6.	Outlook.....	69
7.	Summary	70
8.	Zusammenfassung.....	71
9.	References	73
	Curriculum Vitae.....	91
	Eidesstattliche Erklärung / Declaration under Oath.....	94
	Appendix	95

List of Abbreviations

DNA	Deoxyribonucleic acid	m	Meter
2D	Two-dimensional	RNA	Ribonucleic acid
%	Percentage	M	Molar
°C	Degree celcius	ml	Milliliter
μF	Microfarads	mM	Millimolar
μg	Microgram	ng	Nanogram
μl	Microliter	nm	Nanometer
μM	Micromole	Ø	Diameter
μmol	Micromole	ORF	Open reading frame
ATP	Adenosine Triphosphate	PBS	Phosphate-buffered saline
bp	Basepair	PCR	Polymerase chain reaction
cDNA	Complementary DNA	pmol	Picomole
CDS	Coding sequence	psi	Pounds per square inch
cm	Centimeter	QTL	Quantitative trait loci
dNTP	Deoxynucleoside triphosphate	rpm	Rotation per minute
EDTA	Ethylenediaminetetraacetic Acid	s	Second
Hz	Hertz	siRNA	Short interference RNA
kV	Kilovolt	TTP	Thymidine Triphosphate
w/v	Weight per volume	U	Enzyme unit
DAPI	4',6-Diamidino-2-phenylindole	PI	Propidium iodide
ms	Millisecond	1D	One-dimensional
YEB	Yeast extract broth	Hz/s	Hertz per second
Mbp	Megabasepair	cM	Centimorgen

List of Figures and Tables

Figure 1: Schematic illustration of meiotic recombination in plants.	3
Figure 2: Schematic depiction of the tripartite genome organization of BSMV in the vectors used.....	10
Figure 3: Analysis of male meiotic recombination rate using Naica™ Crystal Miner software.	22
Figure 4: Efficacy of different pollen treatment strategies on pollen nuclei isolation.	25
Figure 5: Pollen treatment strategies for efficient isolation of barley pollen nuclei.	26
Figure 6: Two-plex assay for detecting CO events in pollen nuclei.	28
Figure 7: Multiplex SPNG setup for male CO rate measurement in hybrid barley pollen nuclei.	29
Figure 8: Specificity of the designed TaqMan probes for six selected markers on chromosome 1.	31
Figure 9: Specificity of the designed TaqMan probes for six selected markers on chromosome 3.	32
Figure 10: Pollen nuclei morphology after bursting.	33
Figure 11: Comparison of three- and two-color approaches for estimating CO rate in barley.	35
Figure 12: Increased meiotic recombination rates in <i>recq4</i> hybrid barley pollen nuclei.	38
Figure 13: Male meiotic recombination based on anther developmental stage in hybrid barley.	39
Figure 14: Overview of the BSMVIGE Workflow.	41
Figure 15: BSMVIGE at the <i>ABOSTRIANS</i> locus in barley.	42
Figure 16: BSMVIGE-induced heritable edits at <i>ALBOSTRIANS</i>	43
Figure 17: Offspring transmission of BSMV.	44
Figure 18: BSMVIGE targets within selected meiosis-related genes in barley.	47
Figure 19: Multiplex BSMVIGE using mixed <i>Agrobacterium</i> pool strategy (MEA).	49
Figure 20: BSMV-induced heritable editing within putative meiotic axis- and SC-related genes in barley.	51
Figure 21: Immunolocalization of SC components in barley meiotic mutants.	53
Figure 22: Meiosis in barley meiotic mutants.	54
Figure 23: Male meiotic recombination rate measurements in BSMVIGS treated barley.	56
Table 1: Singleplex BSMVIGE-induced somatic editing in meiosis-related genes.	48

1 Introduction

1.1 Meiosis

Meiosis is a specialized cellular process key for sexual reproduction, facilitating the formation of haploid gametes, that will give rise to pollen and ovules in plants. This process ensures that upon fusion of male and female gametes during fertilization, the diploid state of the zygote is restored, maintaining the organism's chromosome number across generations. It begins with one round of DNA replication, followed by two consecutive and distinct rounds of chromosome segregation: meiosis I and meiosis II. During meiosis I, homologous chromosomes, each consisting of two sister chromatids, segregate to opposite poles. Hence, this reductional division halves the chromosome number. Meiosis II, involves the separation of sister chromatids, resulting in four genetically distinct haploid cells from the original diploid cell. Meiotic prophase I is the longest and most intricate stage of meiosis, characterized by the process of homologous recombination, during which homologous chromosomes exchange genetic material. This exchange generates new combinations of alleles, ensuring that each gamete carries a unique genetic blueprint derived from both parents [1, 2]. Prophase I is divided into five distinct sub-stages—leptotene, zygotene, pachytene, diplotene, and diakinesis—each marked by key molecular and structural events that are cytologically distinguishable and essential for the progression of meiosis. During leptotene, chromosomal condensation begins, making chromosomes visible as thin, thread-like structures under a microscope. In the subsequent zygotene stage, homologous chromosomes initiate pairing and start synapsis. At pachytene, synapsis culminates in the formation of the synaptonemal complex (SC), a tripartite proteinaceous scaffold that ensures precise alignment of homologous chromosomes along their lengths by physical linkage. During this time frame, crossover (CO) formation, i.e. the reciprocal genetic exchange between homologs, occurs. As prophase I advances to diplotene, the SC disassembles but homologs remain connected via chiasmata, cytological manifestations of CO recombination. In the final sub-stage, diakinesis, chromosomes reach their maximum condensation, and the nuclear envelope breaks down, signaling the end of prophase I. The spindle apparatus forms, positioning homologous chromosome pairs, still linked by chiasmata in form of bivalents, for alignment on the metaphase plate [3]. Genetic variation arisen via meiotic recombination underpins the adaptive potential of populations, fueling evolution by providing the raw material upon which natural selection acts. Individuals with advantageous genetic combinations are more likely to reproduce, passing these beneficial traits to their

offspring. Over successive generations, this selective process enhances the ability of populations to adapt to changing environments, thereby increasing their chances of survival. Thus, meiosis not only plays a pivotal role in reproduction but also drives the evolutionary processes that shape diversity and resilience of life [1, 4].

Several genetic factors underlying meiosis have been identified in plants, particularly in *Arabidopsis thaliana*. During leptotene, sister chromatids are organized into a loop-based array along a proteinaceous chromosome axis composed of HORMA domain proteins (ASY1/3/4), cohesin subunit proteins (SMC1/3) [5] and the meiosis-specific protein (SYN1 or DIF1) [6, 7], the ortholog of REC8 in yeast [8]. During zygotene, these chromosome axes become progressively aligned along their length, a process often described as "zipping", based on interhomolog repair interactions. At pachytene, this "zipping" leads to the full assembly of the tripartite SC, that physically connects homologous chromosomes. The SC comprises axial elements (ASY1/3) [9, 10], transverse filaments (TF; ZYP1) [11], and central elements (CE ; SCEP1/2/3) [12, 13]. Meiotic recombination takes place within the context of the chromosome axis and the SC. DNA double-strand breaks (DSBs) occur within chromatin loops that are tethered to the axis, initiating meiotic recombination. Meiotic DSBs are catalyzed by a core DSB-induction complex comprising SPO11 [14-16] and MTOPVIB [17], with co-factors such as PRD1/2/3, and DFO [18-22]. The MRN complex (MRE11-RAD50-NBS1) [23-25] and COM1 [26] resect DSB ends to generate 3'-OH single-stranded (ss) DNA overhangs, which are subsequently bound by RPA [27]. The recombinases RAD51 and DMC1 - the latter being specific to meiosis - form nucleofilaments capable of homology search and heteroduplex formation [28-30].

The complementary strand of the homologous chromatid is displaced by DNA synthesis primed by 3' ssDNA overhangs, leading to the formation of a D-loop. This D-loop is extended by DNA synthesis and ligation, capturing the second end and forming a double Holliday junction (dHJ). Cleavage and ligation of the dHJ result in either CO or non-crossover (NCO) [31, 32]. In *A. thaliana*, approximately 200-300 DSBs are formed during meiosis, but only about 10 CO events occur suggesting that less than 5% of SPO11-catalyzed DSBs are repaired as CO events and that the majority of DSBs (more than 95%) are repaired as NCO events. NCO events can result in the copying of DNA short segments from one chromosome to the corresponding region of the other, either between the sister chromatids or homologous chromosomes – a process known as gene conversion (GC). Alternatively, NCO events may involve no exchange of genetic material at all, occurring through repair pathways such as non-homologous end joining (NHEJ)

or synthesis-dependent strand annealing (SDSA) [1]. In most species, including plants, there are two pathways for CO formation. Class I CO, which account for 85-90% of CO in plants, rely on so-called ZMM proteins (Zip1/2/3/4, Mer3, and Msh4/5 in yeast), including HEI10 (likely Zip3 ortholog in plants) and MLH1/3 [33-35]. Notably, multiple CO occurring on a chromosome tend to be spaced more widely than expected by chance due to the phenomenon of CO interference [36, 37]. Class II CO, which are fewer and do not exhibit CO interference, require in part the endonuclease MUS81 or FANCD2 [38, 39] (Fig 1).

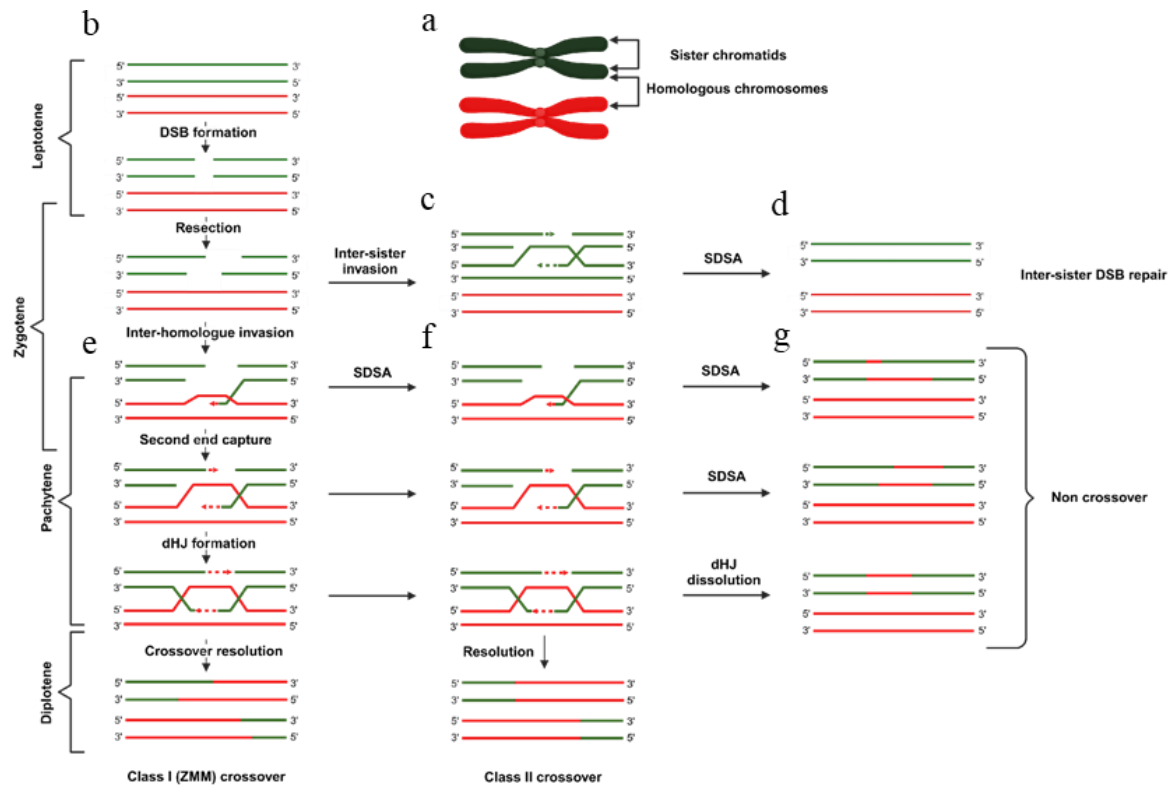


Figure 1: Schematic illustration of meiotic recombination in plants.

(a) A pair of homologous chromosomes with parental chromosomes comprising two sister chromatids. (b-g) For simplicity, only non-sister chromatids are shown in green and red. (b) Programmed meiotic DSBs are introduced by the meiotic DSB induction complex during leptotene, followed by resection of DNA ends to produce 3' single-stranded overhangs. These overhangs can be repaired either by using the sister chromatid (c, d) or the homologous chromosome as a template. (e) RecA-family recombinases (RAD51 and DMC1) bind to the overhangs to promote interhomolog strand invasion during zygotene. (e-g) The resulting joint molecules are processed through multiple parallel pathways, resulting in either CO or NCO outcomes. (e) Second-end capture, DNA synthesis, and ligation lead to the formation of a dHJ, which can be resolved into a class I CO via the ZMM-dependent pathway. (f) Class II CO are generated through ZMM-independent pathways, involving MUS81 and FANCD2. (g) NCO can arise via SDSA or through the dissolution of dHJs or joint molecules.

1.1.1 Meiotic Recombination Distribution and Regulation in Plants

The number of CO formed is limited despite large numbers of DSBs and excess recombination initiation sites. In barley, like in many species, a minimum of at least one CO per homologous chromosome pair is required to ensure the faithful segregation of homologous chromosomes during meiosis I. In the wildtype (WT), ~1.9 chiasmata are formed per chromosome, totalling 12 to 14 chiasmata across seven chromosome pairs during meiosis [40]. In plants, the interplay between pro- and anti-CO pathways restricts CO numbers formed per chromosome arm. Most of the CO sites are associated with the accumulation of ZMM-proteins on the chromosome axis, including the pro-CO factor, E3 ubiquitin ligase HEI10. Initially, multiple HEI10 foci form along synapsed chromosomes but gradually coarsen into a few large foci, which mark future class I CO sites. This process is tightly linked to the SC, which likely provides a structural platform facilitating HEI10 diffusion and focus maturation [41, 42]. Recombination initiation via DSBs is a prerequisite for HEI10 foci formation, and SC integrity is essential for proper coarsening and interference between CO [43]. HEI10 acts in a dosage-dependent manner, and the overexpression of HEI10 increases the CO number but does not influence the CO distribution in *A. thaliana*. Further, in the absence of ZYP1, i.e. the SC, the number of HEI10 foci and CO events increases, associated with (near) absence of CO interference as well as heterochiasmy (differences in CO number between the sexes) [12, 13, 41-43]. The combination of *hei10* and *zyp1* leads to an unprecedented increase in CO events, showing the synergistic effect driven by elevated HEI10 levels in the absence of SC [44]. Anti-CO factors such as RECQ4, FANCM, MHF1/2, FIGL1 and TOP3 α act on the recombination intermediates at various stages, promoting NCO formation and thus limiting CO. It has been shown that depletion of anti-CO factors such as RECQ4 and FANCM increases CO events in Arabidopsis, brassica crops and rice [45-51].

In plants, similar to most organisms, CO are not equally likely to occur at all genomic locations [52]. CO hotspots are defined as genomic regions where CO occur at significantly higher frequencies than the genome-wide average. These regions are typically associated with open euchromatin, DSB hotspots (regions with elevated DSB frequency), gene-rich areas (particularly proximity to gene promoters and terminators), DNA repeat motifs (such as AT, CTT, or CCN), epigenetic marks (including H3K4me3, CHH DNA methylation and H2A.Z) and low nucleosome occupancy. In contrast, CO coldspots, or regions with low or no recombination, are commonly found in genomic areas enriched for DNA methylation (in the context of CG and CHG), chromosome axis-proteins (including ASY1 and REC8), transposons,

or retrotransposons and repetitive elements (flanking centromeres, pericentromeres or telomeres) [53-58]. Notably, in large-genome crops such as barley, wheat, and maize, CO are predominantly found in distal euchromatic regions, while proximal regions exhibit low CO activity [59, 60]. The skewed CO distribution is more pronounced in wheat and barley than in the smaller genome plant species such as *A. thaliana* and rice, possibly due to genome size, repeat content, and chromatin structure [61-65]. Ultimately, both molecular and (epi)genomic factors determine the number and distribution of crossovers in plant species.

1.1.2 Engineering Meiosis for Crop Breeding

Crop pre-breeding programs focus on transferring beneficial alleles from donor germplasm into elite cultivars. However, a skewed CO distribution and a comparatively low CO number in crops such as barley, wheat, and maize lead to strong linkage disequilibrium among alleles across large chromosomal intervals, i.e., alleles within a chromosomal block are inherited together more frequently than expected by chance, thereby limiting genetic diversity [66]. Barley (*Hordeum vulgare* L.) is an important cereal crop that predominantly self-pollinates, however hybrid lines can be developed through breeding strategies. Given that an established genetic transformation protocol, TILLING lines, mutants and extensive genomic data, and that barley has large chromosomes and is diploid, it represents as an attractive model for studying crop plant meiosis [65, 67, 68]. For example, in barley, 20% of the genes are located in non or weakly recombining regions, including interstitial chromosomal regions. Additionally, isolating gene candidates in QTL analysis is challenging due to linkage of undesired chromosomal regions to phenotype-associated regions. Coupling linkage, two alleles with either positive or negative effects on a trait are linked, can result in pseudo-dominance after heterosis when recombination is limited in the confined chromosomal segments. Evolutionarily, low recombination rates may lead to the accumulation of deleterious mutations, negatively affecting fitness and agronomic productivity [69-71]. Therefore, increasing genome-wide recombination can enhance genetic gain as well as plant fitness. A simulation study in maize showed a potential increase in genetic gain of up to 10% over six generations of recurrent selection by using a hypothetical double mutant combination of two hyper-recombination mutants, *ddm1* and *zmet2* [72]. Conversely, reverse breeding, which involves restricting recombination either genome-wide or locally, can help to maintain the desired heterozygous state of a hybrid and to generate chromosome substitution lines, where one chromosome of a line is replaced by that of another line [73].

Unreduced gamete formation, achieved through first-division restitution (FDR) or second-division restitution (SDR), depending on whether the first or second meiotic division is affected, can be used by breeders to produce plants with desired ploidy, exhibiting higher genetic diversity [74]. Both FDR and SDR result in recombined gamete formation, as shown in *A. thaliana* by disturbing spindle orientation through mutations in *parallel-spindle 1* or *Jason*, and by mutating genes controlling entry into the second division, such as *OSD1*, *CYCA1/2*, or *TAM1* [75-78]. Restoring the parental genotype in the offspring through the production of clonal seeds has significant potential in plant breeding, enabling the immediate fixation and seed-based propagation of any plant genotype. This can be achieved by restricting the recombination and bypassing the second division while allowing sister chromatid segregation during the first meiotic division. In rice and *A. thaliana*, *MiMe* mutants (mitosis to meiosis) were generated by simultaneously mutating *SPO11-1* or *PRD1/2/3*, *OSD1*, and *REC8*, resulting in viable clonal seed production [75, 79]. A polyploid genome design using the *MiMe* system was established in tomato hybrids by mutating *SISPO11-1*, *SIREC8* and *SITAM* [80]. This approach enabled the generation of clonally propagated F2 plants referred to as "nonrecombinant, double-cross hybrids" or "4-haplotype" plants that carry the complete genetic makeup of all four inbred F0 grandparents, achieved by crossing two hybrid (F1) *MiMe* plants. Hence, both increasing and limiting the number of meiotic recombination events can accelerate and improve plant breeding.

1.2 Methods to Detect Meiotic Recombination Events in Plants

1.2.1 Cytology Techniques

Cytological techniques for the detection of CO events involve analyzing number and position of either chiasma based on bivalent shape or CO markers such as HEI10 and MLH1/3 based on immunohistochemistry [59, 81]. Additionally, CO interference strength can be estimated through statistical analysis of CO distribution [82]. While cytological methods provide rapid CO rate estimation directly in gametes of both inbred and hybrid plants, they suffer from low throughput and poor resolution, making it difficult to resolve CO breakpoints.

1.2.2 Genotyping and Sequencing Platforms

CO rate measurement in hybrid backgrounds relies on genetic polymorphisms between the two parental genomes. Single nucleotide polymorphism (SNP) genotyping or genotyping-by-sequencing (GBS) can detect genome-wide CO based on segregation of SNP markers in hybrid

offspring populations [83-85]. SNP arrays with varying SNP marker density and distribution allow custom flexibility. KASP (competitive allele-specific PCR) or TaqMan assays can be used to genotype polymorphic markers, facilitating CO rate analysis in hybrid plants [86]. These approaches, however, are labor-intensive because they involve processing a large population of offspring. Whole-genome or targeted sequencing, using both short-read and long-read platforms, offer high-resolution detection of both CO and GC events, as well as CO interference strength [87, 88]. Alternatively, CO events can be directly detected in gametes from single individuals using linked-sequencing [89] or single pollen nucleus genotyping (SPNG) methods, providing resolution akin to single-cell sequencing technologies [90, 91]. Despite their high resolution, these methods are costly and labour-intensive.

1.2.3 Fluorescence-tagged Lines

Fluorescence-tagged lines (FTLs) in *A. thaliana* have been generated by inserting T-DNAs into the genome that express various fluorescent proteins (FPs) specifically in pollen or in seeds under control of the *LAT52* or *napin* promoter, respectively [92, 93]. Hemizygous plants with linked-FP alleles on the same chromosome are isolated by crossing homozygous FP lines with WT or mutants. The CO rate is measured by allowing these hemizygous lines to self-fertilize and then analyzing FP segregation via microscopy for seed-FTLs and flow-cytometry for pollen-FTLs. In pollen *qrt1* mutants, the four products of male meiosis remain physically attached, enabling tetrad analysis of CO and NCO events including CO interference strength assessments [93-96]. Automated analysis tools like *DeepTetrad* and *SeedScoring* enable high-throughput and rapid CO rate measurement using FTLs in *A. thaliana* [97, 98]. *A. thaliana* FTLs have been employed in various genetic studies to elucidate key meiotic players [99] and are extensively used to investigate the impact of (a)biotic factors, environmental conditions, genetic influences or genome structural variations (SVs) on CO rate [100-103]. However, the use of FTLs is restricted by the current limitations in efficient targeted-gene insertion techniques in *A. thaliana*, making it challenging to isolate FTLs with T-DNA insertions in specific genomic regions. Additionally, FTL systems are not yet available in crops, due to the lack of efficient genetic transformation strategies, which further limits crop meiosis studies to traditional methods such as cytological analysis, genotyping, or sequencing techniques.

1.2.4 Crystal digital (d)PCR for CO Rate Measurement

Initially, the evaluation of male CO rates through SPNG was dependent on a costly whole-genome amplification procedure [90, 91]. Although this approach is rapid, its high expense and

low throughput limit its practicality for large-scale studies. To overcome these challenges, a new approach was developed, leveraging the Stilla Technologies Naica™ crystal dPCR system for SPNG-based CO rate measurement [104]. It provides rapid and reliable CO measurement directly in barley hybrid pollen and can be adapted for use in various plant species. However, CO rate measurements are only performed within a single chromosomal interval, which limits throughput and hinders the assessment of CO interference strength. So far, CO interference has only been assessable through sequencing-based approaches, cytological methods, or FTL systems. Furthermore, the current SPNG method has a major drawback: it relies on fresh pollen material, which restricts sample pooling and prevents the simultaneous assessment of samples from different geographical locations.

During a dPCR, the PCR occurs within numerous partitions, where molecules are distributed randomly according to the Poisson distribution. This allows concentration of nucleic acids required for PCR, facilitating efficient amplification even with low template quantities. Unlike quantitative (q)PCR, dPCR provides absolute quantification of nucleic acids and can genotype rare mutations through end-point fluorescence measurement without requiring a calibrator reaction, thereby reducing reaction-to-reaction variation. This is achieved by enumerating digital signals based on positive or negative amplifications within partitions containing nucleic acids [105, 106]. Several dPCR platforms are available, including droplet-based, channel-based, chip-in-tube and nanoplate-based dPCR platforms. These platforms differ in their methodology, material, and partition formation techniques [107].

The droplet crystal-based Naica™ crystal dPCR system generates a 2D array of micro oil droplets to encapsulate nucleic acids from a primed PCR mix in a molded plastic microfluidic chip (Sapphire™ chip). The dPCR is performed using a flat thermocycler block, and subsequently, the chip is scanned by a microscope scanner (Prism™ instrument), revealing positive and negative amplifications within droplets. Each Sapphire™ chip can accommodate four independent dPCR reactions, each with approximately 20,000 partitions. Additionally, three chips can be processed in a single run, significantly enhancing throughput [108]. The current crystal dPCR-based SPNG strategy [104] involves encapsulating the pollen nuclei, each measuring 5-7 μm (\varnothing), within oil droplets of approximately 100 μm (\varnothing), ensuring that each nucleus is isolated and accurately genotyped. This approach enables reliable measurement of CO rates in hybrid pollen nuclei.

1.3 Functional Gene Study Tools for Barley (Meiotic) Research

Despite the overall conservation of meiosis across eukaryotes, genetic analyses have uncovered both similarities and differences in meiotic phenotypes among various species, including plants. For example, loss of the SC component, ZYP1 in *A. thaliana* and partial depletion of its rice ortholog ZEP1 both lead to an increase in CO rates [43, 81, 109]. However, depletion of ZYP1 based on RNA(i) interference resulted in meiotic defects in barley [110]. Induced mutations in the anti-CO factor RECQ4 lead to increased CO rates across several plant species, including *A. thaliana*, rice, pea, tomato, and barley [48, 111, 112] but not in wheat [113]. Similarly, depletion of the anti-CO factor, FIGL1 causes meiosis catastrophe in rice, while it results in increased recombination rates in *A. thaliana* [46, 114]. In wheat, FANCM promotes class I CO, contributing to the obligate CO formation, but restricts class II CO [115]. However, whether FANCM has a similar role in barley remains to be investigated. Thus, it is essential to characterise meiosis-related genes in crops, including barley, to both better understand the regulatory pathways of meiotic recombination and to possibly alter the meiotic recombination landscape, thereby facilitating advancements in crop breeding. To elucidate gene-function relationships, isolation of loss-of-function mutants is invaluable. This can be achieved using targeted genome editing (TGE) through sequence-specific nucleases (SSNs) such as zinc finger nucleases (ZFNs), TAL effector nucleases (TALENs), and the Clustered Regularly Interspaced Short Palindromic Repeats (CRISPR)-Cas9 system [116-118]. Isolation of stable transgenics by SSNs is preferred over Targeting Induced Local Lesions IN Genomes (TILLING) [119] for functional genomics because they allow rapid generation of plants with targeted gene disruptions without extensive backcrossing requirements. The CRISPR/Cas9 system, in particular, has become a versatile tool in plant genetic engineering for crop improvement, enabling gene knockouts or regulation of gene transcription using various Cas9 variants and fusion proteins [120-124]. The commonly used Cas9 variant is derived from *Streptococcus pyogenes*, a component of bacterial adaptive immunity that consists of nuclease domains, HNH and RuvC-like. *S. pyogenes* CRISPR-Cas9 is a RNA-guided DNA endonuclease that uses a dual RNA (tracrRNA:crRNA complex) to direct site-specific DNA cleavage. HNH and RuvC-like domains cut opposite DNA strands; mutating one creates a nickase, while mutating both produces dCas9, which binds DNA without cutting. Targeting requires both 20 bp sequence complementarity and a protospacer adjacent motif (PAM) adjacent to the target site. The dual RNA was engineered into a single guide RNA (sgRNA), simplifying the system to just two components: Cas9 and sgRNA. Unlike ZFNs and TALENs, which need protein reengineering,

CRISPR-Cas9 only requires changing the sgRNA sequence, enabling easy and widespread genome editing across many organisms [125]. However, stable genetic transformation required to deliver CRISPR/Cas9 components can be challenging in crops like barley and in particular multiple genotypes of a given species, which are often recalcitrant to tissue-culture-based transformation methods [126, 127]. Notably, well-established genetic transformation strategies are available only for spring barley cv. Golden Promise due to its amenability to tissue-culture-based genetic transformation; however, standard transformation protocols to other spring and winter barley genotypes have resulted in substantially lower efficiency or are not available [128]. Common transformation protocols use immature embryos as explants; nevertheless, other tissues, including pollen and ovules, have been tested, albeit with lower regeneration efficiency [129, 130].

1.3.1 Virus-Induced Genome Editing and Gene Silencing

Plant viruses have been exploited to deliver genetic elements to induce targeted mutations in the plant genome or elicit RNAi-mediated downregulation of target genes. Virus-induced genome editing (VIGE) is a tissue-culture-free technique emerging as a high-throughput method for TGE in plants. In VIGE, plant viruses are engineered to deliver Cas-compatible guide RNAs into plants expressing the desired Cas protein or to express the complete genome editing components [131-135]. This method has been successfully applied in dicots such as *Nicotiana benthamiana* and *A. thaliana* using plant RNA viruses such as Tobacco rattle virus (TRV) and Pea early browning virus (PEBV) [136, 137]. In monocots, only a few plant viruses, including foxtail mosaic virus (FoMV) and barley stripe mosaic virus (BSMV), have been tested for VIGE [138, 139]. BSMV, a positive-sense RNA virus with a tripartite genome (Fig. 2), has shown promise in delivering sgRNAs into Cas9-overexpressing monocots like wheat and maize, as well as *N. benthamiana*, to elicit CRISPR/Cas9-facilitated TGE [139].

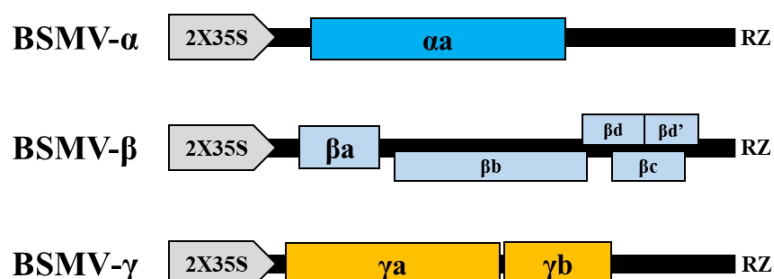


Figure 2: Schematic depiction of the tripartite genome organization of BSMV in the vectors used. Genome organization of BSMV vector used for targeted genome editing in wheat. BSMV-α encodes a single protein: αa, the helicase subunit of the replicase. BSMV-β encodes five proteins: βa, the coat

protein; βb , βc , βd , and $\beta d'$, the triple gene block proteins required for cell-to-cell movement. BSMV- γ encodes two proteins: γa , a polymerase subunit of the replicase; γb , a cysteine-rich pathogenicity-related protein. The three genomes are expressed under two-tandem constitutive Cauliflower Mosaic Virus 35S promoter (2x35S) arrays, and ribozyme sequences added downstream [140].

In my Ph.D. research, I focused on exploring BSMV-mediated virus-induced genome editing (BSMVIGE) in barley. During this work, BSMVIGE was successfully applied in wheat to generate heritable mutations in Cas9-expressing plants [141]. sgRNAs were expressed through the third BSMV subgenome (BSMV- γ) (Fig. 2). The systemic movement and high replication efficiency of BSMV ensure the production of abundant sgRNAs, which are essential for driving CRISPR/Cas9-mediated TGE. Heritable gene editing and multiplex genome editing (MGE) were achieved using BSMVIGE in wheat [142].

Virus-Induced Gene Silencing (VIGS) is a reverse genetics approach utilized in crop research for functional genomics studies. Plants are inoculated with a recombinant virus that carries a target gene fragment. The host's RNAi response triggers sequence-specific degradation of both viral RNA and homologous endogenous mRNA transcripts. Hence, VIGS mediates transient gene silencing, enabling functional gene studies independent of stable genetic transformation. Transient silencing also enables studying dosage-dependent genes that cause host lethality if permanently mutated [143-146]. BSMV has been used for VIGS in barley, wheat, and rye to downregulate genes involved in disease resistance and abiotic stress. Its ability to infect multiple barley genotypes highlights its potential to overcome limitations in reverse genetics and functional genomics [147-155].

2 Aims of this Thesis

Meiosis assures genetic variation through reciprocal DNA exchanges between homologous chromosomes, known as crossovers (CO), that are harnessed during breeding. In cereal crops such as barley (*Hordeum vulgare L.*), CO are limited in number and exhibit an uneven chromosomal distribution. Typically, CO are predominantly found at chromosome ends, leaving extensive interstitial and (peri)centromeric regions largely untouched. Furthermore, CO interference prevents CO from occurring in close proximity of each other along a given chromosome. This together hinders the utilization of all naturally available genetic variation in breeding programs, as for instance genes located in low-recombining regions remain inaccessible for genetic improvement.

In *Arabidopsis thaliana*, various genetic and epigenetic factors regulating the CO landscape (CO frequency and distribution) have been identified. However, it remains unclear whether similar mechanisms operate in cereal crops such as barley. Functional studies are therefore required to elucidate CO regulation in cereals. Despite this need, bottlenecks in barley genetic transformation and in CO rate assessment severely impede functional studies and translational approaches, limiting the ability to study and manipulate meiotic recombination. Hence, novel tools and methodologies are essential for rapidly assessing meiotic gene function in barley, ultimately facilitating advances in crop breeding.

This thesis aims to develop strategies and tools to rapidly assess and study meiotic genes in barley, with the goal of exploring and applying approaches to modify its meiotic recombination landscape. The detailed objectives are:

1. Further development and application of crystal digital PCR-based single pollen nucleus genotyping (SPNG) in barley hybrids to enable high-throughput measurement of CO rates across multiple genomic intervals, including the assessment of CO interference.
2. Exploration and development of virus-based tools (e.g., virus-induced gene silencing (VIGS) and virus-induced genome editing (VIGE)) to rapidly assess meiotic gene function and to isolate meiotic mutants without stable genetic transformation.
3. Application of these tools to manipulate meiotic recombination outcome in barley.

By addressing these objectives, this research aims to deepen our understanding of CO regulation in barley and to develop innovative approaches to harness recombination for crop improvement.

3 Materials and Methods

3.1 Horticultural Work

3.1.1 Plant Materials Used

Nicotiana benthamiana and *H. vulgare* cultivar (cv) Barke (B), Golden Promise (GP), or F1 hybrid B x GP were used as WT.

recq4-1, a non-sense mutation in *RECQ4*, was isolated in a barley cv. B TILLING population [156] and *recq4-2*, CRISPR/Cas9-induced mutations (-2 bp and -3 bp deletions at independent sites) within *RECQ4*, was isolated in barley cv. GP. These lines were isolated by Dr. Mohammad Abdelmordy Ayoub, IPK Gatersleben [157].

ZmUBI::Cas9, barley cv. GP lines expressing *SpCas9* constitutively under control of a maize *polyubiquitin* promoter, were provided by Dr. Jochen Kumlehn, IPK Gatersleben.

3.1.2 Cross-pollination in Barley

Plant crossings were conducted as described [158], using pollen from barley cv. B to fertilize emasculated flowers of barley cv. GP. Briefly, spikes from 8-11-week-old B plants were carefully removed from the leaf sheath. Male anthers were emasculated by trimming the top part of each spikelet with scissors and gently removing the three green immature anthers without damaging the female organ. Two days later, mature anthers were collected from 10-14-week-old GP plants into a petri dish. Using forceps, two to three anthers were inserted into each female spikelet of the emasculated plants. The crossed spike was returned to the leaf sheath and covered with a glassine bag. Mature grains were harvested 1-2 months later.

3.1.3 Plant Growth and Cultivation

N. benthamiana plants were grown in a greenhouse at 22 °C with 65 % relative humidity and a 16/8-hour light/dark cycle, receiving light intensity between 80-100 $\mu\text{molm}^{-2}\text{s}^{-1}$ in plant cultivation pots (13 cm Ø). Upon infection with BSMV, plants were incubated in a growth cabinet (Polyklima) located in a biosafety level S2 containment facility under the same growing conditions except for a constant temperature of 24.5 °C. Barley F1 hybrid B x GP grains (various genetic backgrounds) were placed on moistened Whatman filter paper and subjected to stratification in darkness at 4 °C for two days. Post-stratification, the grains were germinated at room temperature (RT) for up to four days. The germinated seedlings were then transferred to plant germination pots (16 cm Ø) filled with soil. WT or *ZmUBI::Cas9* plants were directly

germinated in plant cultivation pots (13 cm Ø) filled with soil and incubated in a greenhouse at a constant temperature of 19 °C, with 65 % relative humidity and a light intensity of 160-250 $\mu\text{molm}^{-2}\text{s}^{-1}$. Five days prior BSMV infection, plants were transferred to a controlled growth chamber within the same biosafety facility, kept at 24.5 °C, 65% humidity, and 160-250 $\mu\text{molm}^{-2}\text{s}^{-1}$. Progeny of virus-infected plants was cultivated under identical conditions but at a slightly reduced temperature of 21 °C. Both *N. benthamiana* and barley plants were grown in soil made of homemade compost, substrate 2 (Klassmann-Deilmann GmbH), and sand in a 2:2:1 ratio and received a weekly 0.2 % Wuxal fertilizer supplement. Plantacote depot (4 m granulate; Hauert Manna) was applied once at the three-leaf stage and 1% Hakaphos blau fertilizer weekly post-transplantation. During the reproductive phase, 1% Hakaphos rot fertilizer was applied weekly.

3.1.4 Anther Collection for Pollen Nucleus Isolation

Mature anthers (yellow and plump) were isolated using forceps from 8- to 12-week-old barley plants and placed in sterile 2 ml Eppendorf tubes. The tubes with anthers were immediately flash-frozen using liquid nitrogen and stored at -70 °C.

3.2 Molecular Work

3.2.1 Nuclei Acid Extraction

3.2.1.1 DNA

200 mg of plant tissue was collected in a 2 ml microcentrifuge tube and flash-frozen with liquid nitrogen. The frozen tissue was then ground into a fine powder using a TissueLyser at 30 Hz for 2 minutes (Retsch). Subsequently, 800 μl of DNA extraction buffer (composed of 1 % of N-Lauryl-Sarcosin, 100 mM Tris (pH 8), 10 mM EDTA (pH 8) and 100 mM NaCl; autoclaved at 121 °C at 15 psi) was added, and the mixture was vortexed vigorously for 1 minute. Next, 800 μl of Phenol:Chloroform: Isoamyl alcohol (25:24:1) was added, followed by vigorous vortexing for 2 minutes. The suspension was centrifuged at 13,000 rpm for 3 minutes at RT. The top aqueous phase (500 μl) was carefully transferred to a nuclease-free 1.5 ml microcentrifuge tube. To the supernatant, 50 μl of 3M sodium acetate (pH 5.2) and 500 μl of isopropanol were added and mixed well. The mixture was then centrifuged at 13,000 rpm for 10 minutes at 4°C. The supernatant was carefully removed without disturbing the pellet, which was then washed with 1 ml of 70% ethanol. After removing the ethanol, the pellet was dried at 37°C for 1 hour. Finally, the pellet was resuspended in 100 μl of nuclease-free water.

3.2.1.2 RNA and cDNA synthesis

100 mg of plant tissue (leaf or immature anther) was collected in a 2 ml Eppendorf tube and flash-frozen using liquid nitrogen. The frozen tissue was ground into a fine powder using a TissueLyser at 30 Hz for 2 minutes (Retsch). Next, 1 ml of Trizol reagent (Ambion) and 200 µl of chloroform were added, and the mixture was vortexed well for 30 s and incubated for 10 minutes at RT. The suspension was then centrifuged at 11,000 rpm for 15 minutes at 4°C. The top aqueous phase was carefully transferred to a new 1.5 ml nuclease-free microcentrifuge tube. The supernatant was centrifuged again at 11,000 rpm for 10 minutes at 4°C. The resulting pellet, after removing the supernatant, was washed twice with 1 ml of 75% ethanol. After removing the ethanol, the pellet was dried for 30 minutes at RT. The dried pellet was resuspended in 100 µl of nuclease-free water and stored at -20°C. cDNA synthesis was performed employing the RevertAID H minus first strand kit using random hexaprimers (NEB) and barley anther RNAs.

3.2.2 Genotyping

To evaluate the zygosity of F1 hybrid B x GP seedlings, PCR-based genotyping (GoTaq® polymerase) together with agarose gel electrophoresis was employed. Insertion and deletion (InDel) polymorphisms were genotyped using qPCR with 1x PerfeCTa Multiplex qPCR ToughMix Reagent (Quantabio). For genotyping *recq4-1*, the Derived Cleaved Amplified Polymorphic Sequences (dCAPS) method was employed [157]. In brief, the PCR product was digested with PvuI-HF and analyzed on a 2.5% agarose gel. The primers were designed to introduce a restriction site within the WT amplicon: complete digestion indicated a WT genotype, partial digestion indicated a heterozygous genotype, and no digestion indicated a homozygous mutant. For genotyping mutants isolated through CRISPR-Cas9 (*recq4-2*), allele specific primers were used. Primers used in the section 2.2.2 and 2.23 are listed in Table S1.

3.2.3 PCR

3.2.3.1 Reverse Transcriptase (RT) PCR

BSMV-presence and *SpCas9* expression were analyzed using the One Taq one-step reverse transcriptase (RT)-PCR kit (NEB).

3.2.3.2 Touch-down PCR

To amplify target DNA sequences containing 5' and 3' overhangs, touch-down PCR was performed using Phusion™ High-Fidelity DNA Polymerase (Thermo Fisher) under the following conditions: initial polymerase activation at 98 °C, followed by 10 cycles of

denaturation at 98 °C for 10 s, annealing at 65 °C for 30 s with a stepwise temperature reduction of 0.7 °C per cycle, and extension at 72 °C for 30 s. This was followed by 30 cycles consisting of denaturation at 98 °C for 10 s, annealing at 60 °C for 30 s, and extension at 72 °C for 30 s. A final extension step was performed at 72 °C for 10 minutes.

3.3 Molecular Cloning

3.3.1 Plasmid DNA Transformation, Screening and Verification

4 µl of ligated/hybridized product was mixed with 50 µl of *Escherichia coli* competent cells and incubated on ice for 30 minutes. The mixture was heat-shocked at 42 °C in a water bath for 30 s without shaking, followed by a 2 minutes incubation on ice. After adding 950 µl of Liquid broth (LB) medium (0.1 w/v % of tryptone, 0.05 w/v % of yeast extract, 0.1 w/v % of NaCl dissolved in water; autoclaved at 121 °C at 15 psi), the mixture was incubated at 37 °C for 1 h at 500 rpm in a shaking incubator. The cells were pelleted by centrifugation at 6,000 rpm for 3 minutes, and the pellet was resuspended in 150 µl of LB medium. The bacterial suspension was then spread onto LB agar plates (LB medium with 0.15 w/v % of bacto agar) containing 50 µg/ml Kanamycin and incubated overnight at 37 °C. Positive colonies were identified by colony PCR to verify the presence of respective DNA fragments cloned into the respective plasmid. Verified positive colonies were then cultured overnight in LB medium at 37 °C at 500 rpm in a shaking incubator. Plasmid DNAs were isolated using the QIAprep Spin Miniprep Kit (Qiagen). The isolated plasmids were then confirmed by restriction digestion assay using BamHI (for all BSMV plasmids) and further validated by Sanger sequencing.

3.3.2 Generation of BSMV- γ -sg Plasmid for Expression of sgRNA

A 1065 bp custom sequence comprised of the BSMV- γ bCDS, the sgRNA scaffold sequence compatible with SpCas9, and the *ccdB* gene flanked on both sides by AarI restriction sites for sgRNA target sequence insertion was designed, synthesized (GENEWIZ) and cloned into the pCa-LIC γ b plasmid [149] downstream of the γ b ORF, replacing a 359 bp sequence flanking the ligation-independent cloning (LIC) site via HpaI/BamHI restriction sites, resulting in the BSMV- γ -sg plasmid that enables the expression of sgRNAs for BSMVIGE.

3.3.3 Cloning of sgRNA into BSMV- γ -sg Plasmid

To generate a double stranded (ds)DNA fragment for a selected sgRNA, an oligonucleotide pair according to Table S1 was synthesized (Eurofins). 10 µM of each oligonucleotide were

annealed using 5 U of T4 Polynucleotide Kinase in presence of 1X T4 DNA ligase buffer containing 1 mM ATP in a 30 µl reaction volume. Annealing was performed in a thermocycler: 37 °C for 1 hour, followed by 95 °C for 5 minutes, then a ramp down to 85 °C at a rate of -2 °C/s and a final ramp down to 25 °C at a rate of -0.1 °C/s. To clone the annealed dsDNA into BSMV- γ -sg, modified Golden Gate cloning [159] was employed. In brief, 50 ng of BSMV- γ -sg plasmid, 250 pg of dsDNA insert, 5 U of PaqCI enzyme (isoschizomer of AarI), 5 pmol of PaqCI activator, 200 U of T4 DNA ligase and 1X T4 DNA ligase buffer were mixed in a 20 µl reaction. The Golden Gate assembly was performed in a thermocycler: 10 cycles of 37 °C for 5 minutes, followed by 16 °C for 10 minutes, 37 °C for 15 minutes, and enzyme inactivation at 80 °C for 5 minutes. The mixture was transformed into DH α competent cells (NEB). Subsequent steps involved plasmid screening, isolation, and verification.

3.3.4 Cloning of gene fragment BSMV- γ bCDS Plasmid

The PCR-amplified DNA insert, containing 5' and 3' overhangs, was cloned into BSMV- γ bCDS [149] using LIC. 1 µg of BSMV- γ bCDS was digested in a 20 µl reaction containing 1X FastDigest buffer (Thermo Fischer) and 2 U of FastDigest ApaI (Thermo Fischer). The reaction was incubated at 37 °C for 1 hour, followed by heat inactivation at 75 °C for 10 minutes. The digested plasmid was purified using QIAquick® Nucleotide Removal Kit (Qiagen). To generate sticky ends via 3'→5' exonuclease activity of T4 DNA polymerase, a 10 µl reaction was assembled, containing 2.5 U of T4 DNA polymerase, 1x reaction buffer, 0.5 mM dNTPs (dTTP for the plasmid and dATP for the insert) and 0.1 pmol of DNA (digested plasmid and insert). The mixture was incubated at 22 °C for 10 minutes, followed by heat inactivation at 65 °C for 10 minutes. For the hybridization reaction, T4 DNA polymerase-treated plasmid and insert DNAs were mixed in a ratio of 1:10, incubated at 66 °C for 2 min in a heated water bath, and then cooled down at RT for 45 minutes in the presence of 0.5 µM of EDTA. The hybridized mixture was subsequently transformed into DH α competent cells.

3.4 Cytology – Male Meiotic Chromosome/Nuclei Preparations

Spikes (1-3 cm in length) were fixed in 3:1 solution (75% ethanol, 25% glacial acetic acid) for at least 24 hours. Under a stereomicroscope, spikes were dissected, and one anther per spikelet was squashed in a drop of acetocarmine on a slide, briefly heated, covered with a coverslip, and examined under a light microscope to determine the meiotic stage. The remaining two anthers from selected spikelets were either processed immediately or stored in freshly-prepared 3:1.

Male meiotic chromosomes were prepared as described by [160]. Anthers were macerated with forceps in a drop of acetocarmine solution. The preparation was gently heated by passing the slide 2-3 times above a flame (without boiling the stain), a coverslip was placed on top, and pressure was applied with a thumb between filter paper sheets. Chromosomes were then observed under a light microscope. Slides containing meiocytes at the desired stage were flash-frozen in liquid nitrogen. Coverslips were removed with a razor blade, and slides were immediately washed in an ethanol series (70, 85, 96%). DNA was counterstained with DAPI in Vectashield mounting media (1.5 µg/ml, Vector Laboratories). Images were captured using a Nikon Eclipse Ni-E microscope equipped with a Nikon DS-Qi2 camera and NIS-Elements-AR version 4.60 software (Nikon). The minimum chiasmata number (MCN) was scored from cells in which individual bivalents and univalents could be clearly distinguished.

Immunostaining was performed according [40]. Briefly, two anthers per slide were digested for 8 minutes in 25 µl of EM digestion mix (0.1 g cytohelicase, 0.25 g polyvinylpyrrolidone, and 0.375 g sucrose made up to 25 mL with MilliQ water) at 37 °C in a moist chamber, with mechanical disruption using a brass rod after 4 minutes. Spreading was performed using 17 µl of 1.5% Lipsol solution, followed by fixation with 17 µl of 4% paraformaldehyde. Primary antibodies were applied overnight at 4 °C, followed by secondary antibody incubation for 1 hr at 37 °C. The following antibodies and dilutions were used: primary (1:500): anti-ZYP1 [40], anti-ASY1 [40] and anti-SCEP3 (unpublished); secondary (1:500): Cy3 (JIR; Jackson Immuno Research), Cy5 (Abcam) and Alexa Fluor 488 (JIR). Finally, DAPI staining of DNA was performed prior microscopic analysis as described above.

3.5 *In silico* Methods

3.5.1 Oligonucleotide Design

Oligonucleotides including dual-labeled probes were designed using Primer3 [161]. Uniqueness of sequences was verified *in silico* using BLAST® [162].

3.5.2 SgRNA Design

sgRNAs with high target specificity and minimal off-target scores were selected using CRISPOR [163]. Following [164], at least two sgRNAs for each target were chosen based on their secondary structures, ensuring the presence of intact repeat duplexes and stem-loops. Structures were assessed using RNAfold [165].

3.5.3 Mutation Analysis

Mutations induced by CRISPR/Cas9 at the target sites were analyzed using the ICE Synthego tool employing generated Sanger sequencing reads [166].

3.5.4 Statistical Analysis

Statistical analysis was performed by comparing the means of recombination rate estimates from two distinct groups. The significance level, or p-value (set at 5%), was determined using Welch's unpaired t-test through the GraphPad Prism online tool [167].

3.5.5 RNAi-target design

To identify regions with potentially high-efficiency siRNA expression, cDNA sequences were analysed using si-Fi software with default parameters [168]. Regions predicted to generate a high number of siRNAs with minimal or no off-target effects were selected.

3.5.6 Plot Generation

Plots were generated using RStudio (version 4.3.3).

3.6 Multiplex Crystal digital (d)PCR-based single pollen nucleus genotyping (SPNG)

3.6.1 Pollen Nuclei Isolation

Frozen anther samples were thawed on ice for 5 minutes before adding 500 µl of ice-cold nuclei isolation buffer (45 mM MgCl₂, 20 mM MOPS, 30 mM sodium citrate, and 0.1% Triton X-100; pH 7.0; sterilized through 0.22 µm filtration). The anthers were then cut into at least three pieces using sterile scissors and vortexed vigorously for 2 minutes. The resulting pollen suspension was pipetted onto a 100 µm mesh filter (Celltrix, Sysmex-Partec) and placed over an empty 1.5 ml microcentrifuge tube containing two metal beads (3.5 mm Ø; Askubal). Pollen on the filter was gently ground with a micro pestle (Carl Roth) for 15 s, followed by flushing with 250 µl of nuclei isolation buffer. The suspension was then processed using either a tissue grinder (Retsch) at 30 Hz for 30 s and 1 minutes or sonicated using a Sonorex TK-30 with default settings (50 kHz) for 1 and 3 minutes followed by filtering through a 20 µm mesh filter (Celltrix, Sysmex-Partec) placed on an empty 5 ml polystyrene sample tube. Any intact pollen remaining was disrupted by gently grinding with a micropestle on the filter for 15 s. The filter was flushed with 250 µl of nuclei isolation buffer, with grinding and flushing repeated as needed. The nuclei

suspension was stained with 50 µg/ml of propidium iodide (PI; Thermo Fisher), gently mixed with a sterile pipette, and incubated on ice for 30 minutes before flow sorting. To isolate pollen nuclei from fresh anthers, the same procedure was followed, except thawing and bead-beating were omitted. All steps were performed on ice to preserve sample integrity.

3.6.2 Flow Sorting of Pollen Nuclei

The BD Influx™ Cell Sorter (BD Biosciences) was calibrated according to the manufacturer's instructions, using 0.5x phosphate-buffered saline (PBS) (10x PBS: 1.37 M NaCl, 27 mM KCl, 80 mM Na₂HPO₄, 15 mM KH₂PO₄; pH 7.4) as sheath fluid. A 5 ml polystyrene sample tube containing the nuclei suspension was placed in the cell sorter's sample holder, and the sample was processed at a rate of 200 to 1,000 events per second. The thresholds for PI fluorescence (e.g., 575/40 log scale), the gain for forward scatter (FSC) and side scatter (SSC) as well as the PI fluorescence (610/40) detectors, were adjusted to ensure that the nuclear populations were displayed within the instrument's dynamic range. A region encompassing the haploid pollen nuclei populations was defined on the dot plot of PI fluorescence versus FSC/SSC and displayed in a histogram of PI fluorescence (610/40). A sort gate was established within the PI fluorescence histogram. The appropriate sort device and mode (e.g., '1.0 Drop Pure') were selected, and a 1.5 ml microcentrifuge tube containing 23.5 µl of the Crystal dPCR mix containing 1x Buffer A - naica® multiplex PCR MIX, 3% Buffer B - naica® multiplex PCR MIX and oligonucleotides at their optimal concentrations (Table S2) was placed in a preselected position on the sort device. The target number of nuclei to be sorted was specified, and the sorting process was initiated. After sorting, the collection tube was briefly centrifuged using a mini centrifuge and stored on ice.

3.6.3 Loading and Scanning of Naica™ Sapphire Chips

Before sorting, the Naica™ Geode (Stilla Technologies) was activated, ensuring pressure at 1200 ± 50 mbar. A Naica™ Sapphire chip (Stilla Technologies) was placed on tissue wipes pre-sprayed with an anti-static spray (Screen Clean; AF International) inside a petri dish. Subsequently, 25 µl of the master mix containing a given number of sorted nuclei was carefully loaded into each inlet over the oil phase, avoiding tip insertion into the oil phase to prevent air bubble formation. After sealing, the chips were positioned on the thermal plate of the Naica™ Geode and subjected to the following cycling program: sample partitioning at 40 °C, an initial denaturation at 95 °C for 3 minutes, followed by 45 cycles of 95 °C for 15 s and 58 °C for 30 s, concluding with a final pressure release step. The Naica™ Sapphire template, designed for

the Naica® multiplex PCR Mix provided by Stilla™ Technologies, was loaded into the Crystal Reader application on the Naica™ Prism6 instrument (Stilla Technologies). All necessary parameters for scanning the chips were set, including the experiment name, Chip Unique Identifier, chamber details, fluorophore names, and target names. The exposure times for the fluorescence detection channels were set as follows: Blue at 100 ms, Teal at 350 ms, Green at 100 ms, Yellow at 125 ms, Red at 500 ms, and Infra-red at 500 ms. After dPCR completion, the Naica™ Sapphire chips were gently cleaned with wet tissue wipes (Kim-tech Science), sprayed with anti-static spray and then loaded into the Naica™ Prism6 instrument for scanning.

3.6.4 Recombination Rate Analysis

The Naica crystal compensation matrix was loaded into the Crystal Miner application 3.1.6.3. Non-analyzable droplets, typically due to air bubbles, were excluded using the polygon tool. Fluorescence spillover compensation coefficients were manually adjusted to ensure positive clusters of marker pairs for each locus aligned perpendicularly. The analysis configuration setup, created using the population editor tool, which quantifies combinations of pollen nuclei genotypes (including non-recombinants and recombinants) (Table S3), was loaded. Two approaches (three-color and two-color) were developed to detect pollen nuclei genotypes. In the three-color approach, only droplets positive for all three colors were selected, while in the two-color approach, droplets with any two colors corresponding to a single interval were chosen for recombination rate analysis. The threshold for each fluorescence channel was set in the 1D plot at 2,000 fluorescence units above the cluster representing negative droplets (Fig. 3a). Droplets slightly above the negative cluster of a given fluorescence channel but separated from the positive clusters due to improper spillover compensation were considered negative. To ensure balanced genotyping calls between marker pairs (Blue versus Red, Teal versus Yellow, and Green versus Infrared channels), the fluorescence threshold of the channel with the higher genotyping calls was increased in the 1D plot until a balanced call rate was achieved (Fig. 3b).

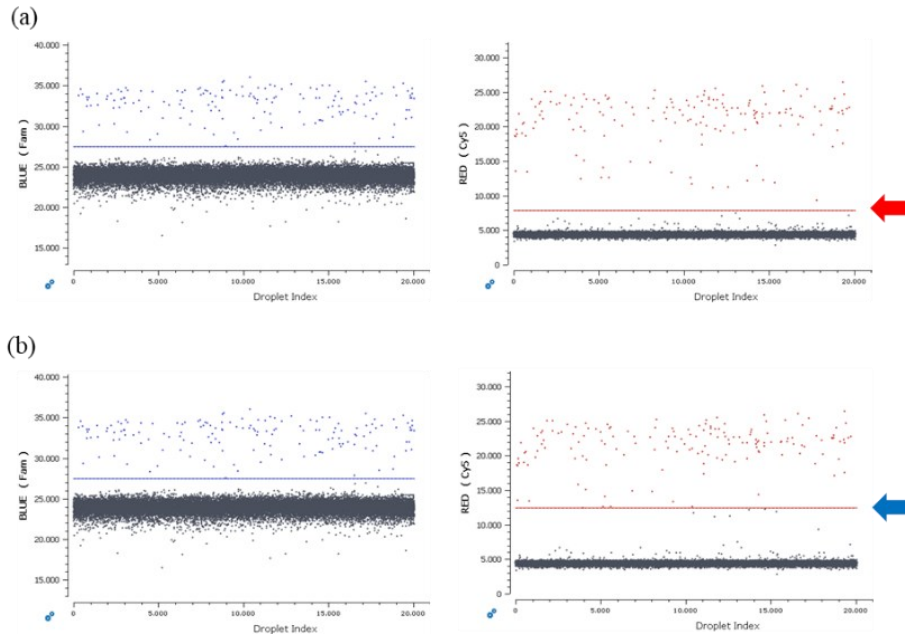


Figure 3: Analysis of male meiotic recombination rate using Naica™ Crystal Miner software.

2D plots for each fluorescence channel: BLUE and RED representing pollen nuclei genotyped positive for marker pair at a locus representing Fam and Cy5 fluorophores. **(a)** Fluorescence thresholds (blue or red line) set around 2000 units above the negative droplets' population (droplets in grey color). Red and blue arrows indicate the threshold baseline for the RED channel before **(a)** and after **(b)** normalization. After estimating the number of positive droplets for all possible genotypes (non-recombinant and recombinants) upon normalization of three selected marker pairs of given chromosomes, the meiotic recombination rate is estimated using the formula shown in **(c)** for each genetic interval.

This normalization of genotyping calls among non-recombinants and recombinants allowed for the calculation of the recombination rate and the CO interference strength for each chamber, based on estimations of positive calls for non-recombinant and recombinant populations.

$$\text{Meiotic recombination rate (cM)} = \left(\frac{\text{Total recombinants}}{\text{(Total non-recombinants + Total recombinants)}} \right) * 100$$

$$\text{CO interference strength} = 1 - \left(\frac{\text{Actual double recombinant frequency}}{\text{Expected double recombinant frequency}} \right)$$

3.7 BSMV Infection Methods

3.7.1 Agrobacterium-Mediated Infection of *N. benthamiana* with BSMV

50 ng of each plasmid (BSMV- α , BSMV- β , and BSMV- γ -sgTarget) were introduced individually into *Agrobacterium tumefaciens* strain AGL1 via electroporation as follows: a single pulse of 2.2 kV, 100 Ω , and 25 μ F for approximately 2.6 ms. Transformed bacteria were resuspended in 950 μ l of YEB medium (0.05% w/v meat extract, 0.05% w/v tryptone, 0.05% w/v sucrose, 0.01% w/v yeast, 250 mM autoclaved MgSO₄, pH 7.2) and incubated at 28 °C for 2 hours with shaking at 500 rpm. 1 ml inoculum was then cultured in 25 ml of YEB medium supplemented with 50 μ g/ml Kanamycin and Rifampicin at 28 °C for 20 hours with shaking at 200 rpm. Following centrifugation at 3,500 rpm for 30 minutes at 4 °C, the resulting pellets were resuspended in freshly prepared infiltration buffer (composed of autoclaved 10 mM MES (2-(N-morpholino) ethanesulfonic acid) and 33.3 mM MgCl₂, pH 5.6) and the optical density was adjusted to approximately 1.2 at 600 nm. For singleplex BSMV-Induced Genome Editing (BSMVIGE), an equal mixture of *Agrobacterium* cultures containing BSMV- α , BSMV- β , and BSMV- γ -sgTarget-1 was used. For multiplex BSMVIGE with a mixed *Agrobacterium* pool (MEA), *Agrobacterium* cultures containing BSMV- α , BSMV- β , BSMV- γ -sgTarget-1, and BSMV- γ -sgTarget-2 plasmids were combined in a ratio of 1:1:0.5:0.5. *Agrobacterium* mixtures were infiltrated into leaves of 21-day-old *N. benthamiana* plants using a 1 ml needleless syringe.

3.7.2 *In vitro*-BSMV Transcript Preparation

Alternatively, *in vitro*-transcribed BSMV RNAs were used to directly infect barley plants, eliminating the need for tobacco virus sap preparation. To do so, BSMV-specific primers (Table S1) with an upstream T7 promoter sequence at the 5' end were designed to amplify BSMV segments (α , β , and γ b-CDS) using Ex Taq® Hot Start polymerase (TaKaRa). The amplification reaction was performed with 100 ng of BSMV- α , BSMV- β , and BSMV- γ b-CDS as template DNA, following the manufacturer's protocol. The resulting amplicons served as templates for an *in vitro* transcription to generate 5'-capped BSMV RNAs. This was achieved using the HiScribe T7 High Yield RNA Synthesis Kit (NEB) in the presence of m⁷G(5')ppp(5')G RNA Cap Structure Analog (NEB), with 1 μ g of purified PCR amplicon as the starting material, according to the manufacturer's instructions. For BSMV RNA inoculation, 0.05 μ g of each BSMV RNA was mixed in 10 mM phosphate buffer supplemented with 0.5% Celite 545 and 0.5% silicon carbide, and kept on ice until application.

3.8 BSMV Inoculation in Barley

To obtain virus sap, systemic leaves (8-10 leaves) with virus symptoms were harvested from infiltrated tobacco plants 10-12 days post-inoculation (dpi). These were ground on ice in 2 ml of 10 mM phosphate buffer (6.15 mM dipotassium phosphate, 3.85 mM monopotassium phosphate, 0.5% celite 545 (Carl Roth), 0.5 % silicon carbide (400 mesh particle size, Sigma-Aldrich), pH 7.0). The tobacco virus sap (only fresh saps were used) or BSMV RNA inoculum (can be stored at -20 °C) was used to inoculate 3- to 4-week-old barley plants by finger-rub inoculation on the fully-emerged second and third leaves.

4 Results

4.1 Multiplex Crystal Digital (d)PCR-based Single Pollen Nucleus Genotyping (Multiplex SPNG) in Barley: Male Meiotic Recombination Measurements

4.1.1 Storage of Barley Anthers for Multiplex SPNG

Assessment of male meiotic recombination rates using multiplex SPNG requires fresh barley anther material to be processed immediately [104]. This limits the simultaneous evaluation of pollen samples from plants flowering at different time points or from diverse geographic locations. To overcome this limitation, a rapid anther storage method was tested using cv. B anthers as a benchmark. This method involves flash-freezing of 80-100 anthers isolated from two or three spikes using liquid nitrogen, followed by long-term storage at -70°C .

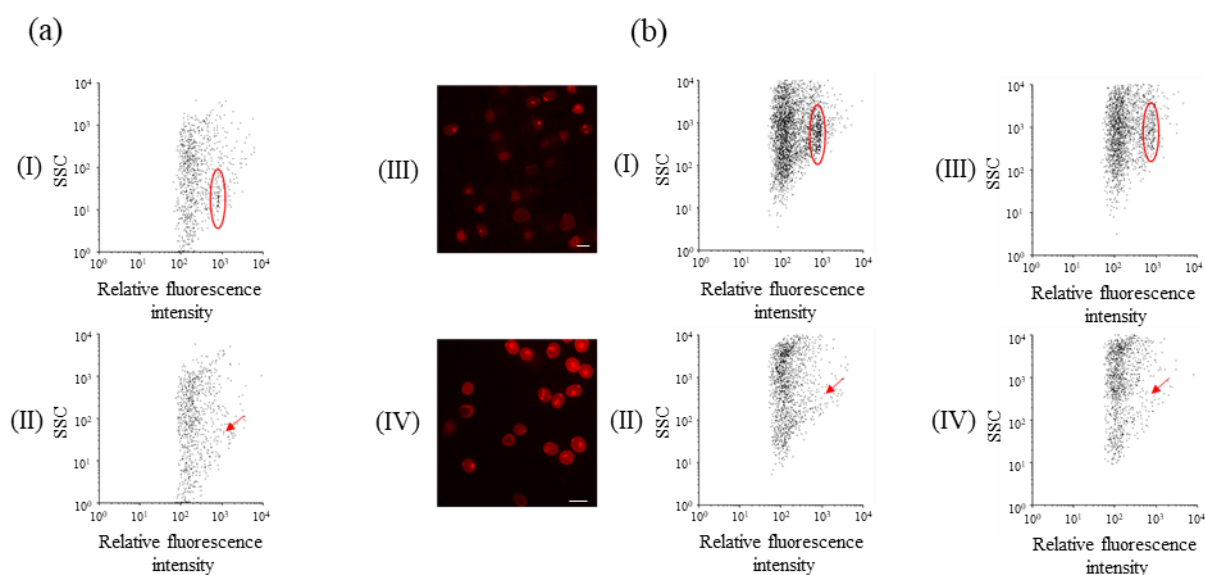


Figure 4: Efficacy of different pollen treatment strategies on pollen nuclei isolation.

(a) Flow cytometric analysis of pollen nuclei isolated from fresh (aI) and flash-frozen stored (aII) anthers without employing any pollen treatment strategy. Representative microscopic images of $20\ \mu\text{m}$ filter after passing the pollen suspension isolated from fresh anthers (aIII) and stored anthers (aIV). PI was used for staining of pollen nuclei (Scale bar = $20\ \mu\text{m}$). **(b)** Flow cytometric analysis of pollen nuclei isolated from stored anthers based on different pollen treatment strategies: Bead beating using TissueLyser at $30\ \text{Hz/s}$ for 1 minutes (bI) and at $30\ \text{Hz/s}$ for 30 sec (bIII); sonication for 1 min (bII) and for 3 minutes (bIV). A distinct haploid pollen nuclei population indicated using the red circle whereas the red arrow indicates the absence of such a distinct population at the expected position when plotting the side scatter parameter (Y-axis) against relative fluorescence intensity (X-axis).

Initially, the feasibility of isolating pollen nuclei from stored barley anthers using the conventional filter-bursting method with Galbraith buffer [169, 170] was tested. Flow cytometry analysis was performed on pollen nuclei suspensions isolated from fresh anthers as a positive control. Unlike fresh anthers, a distinct haploid nuclei population was not observed in suspensions from stored anther material (Fig. 4a). To find out whether the pollen (nuclei) were lost during the isolation procedure, 20 μm filters, which were used for isolating pollen from macerated anthers, were examined. A large number of intact pollen grains remained on the 20 μm filter compared to fresh anthers, indicating that storage affected the ability of pollen to burst readily via the filter-bursting method (Fig. 4a).

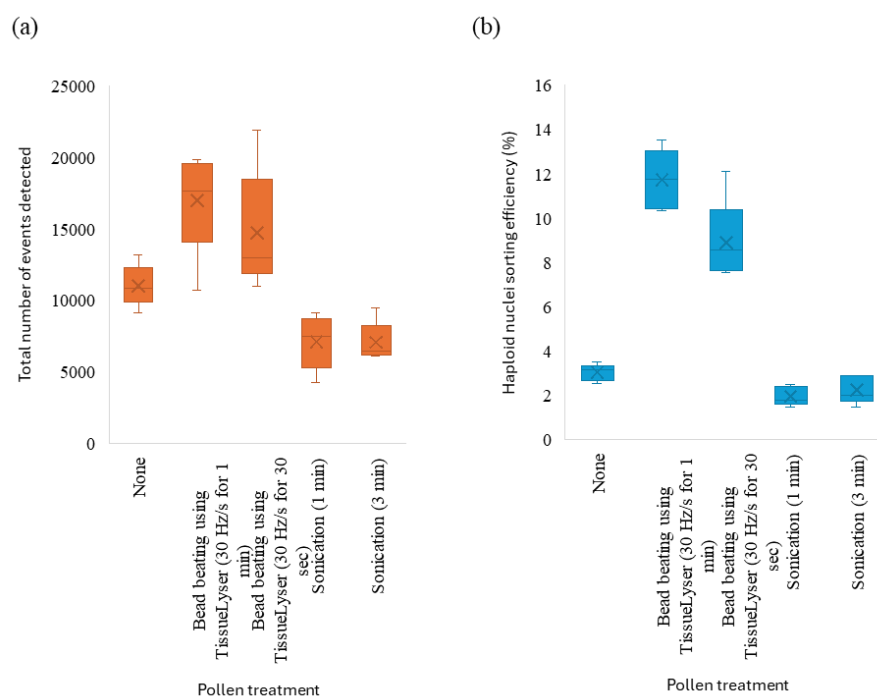


Figure 5: Pollen treatment strategies for efficient isolation of barley pollen nuclei.

(a) Total number of events detected within the selected sorting gate for each pollen treatment (n, replicates for each treatment = 5). **(b)** Haploid pollen nuclei sorting efficiency (the percentage of haploid nuclei sorted from the total number of events detected within a 2 minutes sorting window) for each pollen treatment (n = 5).

To improve the isolation of pollen nuclei from frozen anthers, mechanical disruption of the pollen wall was tested. This was achieved by beating the pollen suspension with metal beads using a TissueLyser or by sonication. Bead-beating at 30 Hz/s for 1 minute using a TissueLyser yielded the highest efficiency in isolating haploid pollen nuclei, compared to bead-beating at

30 Hz/s for 30 s, sonication for one or three minutes, or no treatment. Flow cytometry analysis of pollen suspensions revealed the total number of events (an event is defined as a single particle detected during flow cytometry analysis) generated was higher with bead-beating at 30 Hz for 1 minute compared with all other treatments (Fig. 4b; Fig. 5; Table S4). Pollen nuclei suspensions isolated from anthers stored for up to 12 months yielded nuclei populations that were suitable for flow sorting. Thus, stored barley anthers can be effectively used for pollen nuclei isolation and flow sorting, facilitating the analysis of male meiotic recombination rates from plants grown at different time points and locations.

4.1.2 Marker Selection and Validation for Multiplex SPNG

The development of a SPNG method using three-color Crystal dPCR (Naica®, Stilla Technologies®) (Madic et al., 2016) enables the measurement of male CO rates within a single chromosomal interval in a hybrid barley cv. Morex x Barke pollen nucleus [104]. However, it does not allow for the simultaneous measurement of multiple genetic intervals and it depends on fresh pollen samples, leading to low-throughput CO rate analysis. Furthermore, no standard genetic transformation procedures are available for barley cv. Morex, which limits the application of CO rate analysis in these hybrid materials. The latest six-color Crystal dPCR system (Naica®, Stilla Technologies®), utilizing the prism6, can simultaneously read up to six different fluorescence light channels [171]. This technological advancement makes it theoretically possible to measure CO rates across multiple chromosomal intervals within a single pollen nucleus using the six-color Crystal dPCR system. To leverage this potential, barley cultivars B and GP were chosen. This selection was based on the availability of a TILLING population in B [156] and established genetic transformation in GP [127]. A dataset of genome-wide structural variations (SVs), consisting of InDel polymorphisms from 4,000 barley accessions called against the Morex V3 genome assembly provided by Dr. Murukarthick at IPK, Gatersleben, was utilized [172]. From this dataset, 85,547 InDels were identified between B and GP. Six genomic loci, labelled ‘a’ to ‘f’, containing distinct InDel polymorphisms differentiating B and GP on chromosome 1 were selected (Table S5). The loci ‘a’ to ‘d’ are located on the short arm of chromosome 1, while loci ‘e’ and ‘f’ are on the long arm. To genotype these InDel polymorphisms, six allele-specific fluorescent oligonucleotide probe pairs were designed, along with oligonucleotides to amplify short amplicons containing these polymorphisms (Table S2). To verify the efficacy of the designed oligonucleotides for genotyping the selected markers, dPCR genotyping was performed for individual markers. This analysis used a mixture of 3,000 non-recombinant nuclei (comprising 1,500 B and 1,500 GP

nuclei) as the template for the positive control, along with a non-template control (dH₂O). This approach allowed for the assessment of marker specificity. The results indicated that all markers, except for ‘a’ and ‘e,’ were successfully genotyped for both B and GP alleles.

4.1.3 Six-color Crystal dPCR: Multiplex Male Meiotic Recombination Rate Assessment

A two-plex dPCR assay, as described by [104], employs oligonucleotides specific to a single parent at two loci, both labelled with the same fluorophore (Fig. 6a). This setup enables the estimation of CO rates within a single interval by analyzing the three distinct positive clusters formed after successful SPNG, representing two non-recombinant clusters and one recombinant cluster (Fig. 6b).

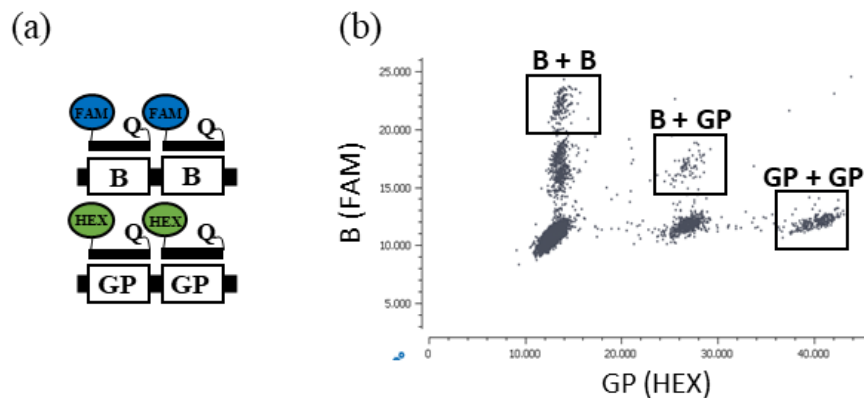


Figure 6: Two-plex assay for detecting CO events in pollen nuclei.

(a) Design of two-color allele-specific oligonucleotides, with FAM-tagged probes indicating B-alleles and HEX-tagged probes indicating GP-alleles at two loci. (b) Example plot illustrating positive clusters that readily distinguish non-recombinant and recombinant genotypes (highlighted in box).

To achieve multiplex CO rate measurements, i.e. measuring CO rate within more than one interval in a given pollen nucleus, simultaneously, a three-plex assay utilizing a six-color multiplex approach was established. It allows for the simultaneous quantification of CO rates within two genetic intervals. Three markers (b, d and f) defining two independent genetic intervals (1bd and 1df) were selected for further analysis. These intervals span the chromosomal regions between the markers b and d or d and f, respectively. Interval 1bd is located at the distal end of the chromosome, while interval 1df encompasses (peri)centromeric regions across both arms of chromosome 1 (Fig. 7a). In contrast to the two-plex assay, the three-plex assay employs allele-specific oligonucleotides labelled with distinct fluorophores, as recommended by Stilla Technologies, for each allele (Fig. 7b; Table S2).

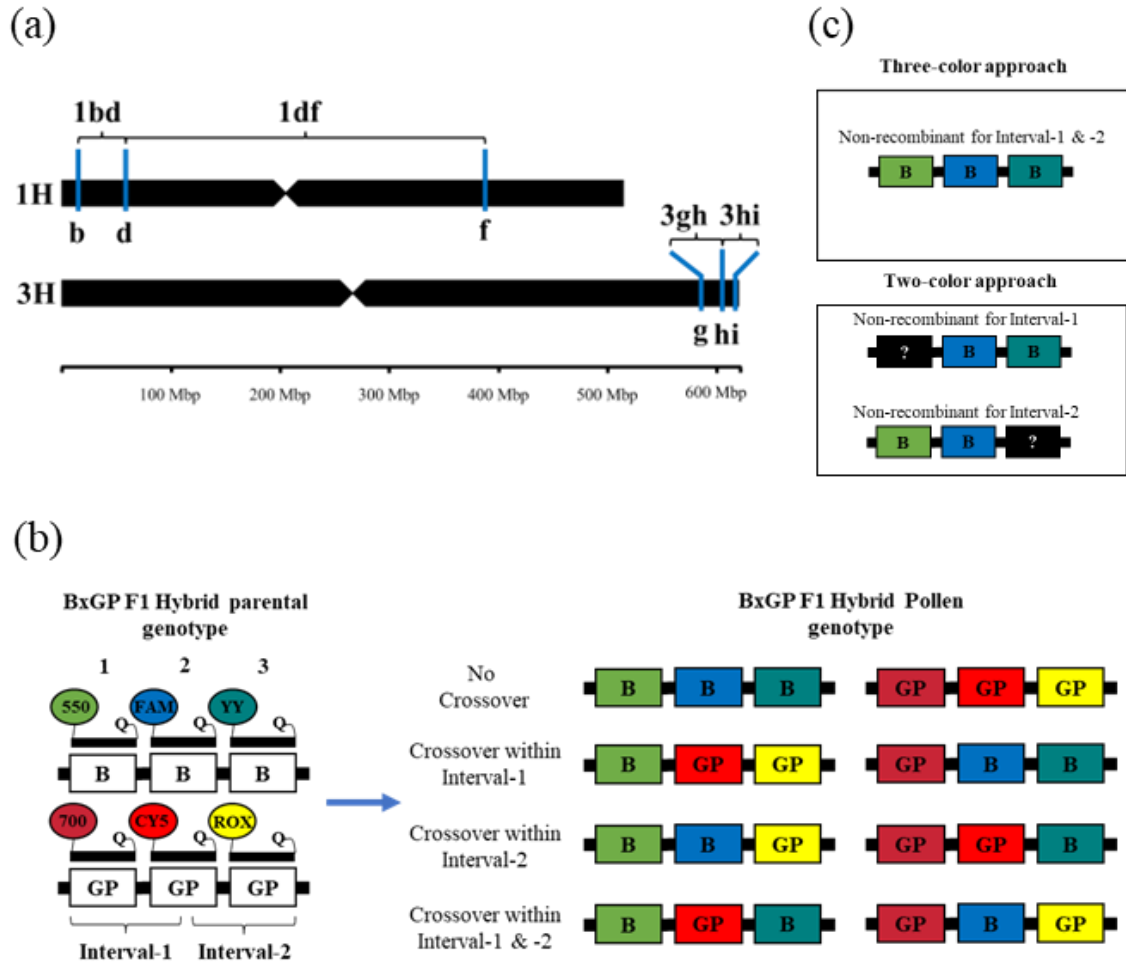


Figure 7: Multiplex SPNG setup for male CO rate measurement in hybrid barley pollen nuclei.

(a) Chromosomal genetic interval setup for multiplex SPNG. Three loci per chromosome form two linked genetic intervals on chromosomes 1 and 3 of barley, respectively. The physical distance is based on the Morex V3 genome assembly. (b) Schematic depiction of haploid pollen nuclei genotypes based on multiplex Crystal dPCR. TaqMan probes with six different fluorophores (oval) designed for six selected polymorphisms at three loci forming two linked genetic intervals on chromosomes of Barke (B) and Golden Promise (GP). Haploid pollen nuclei genotypes are assessed based on the presence of different combinations of fluorescence developed within a droplet upon successful genotyping of the given pollen nucleus. (c) In the three-color approach (top), only droplets positive for three colors were selected while in the two-color approach (bottom), droplets with any two-color corresponding to a single interval were selected for recombination rate analysis using Crystal dPCR.

Two different approaches (three- or two-color approach) for estimating the recombinant and non-recombinant populations were established. In the three-color approach, only droplets positive for three colors were selected, while in the two-color approach, droplets with any two

colors corresponding to a single interval were selected for recombination rate analysis (Fig. 7c). The feasibility of this six-plex setup in genotyping both non-recombinant and recombinant pollen nuclei was then explored. For this purpose, two samples were used: a mixture of 3,000 non-recombinant nuclei (1,500 B and 1,500 GP) and 3,000 B x GP F1 hybrid pollen nuclei. A semi-automated analysis pipeline (see Materials and Methods 3.6.4) was developed to estimate all possible genotype combinations, including both non-recombinant and recombinant populations (Fig. 7b). In the non-recombinant nuclei mixture, only positive populations for non-recombinants were observed. In contrast, for the F1 hybrid nuclei, both non-recombinant and recombinant positive populations were detected. This confirmed the ability of the six-plex assay to detect recombined pollen nuclei. Subsequently, three small-scale InDel polymorphisms (3g, 3h, and 3i) between barley cultivars B and GP, defining two genetically linked chromosomal intervals on chromosome 3, were selected (Fig. 7a). A similar six-plex crystal dPCR assay to that used for chromosome 1 was established for chromosome 3. The efficacy of this chromosome 3 six-plex setup in distinguishing non-recombinant and recombinant nuclei populations was confirmed using B x GP F1 and non-recombinant pollen nuclei suspensions.

According to the genomic zone classification described by [173]: zone 1 is highly recombinogenic, zone 2 has low recombinogenic activity, and zone 3 exhibits very limited recombinogenic activity. The interval 1bd spans the entire zone 1 and a small portion of zone 2 on the short arm of chromosome 1. In contrast, the interval 1df, which flanks the (peri)centromeric region of chromosome 1, covers large portions of zones 2 and 3. These intervals span physical distances of approximately 39.6 Mbp and 331.3 Mbp, respectively. The 1bf interval encompasses the chromosomal segment from marker b to marker f. Intervals 3gh and 3hi are subtelomeric on the long arm of chromosome 3, each covering a small portion of zone 2 and spanning physical distances of approximately 19.4 Mbp and 12.6 Mbp, respectively. The interval 3gi extends from marker g to marker i (Table S5).

4.1.4 Optimizing the novel Crystal dPCR Setup for Enhanced SPNG in Barley

To validate the specificity of the individual probes for their respective targets (InDels), a chromosome-specific multiplex SPNG was performed. This assay utilized all six probe and primer sets with 4,000 pollen nuclei isolated from either B or GP as templates.

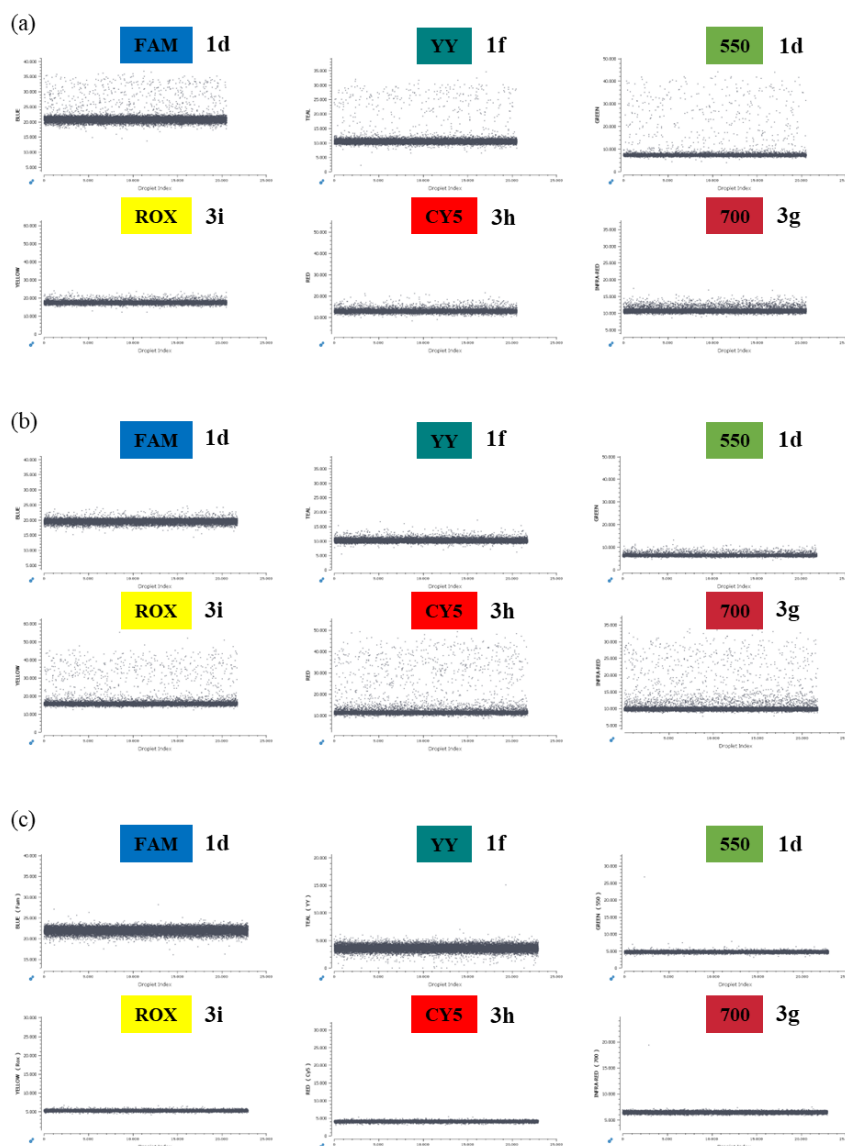


Figure 8: Specificity of the designed TaqMan probes for six selected markers on chromosome 1. 1D amplification plots display all six fluorescence channels of the dPCR assays conducted using nuclei templates from Barke (a), Golden Promise (b), or beads (c). The fluorescence channels (box) and their corresponding locus are indicated.

As a non-template control (NTC), 4,000 beads were sorted from a standard 500 μ l F1 B x GP pollen suspension containing one drop of bead solution (SPHERO™ 6.1 μ m rainbow calibration particles, Spherotech).

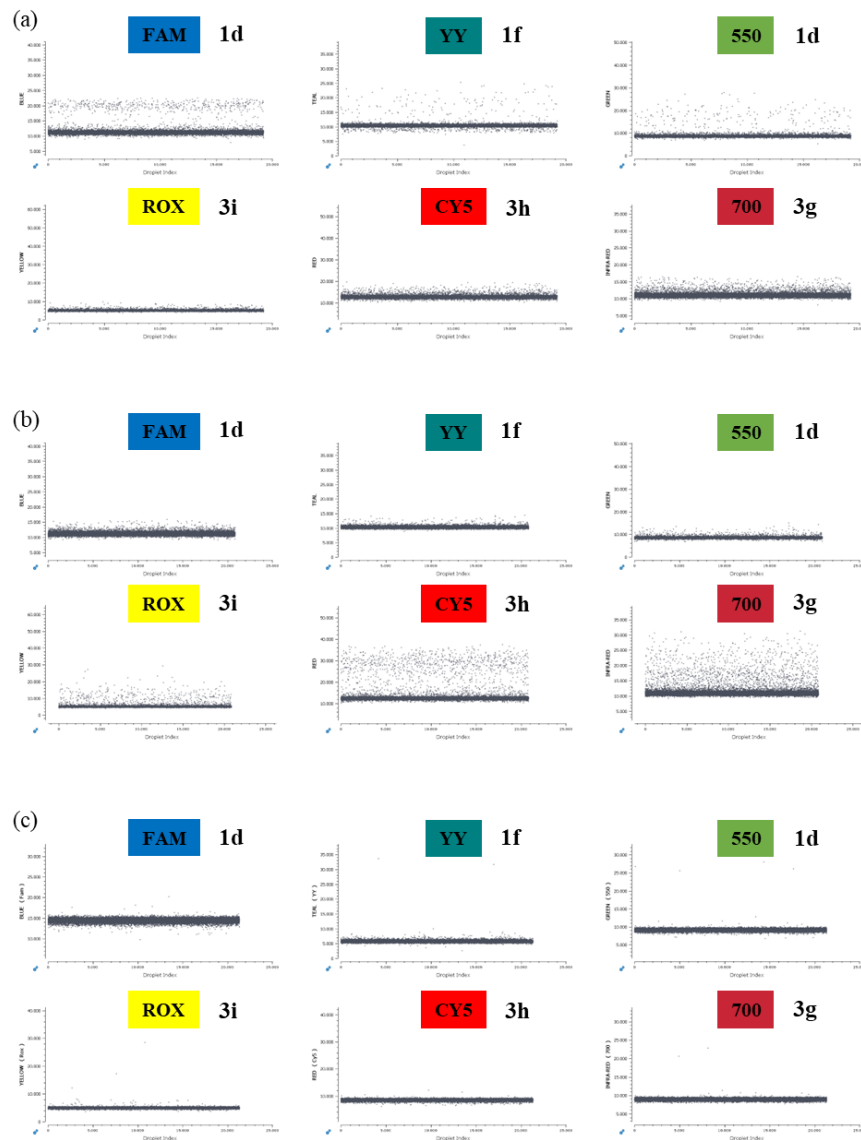


Figure 9: Specificity of the designed TaqMan probes for six selected markers on chromosome 3.

1D amplification plots display all six fluorescence channels of the dPCR assays conducted using nuclei templates from Barke (a), Golden Promise (b), or beads (c). The fluorescence channels (box) and their corresponding locus are indicated.

The NTC served to identify any encapsulation of DNA fragments within droplets, which could lead to false-positive genotyping calls. The results showed that only markers corresponding to B or GP were successfully genotyped with the respective template nuclei from B or GP for both chromosomes 1 and 3. For the NTC, no false-positive droplets were detected across all combinations, except for markers B-allele specific to loci d and h, as well as GP-allele specific to h and i, where up to five false positives were detected (Fig. 8 and 9). Together, the designed markers were successfully genotyped using barley pollen nuclei as a template, demonstrating

their effectiveness for setting up multiplex Crystal dPCR for measuring meiotic recombination in the chosen barley hybrid.

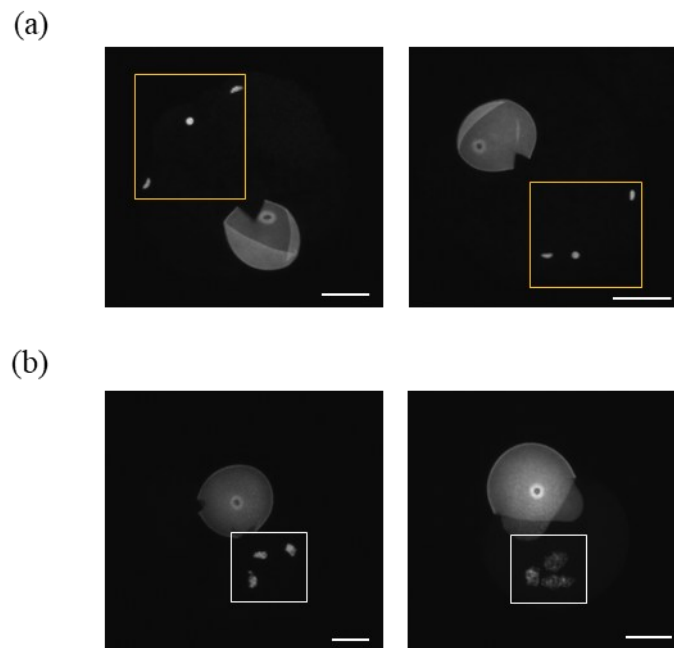


Figure 10: Pollen nuclei morphology after bursting.

Microscopic images of pollen nuclei from freshly isolated (a) and stored (a) anthers of Barley cv. GP after bursting (Scale bar = 10 μm).

To evaluate the feasibility of using six-color Crystal dPCR to measure male meiotic recombination rates within the selected linked genetic intervals on chromosomes 1 and 3 in barley B x GP hybrid pollen nuclei, chromosome-specific multiplex Crystal dPCR assays were conducted. The assay setup (referred hereafter as ‘multiplex SPNG’) was modified from a previous study [104] in two ways:

- 1) The input number of haploid nuclei was increased from 3,000 to 4,000 per chamber to enhance the total number of genotyping calls per chamber. This adjustment was made considering that the frequency of double nuclei encapsulation increases only minimally with the higher input [104]. It was observed that PCR efficiency, in terms of fluorescence intensity, is negatively impacted by an increased volume of PBS buffer (used as a sheath buffer for flow sorting) sorted along with the increasing nuclei number in the dPCR mix. To accommodate the increased number of pollen nuclei in a relatively low volume of 0.5x PBS buffer, a narrower nozzle (70 μm) for flow-sorting was used, compared to the 86 μm nozzle employed in the earlier study [104].

2) Pollen nuclei from stored anthers exhibited varying degrees of compaction compared to those from freshly isolated anthers, as observed through visual inspection following pollen bursting during the nuclei isolation procedure (Fig. 10). This suggests that pollen nuclei from stored anthers may already have increased accessibility to Taq polymerase. However, the presence of TaqI restriction sites within amplicons inhibited the employment of an enzymatic treatment of nuclei during encapsulation/dPCR to enhance genotyping efficiency [104].

4.1.5 Assessing Male Meiotic Recombination Rates Using Multiplex SPNG in Barley Hybrid Pollen Nuclei

To reduce the potential variability in meiotic recombination rates caused by differences between individual plants and spikes, pollen nuclei were extracted from pooled anthers isolated from 12 individual spikes of six independent F1 plants (two spikes per plant) grown in a greenhouse. Subsequently, chromosome-specific multiplex SPNG assays were conducted using 4,000 haploid pollen nuclei as template per reaction for three independent pooled plant populations. The recombination rate within selected intervals of chromosomes 1 and 3 was estimated across 15 and 18 chambers, respectively, for three biological replicates using both three-color and two-color approaches. The average three-color genotyping call (total number of positive droplets comprising non-recombinants and recombinants after normalization) per chamber was 130.67 ± 76.85 and 105.41 ± 78.12 for chromosomes 1 and 3, respectively (Fig. 11a; Table S6). A higher average genotyping call rate per chamber was achieved with the two-color approach: 172.8 ± 101 for 1bd, 203.67 ± 113.53 for 1df, 197.33 ± 103.83 for 1bf, 149.71 ± 99.56 for 3gh, 195.24 ± 144.68 for 3hi, and 146.47 ± 106.46 for 3gi (Fig. 11a; Table S7). Substantial variation in genotyping calls between chambers was observed in all intervals measured. This is likely attributed to several factors, such as the inclusion of chambers with improper droplet formation for analysis, which usually results in comparatively low genotyping calls as well as the variability in dPCR efficiency, random noise due to the small sample size, or inconsistencies in the quality of pollen nuclei samples across different chambers and experiments.

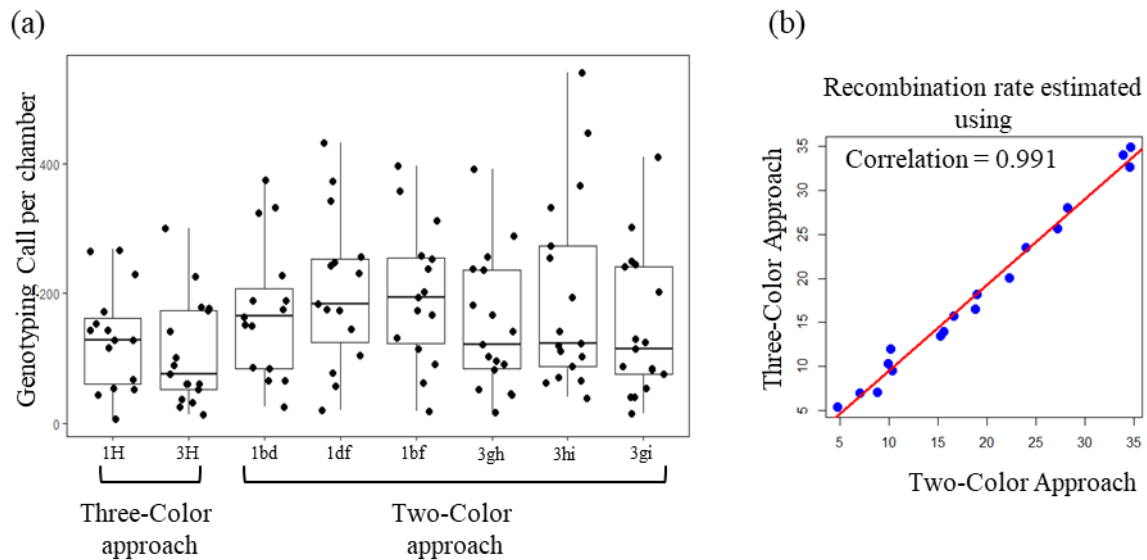


Figure 11: Comparison of three- and two-color approaches for estimating CO rate in barley.

(a) Total genotyping call per chamber obtained across all experiments performed using WT F1 B x GP pollen isolations, plotted for all selected genetic intervals on chromosomes 1 and 3, based on three-color, or two-color approaches. (b) Correlation plot of estimated recombination rates from both three- and two-color approaches, showing a Spearman correlation coefficient of 0.991 for estimated recombination rates within six-tested genetic intervals in three biological replicates of WT F1 B x GP.

Importantly, the average recombination rates measured within the six intervals using these two methods were similar: 14.18 ± 0.99 or 15.74 ± 0.57 cM for 1bd; 6.43 ± 0.74 or 6.84 ± 1.65 cM for 1df; 17.96 ± 1.45 or 19.46 ± 1.56 cM for 1bf; 26.12 ± 1.85 or 26.92 ± 1.81 cM for 3gh; 10.38 ± 1.01 or 10.18 ± 0.17 cM for 3hi; and 34.04 ± 0.92 or 34.42 ± 0.33 cM for 3gi (Table S6 and S7). A significant correlation (Spearman's rank correlation coefficient of 0.9917) was found between recombination rates acquired by the three- and two-color approaches (Fig. 11b). As expected, 1bd exhibited a higher recombination rate than 1df, located in low-recombinogenic zone 3. Among the 3H intervals located in zone 2 of chromosome 3, 3gh displayed a higher recombination rate than 3hi. A similar trend was found in sequencing data of hybrid barley populations derived from cultivars M x B [174] (Table S5).

4.1.6 Validating Male Meiotic Recombination Rate Measurements

To evaluate the influence of false-positive genotyping calls caused by droplets encapsulating more than one nucleus on the measured male meiotic recombination rates, PI-stained droplets were assessed. Those identified as recombinants and containing more than one nucleus were

manually excluded based on visual inspection of crystal images in the Crystal Miner application. Among five randomly selected chambers analyzed using the two-color approach, no significant differences were observed in the measured average recombination rates within genetic intervals 1bd, 1df, 1bf, 3gh, 3hi and 3gi before (16.12 ± 1.81 cM, 5.94 ± 2.9 cM, 20.19 ± 1.59 cM, 25.86 ± 2.86 cM, and 10.69 ± 0.59 cM, 36.02 ± 5.17 cM) and after correction (15.87 ± 1.88 cM, 5.78 ± 2.89 cM, 20.19 ± 1.59 cM, 25.42 ± 2.08 cM, 10.29 ± 0.79 cM, and 35.94 ± 4.69 cM) (Table S8). Given the minimal impact of false-positive on measured recombination rates across all selected intervals, and considering that the manual removal of these false-positive droplets is time-consuming due to differences in fluorescence detection filters between the prism6 and prism3 instruments, no further manual removal of these false-positives was conducted throughout the study.

To validate the male meiotic recombination rate measurements obtained for WT F1 hybrid B x GP barley pollen, qPCR-TaqMan™ genotyping of the selected markers along chromosomes 1 and 3 in segregating F2 offspring populations (obtained from 5 F1 B x GP hybrid plants) was performed and recombination rates within the selected genetic intervals were estimated. Within some tested intervals variation in recombination rates between pollen samples (male meiosis), utilizing either three- or two-color approaches, and offspring populations (male and female meiosis), determined based on marker segregation analysis, were observed. In the case of genetic intervals 1bd, 1df, and 3gh, slight variations in recombination rate measurements between pollen based on two-color approach and offspring were found. For example, in 1bd, the recombination rate observed was 15.74 cM in pollen vs 18.28 cM in offspring populations. Similarly, for 1df, the recombination rate varied between 6.84 cM in pollen and 4.57 cM in offspring, and for 3hi, it varied between 10.18 cM in pollen and 11.6 cM in offspring. However, within the genetic interval 3gh, a substantial difference in recombination rates was observed. In this case, the recombination rate varied between 26.92 cM in pollen and 18.23 cM in the offspring population. These observations indicate that in some selected intervals, variations in recombination rate between pollen and offspring populations are found. Unlike in pollen, recombination rate estimates in offspring are influenced by both male and female recombination rates, as well as selective processes affecting gamete viability, function, or competition, leading to post-meiotic distortion [175]. Therefore, variation in CO rates between pollen and offspring is expected. In summary, male meiotic recombination rates within two genetically linked chromosomal intervals in barley pollen nuclei populations can be measured using multiplex SPNG without being influenced by post-meiotic distortion.

4.1.7 CO Interference Strength within Selected Genetic Intervals in Barley Pollen Nuclei

The multiplex SPNG setup allows parallel genotyping of three loci forming two genetically linked intervals on chromosomes 1 and 3. Hence, the possibility to measure CO interference strength in pollen nuclei was explored. The two intervals on chromosome 1 span a physical distance of over 300 Mbp across the centromere, covering large regions of both chromosome arms, which typically receive at least one CO. Thus, negative CO interference, as commonly observed over large chromosome distances, including arms, was expected. In contrast, the two intervals on chromosome 3 are physically close and subterminal on one chromosome arm. Given their proximity, positive CO interference was anticipated [176].

Analysis of F1 B x GP WT hybrid pollen nuclei data using a modified six-color approach, that considers the droplets genotyped for all three selected loci along a given chromosome, revealed negative CO interference of -0.45 (1960 pollen nuclei analysed, 15 chambers) between the two linked intervals on chromosome 1, while strong positive CO interference of 0.55 (1792 pollen nuclei analysed, 18 chambers) was found for the two linked intervals on chromosome 3 (Table S6). Thus, multiplex SPNG enables a reliable assessment of male meiotic recombination rates (via two- and three-color approaches) and CO interference strength (via a modified three-color approach) within two linked chromosomal intervals in barley pollen nuclei.

4.1.8 Multiplex SPNG Enables Measurement of Altered Meiotic Recombination Rates

In barley, an induced mutation in *HvRECQ4*, being identified as an anti-CO factor, results in a significant increase in genome-wide CO, both in a *zmm* (*Hvmlh3*; deficient in interference-sensitive class I CO formation) and WT background [112]. Given that *RECQ4* regulates the number of interference-insensitive class II CO, defects in *HvRECQ4* may alter CO interference in barley. This hypothesis led to the utilization of available *hvrecq4* mutants (unpublished materials; provided by Dr. Mohammad Abdelmordy Ayoub; IPK Gatersleben) in the two cultivars B (*recq4-1*; TILLING mutant) and GP (*recq4-2*; CRISPR/Cas9-based mutant) to test whether changes in meiotic recombination rates, including variations in CO interference strength, can be reliably detected using the multiplex SPNG method. Accordingly, segregating F1 populations were generated by crossing *recq4-1*^{+/-} with *recq4-2*^{+/-}. Recombination rates were subsequently measured within selected intervals on chromosomes 1 and 3 in F1 pollen populations, WT for *recq4-1* x *recq4-2* (*RECQ4*) alleles and mutant for *recq4-1* x *recq4-2*

(*recq4*) alleles, using multiplex SPNG. Recombination rates were assessed for three biological replicates, each consisting of four spikes isolated from two plants.

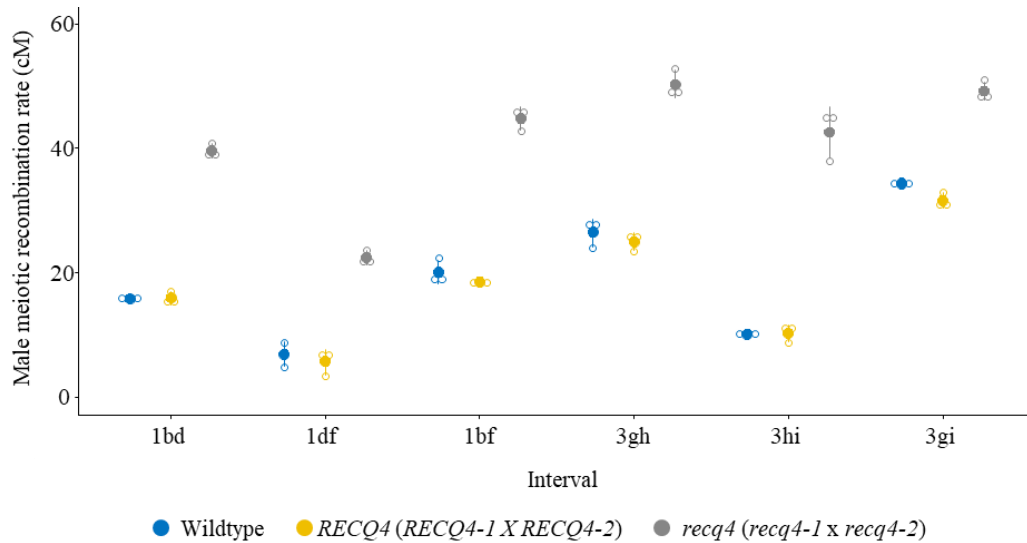


Figure 12: Increased meiotic recombination rates in *recq4* hybrid barley pollen nuclei.

Male meiotic recombination rate in selected genetic intervals in *RECQ4* (*RECQ4-1 X RECQ4-2*; WT) and *recq4* (*recq4-1 x recq4-2*; mutant) hybrid barley based on multiplex SPNG (two-color approach).

Recombination rates based on the two-color approach in F1 *RECQ4* (*RECQ4-1 x RECQ4-2*; WT) were similar to those in F1 WT B x GP hybrid plants. However, a significant increase, ranging from 1.4- to 4.3-fold, in the average recombination rate was observed in *recq4* when compared to *RECQ4* or F1 WT B x GP hybrid plants across all tested intervals: 39.81 ± 0.95 vs 16.12 ± 0.82 or 15.74 ± 0.57 cM for 1bd; 21.54 ± 0.97 vs 5.99 ± 1.71 or 6.84 ± 1.65 cM for 1df; 44.83 ± 1.45 vs 18.43 ± 0.6 or 19.46 ± 1.56 cM for 1bf; 50.60 ± 1.79 vs 25.05 ± 1.22 or 26.92 ± 1.81 cM for gh; 43.39 ± 3.28 vs 10.28 ± 1.08 or 10.18 ± 0.17 cM for 3hi; and 49.50 ± 1.21 vs 31.81 ± 1.02 or 34.42 ± 0.33 cM for 3gi (Fig. 12; Table S7; Table S9). This agrees with previous reports indicating a ~2- to 5-fold rise in genome-wide CO in *hvrecq4* mutants in both WT and *hvm1h3* backgrounds when compared with WT plants [112].

CO interference strength, based on the three-color approach, was increased in *recq4* compared to *RECQ4* or F1 WT B x GP hybrids between chromosome 1 intervals (0.05 vs -0.53 or -0.45), while decreased between chromosome 3 intervals (0 vs 0.23 or 0.55) (Table S6), suggesting chromosome region-specific differences in *recq4* on CO interference. Altogether, the multiplex SPNG approach represents a rapid and reliable method for measuring male meiotic recombination rates, including CO interference strength, in hybrid barley pollen nuclei.

4.1.9 Meiotic Recombination Rates in Pollen Nuclei at Different Developmental Stages

In cereals such as barley, tillering (branching) is a crucial trait linked to yield and environmental adaptation. Anthers vary in age and develop at different times during plant growth across tillers. The influence of plant development stage, age, sex, and growth conditions on the CO landscape in *A. thaliana* [93, 102] triggered to investigate whether CO rates in pollen nuclei may vary depending on the developmental position of anthers within and across spikes from different barley tillers. Hence, anthers were isolated from the top four and bottom four spikelets, representing the apical and basal regions of a spike, respectively, with the remaining spikelets classified as intermediate (Fig. 13a).

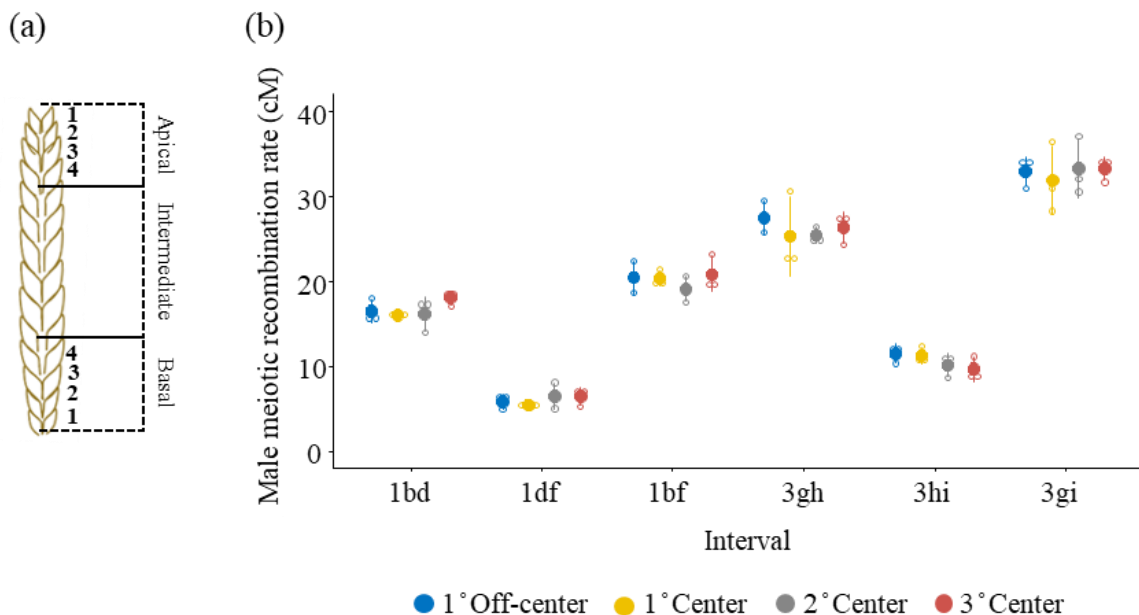


Figure 13: Male meiotic recombination based on anther developmental stage in hybrid barley.

(a) The first four (apical) and last four spikelets (basal) were grouped as off-center while the remaining spikelets were grouped as center. (b) Meiotic recombination in cM plotted for all tested intervals on chromosomes 1 and 3 of hybrid barley.

Subsequently, the male meiotic recombination rates within selected genetic intervals on chromosomes 1 and 3 were measured in anthers from central spikelets (intermediate) of the first, second, and third emerging spikes, as well as in anthers from the off-center (apical and basal spikelets) of the first emerging spike, in 15 F1 B x GP hybrid plants (five plants per biological replicate) grown under controlled conditions. The data showed no significant differences in recombination rates across all six tested intervals using the two-color approach

(Fig. 13b; Table S7; Table S9). These findings suggest that population-wide CO rates in F1 B x GP hybrid pollen are consistently regulated across various developmental positions (at least) for the selected genetic intervals.

4.2 Barley Stripe Mosaic Virus-Induced Genome Editing (BSMVIGE) in barley

VIGE involves delivering target-specific sgRNAs into *Cas9*-expressing plants using an RNA virus to induce TGE. Thus, the requirement of stable genetic transformation for *Cas9*-based mutant isolation is omitted once a *Cas9*-expressing plant has been established. To investigate the applicability of this approach in barley, *Cas9*-expressing barley plants were generated, and rapid BSMV inoculation and TGE-analysis strategies were explored.

4.2.1 Generation of *SpCas9* Expressing Barley Plants

To assess the feasibility of BSMV-mediated TGE in barley, it was necessary to isolate a barley transgenic line expressing *SpCas9*. Thus, five transgenic barley cv GP lines, engineered to constitutively express *SpCas9* under the control of the *ZmUBI* (maize ubiquitin) promoter, was obtained from Dr. Jochen Kumlehn at the IPK in Gatersleben. A transgenic barley line expressing *SpCas9*, confirmed by RT-PCR and designated *ZmUBI::cas9*, was selected for the BSMVIGE experiments.

4.2.2 BSMVIGE Targeted Somatic Gene Editing at the *ALBOSTRIANS* locus in Barley

To deliver sgRNAs compatible with *SpCas9* for TGE, the BSMVIGS vector [149] was modified into BSMV- γ -sgTarget plasmid by inserting a *SpCas9*-compatible sgRNA scaffold sequence and a unique *PaqCI* restriction site, allowing the integration and expression of sgRNAs downstream of the γ b ORF in RNA γ . To assess BSMVIGE in barley, a previously employed sgRNA targeting the *ALBOSTRIANS* gene, *CMF7* [177] was chosen. Efficient *in planta* virus-mediated gene editing largely relies on the systemic movement of the virus, facilitating diverse *Cas9*-induced mutations in various plant tissues, along with the high-level accumulation of viral RNA containing the target-specific sgRNA. Therefore, BSMVIGE-induced editing at the *CMF7* target site across multiple leaf tissues and emerging awns of different tillers in *ZmUBI::cas9* plants inoculated with either BSMVIGE-*CMF7* or BSMVIGE-GFP was initially examined (Fig. 14d). DNA regions flanking the *CMF7* target region were

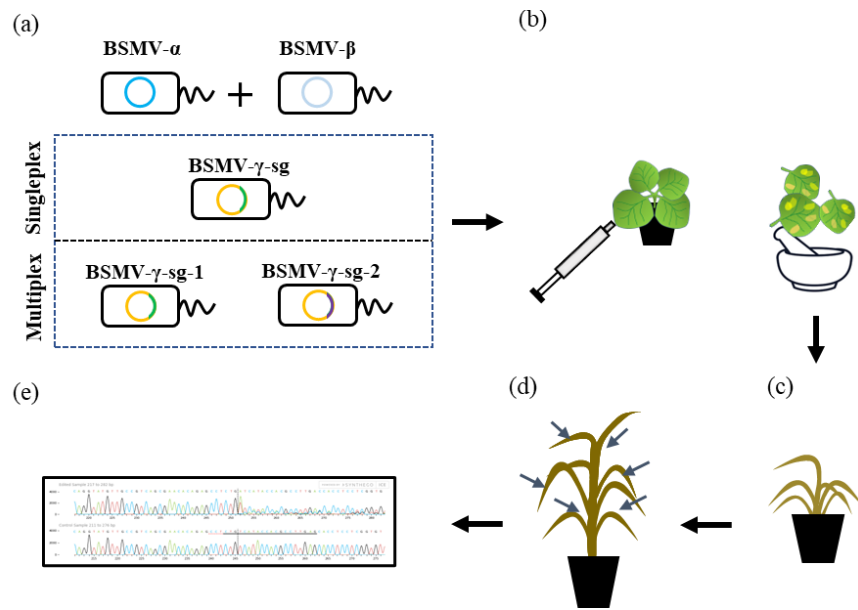


Figure 14: Overview of the BSMVIGE Workflow.

(a) Cloning of sgRNAs into the BSMVIGE vector and transformation of BSMVIGE plasmids into *Agrobacterium* for both singleplex and multiplex BSMVIGE. (b) Infiltration of *Agrobacterium* cultures into tobacco leaves, followed by virus sap preparation. (c) Leaf-rub inoculation of barley seedlings using virus sap. (d) Collection of somatic tissues from various plant parts. (e) Detection of mutations through Sanger sequencing. The depiction is modified according to [178].

amplified using gDNA extracted from pooled tissue samples obtained from individual plants at 5 weeks post-inoculation (wpi). Subsequently, Sanger sequences were analyzed using the ICE Synthego tool [166] to estimate the editing frequencies and types (Fig. 14e). Editing at the *CMF7* target site was observed in 8 out of 14 *ZmUBI::cas9* plants infected with BSMVIGE-*CMF7* ($\alpha=95\%$), with mutation efficiencies reaching up to 94% and a mean mutation efficiency (the average mutation efficiency across all analysed plants) of 35% in two independent experiments (Fig. 15a). In contrast, no editing at the target site was detected in any *ZmUBI::cas9* plant infected with BSMVIGE-GFP ($n=3$), confirming specificity of BSMVIGE-induced mutations at the *CMF7* target site. The predominant mutation type observed among the analyzed plants was a single base 'T' insertion at the expected SpCas9 cut site, located three bases upstream of the PAM within the *CMF7* target site. Other mutation types, including two-base deletions around the expected cut site, were also found but at lower frequencies.

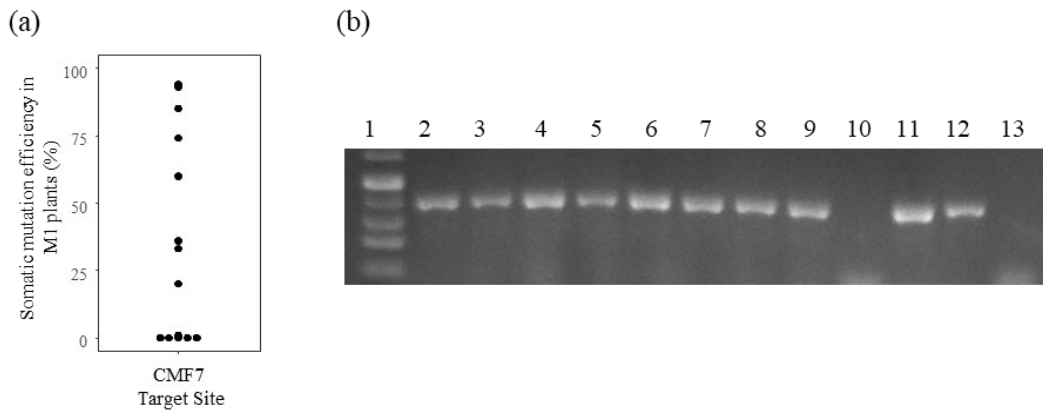


Figure 15: BSMVIGE at the *ABOSTRIANS* locus in barley.

(a) Somatic mutation efficiency at the CMF7 target site 5 wpi in 14 M1 *ZmUBI::cas9* plants (black dots) inoculated with BSMVIGE-CMF7 virus sap. **(b)** The presence/absence of BSMV RNA analyzed using one-step RT-PCR and agarose gel electrophoresis in BSMVIGE-CMF7 and BSMVIGE-GFP inoculated M1 plants. Lane 1, 1 kb plus DNA ladder (Invitrogen). Lanes 2-4, BSMVIGE-GFP infected M1 plants; lanes 5-11, BSMVIGE-CMF7 inoculated M0 plants; lane 12, BSMVIGE-CMF7 plasmid control; lane 13, non-template control.

To identify whether virus presence is sufficient for BSMVIGE at target sites, one-step RT-PCR, amplifying a fragment of BSMV- γ was performed. RNA was extracted from the same pooled somatic tissue at 5 wpi from seven randomly selected *ZmUBI::cas9* barley plants infected with BSMVIGE-CMF7 and all three *ZmUBI::cas9* barley plants infected with BSMVIGE-GFP. The virus was detected in all plants exhibiting targeted editing as well as in a plant showing no editing (Fig. 15b). This indicates that while the presence of the virus is essential for BSMVIGE, not all infected plants display detectable somatic editing by Sanger sequencing.

4.2.3 Heritable Editing at the *ALBOSTRIANS* Locus in Barley

To examine whether induced somatic edits were transmitted to the offspring and if any positive correlation between the somatic mutation and the heritable editing frequency was found, three BSMV-positive M1 plants with varying editing efficiencies of 0%, 33%, and 94%, designated as M1-Null, M1-Medium, and M1-Highest, respectively, were selected. Subsequently, the *CMF7* target region was sequenced in at least 20 M2 offspring plants from each of the three selected M1 plants. Interestingly, 33 out of 61 analyzed M2 plants (~55%), representing 8, 9, and 16 M2 from M1-Null, M1-Medium, and M1-Highest, respectively, exhibited target site mutations. Editing in offspring from M1-Null, tested virus-positive five wpi without detectable somatic editing, suggested that BSMVIGE might occur after tissue sampling, possibly in

reproductive tissues such as the germline or developing embryos. Thus, Sanger-based analysis using pooled somatic tissues, hindered the identification of BSMVIGE edits in M1-null that likely occurred after 5 wpi. In any case, among 33 M2 plants with editing at the *CMF7* target region, 9, 8, 3, and 13 plants were homozygous, heterozygous, bi-allelic, or chimeric, respectively (Fig. 16a). Three M2 plants displayed an albino phenotype, indicative of a complete *CMF7* loss-of-function phenotype (defective chloroplast development), while five M2 mutants exhibited a variegated phenotype likely due to residual/hypomorphic *CMF7* activity (Fig. 16b). Altogether, BSMVIGE induces diverse somatic mutations at the *CMF7* target site (evaluated by a rapid and cost-effective Sanger sequencing-based method) in BSMV-infected *ZmUBI::cas9* barley plants, which can be inherited to offspring plants.

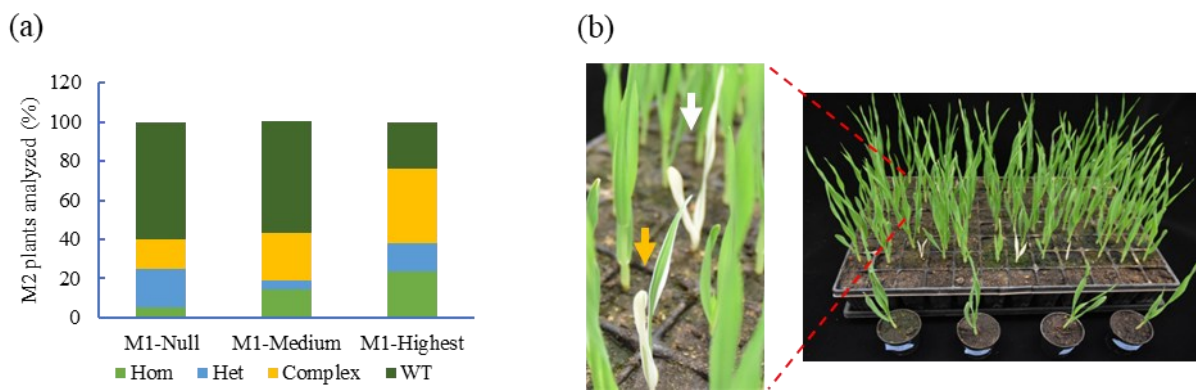


Figure 16: BSMVIGE-induced heritable edits at *ALBOSTRIANS*.

(a) Mutations based on Sanger-ICE Synthego at the *CMF7* target site in M2 offspring from three selected M1 plants (M1-Null, M1-Medium, and M1-Highest with somatic mutation frequencies of 0, 33 and 94%, respectively). Frequency of M2 plants with/without mutation: no mutation (WT); two or more diverse mutations (complex); single mutation at a frequency of ~50% (heterozygous, Het) or ~100%, (homozygous, Hom). **(b)** M2 plants with albino (white arrow) or variegated (orange arrow) phenotypes.

4.2.4 Isolation of Virus-free *cmf7* Mutants

BSMV transmission via grains into the offspring relies on factors such as viral entry into early gametophytes/developing embryos, the BSMV strain, and/or the host genotype [179, 180]. Hence, the generative transmission rate of the BSMVIGE-*CMF7* virus in randomly selected M2 offspring plants screened for heritable editing at the *CMF7* target site was investigated using one-step RT-PCR followed by agarose gel electrophoresis to detect BSMVIGE-*CMF7* viral RNA. Among 38 analyzed M2 plants, 14 were virus-free, including 10 mutants and 4 WT for the *CMF7* target site, while 24 were virus-positive, comprising 16 mutants and 8 WT for

CMF7 (Fig. 17). Hence, while BSMV is transmitted via grains at a high rate, BSMVIGE-induced mutations are inherited regardless of virus transmission.

To assess whether the mutations identified in *cmf7* M2 plants segregate in the M3 generation, Sanger sequencing analysis at the *CMF* target site in a limited number of M3 progenies from a virus-free M2 plant heterozygous for an 'A' insertion (*cmf7-1*) was conducted. Among the analyzed M3 individuals, plants WT, homozygous, or heterozygous for *cmf7-1* were observed, indicating Mendelian segregation of *cmf7-1*. To determine also if virus-free M3 *cmf7* mutant progenies could be obtained from a virus-positive *cmf7-2* M2 mutant, both editing at the *CMF7* target site and presence of BSMV in M3 progenies from a virus-positive M2 *cmf7-2* mutant with multiple editing events (chimeric) were investigated. Four virus-free and four virus-positive M3 plants (n=8) were found. Among those, diverse editing events at the *CMF7* target site were detected, inherited from the M2 parent. Thus, BSMVIGE-induced mutations at the *CMF7* target site are inherited by M3 progenies from M2 plants. Altogether, even though BSMV can be transmitted to subsequent generations, virus-free *cmf7* offspring plants can readily be obtained.

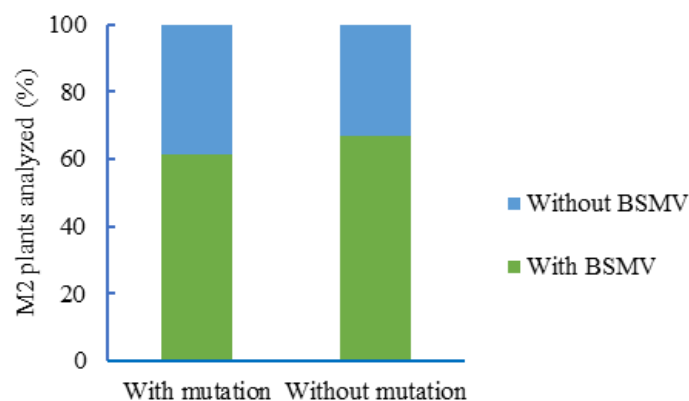


Figure 17: Offspring transmission of BSMV.

BSMV presence or absence in M2 progeny analyzed for editing at the *CMF7* target site. Frequency of M2 offspring plants with or without mutation.

4.3 Modification of the Meiotic Recombination Landscape Using BSMV

The formation of a limited number of CO and their uneven distribution across the genome constrain the effective use of allelic variation in barley breeding. BSMV-based tools, such as BSMVIGE and BSMVIGS, offer promising approaches to alter the CO landscape in barley by targeting meiotic regulators known to influence CO formation in other plant species, including

A. thaliana and rice. In *A. thaliana*, the SC is composed of multiple proteins, including TF protein ZYP1 [11] and CE protein SCEP1/2/3 [12, 13]. Disruption of the SC leads to an increase in CO rates, accompanied by reduced CO interference and a loss of heterochiasmy. The axis-associated protein ASY1 is essential for proper synapsis [9], however, altered *AtASY1* dosage results in CO redistribution toward subtelomeric regions at the expense of the pericentromeres [55]. In *atpch2*, the removal of ASY1 from synapsed chromosome regions is delayed or incomplete, leading to synapsis defects and altered CO distribution [181]. Alteration of DNA methylation pattern through depletion of the epigenetic regulator *CHROMOMETHYLASE 3* (*AtCMT3*) has been shown to enhance interstitial recombination in Arabidopsis [182]. MUS81, a key component of the class II CO pathway, functions independently of CO interference. Therefore, *mus81* could represent a valuable resource for dissecting the relative contributions of this rather minor crossover pathway in barley, as so far only mutants in class I CO genes, such as *mlh3* and *hei10*, were dissected [157, 183]. Hence, selected barley orthologs of well-characterized meiotic genes from *A. thaliana* - including SC components (*ZYP1* and *SCEP3*), CO modifiers (*ASY1*, *PCH2* and *CMT3*) and CO interference-insensitive Class II CO mediator (*MUS81*) - were selected as potential targets.

4.3.1 Identification of Putative Meiosis-related Genes

To identify the putative orthologs of *A. thaliana* genes *ZYP1*, *SCEP3*, *ASY1*, *PCH2*, *CMT3* and *MUS81* in *H. vulgare*, a protein-protein BLAST was performed using the UniProt BLASTp tool with default parameters. Amino acid sequences of the respective *A. thaliana* proteins were used as queries [184, 185]. This analysis identified high-confidence barley orthologs - HORVU.MOREX.r3.2HG0172550 for *AtZYP1*, HORVU.MOREX.r3.3HG0289610 for *AtSCEP3*, HORVU.MOREX.r3.5HG0494140 for *AtASY1*, HORVU.MOREX.r3.2HG0175590 for *AtPCH2*, HORVU.MOREX.r3.6HG0628050 for *AtCMT3*, and two paralogous genes, HORVU.MOREX.r3.3HG0257160 (*HvMUS81a*) and HORVU.MOREX.r3.3HG0319570 (*HvMUS81b*) for *AtMUS81* - annotated in the MorexV3 pseudomolecule genome assembly of barley cv. Morex [186].

HvZYP1 shares 39.5% amino acid similarity with both AtZYP1A and AtZYP1B proteins, and it contains extended coiled-coil regions, a hallmark for ZIP1/ZYP1 orthologs [11, 187]. HvSCEP3 shows 57% amino acid similarity to AtSCEP3 and is predicted to possess a coil-coil domain. HvASY1 displays 55.7% similarity to AtASY1 and possesses a HORMA domain, characteristic of HOP1/ASY1 family proteins involved in meiotic chromosome axis [9, 188].

HvPCH2 and HvCMT3 exhibit amino acid similarities of 67.1% and 60.3% to their Arabidopsis counterparts, respectively. HvPCH2 contains a conserved AAA+ ATPase domain, while HvCMT3 features characteristic domains including a bromo-adjacent homology (BAH) domain, a chromodomain, and a C-5 cytosine-specific DNA methyltransferase domain. Two paralogs of MUS81 were identified in barley: HvMUS81a and HvMUS81b, showing 57.1% and 52.3% similarity to AtMUS81, respectively. These paralogs share 50.6% similarity and both contain hallmark features of MUS81 proteins, including a helix-hairpin-helix (HhH) DNA-binding motif and an ERCC4 endonuclease domain. The combination of high amino acid similarity and the presence of conserved, functionally relevant domains strongly supports the identification of these barley genes as orthologs of selected *A. thaliana* meiotic regulators.

4.3.2 BSMVIGE-Directed Targeting of Identified Meiosis-related Genes

Two BSMVIGE strategies were employed to target identified meiosis-related candidate genes: singleplex, which targets a single genomic site, and multiplex, which targets multiple genomic sites. For each gene - *ZYP1* (*ZYP1-E2* and *ZYP1-E6*), *SCEP3* (*SCEP3-E6-1* and *SCEP3-E6-2*), *ASY1* (*ASY1-E4* and *ASY1-E6*), *PCH2* (*PCH2-E3* and *PCH2-E4*) and *CMT3* (*CMT3-E6* and *CMT3-E9*) - two target sites located within the same or different exons (denoted as 'E') were selected. One target site was selected for each paralog, *MUS81a* and *MUS81b* (Fig. 18). Then, BSMV- γ -sgTarget plasmids targeting selected sites within the candidate genes were generated.

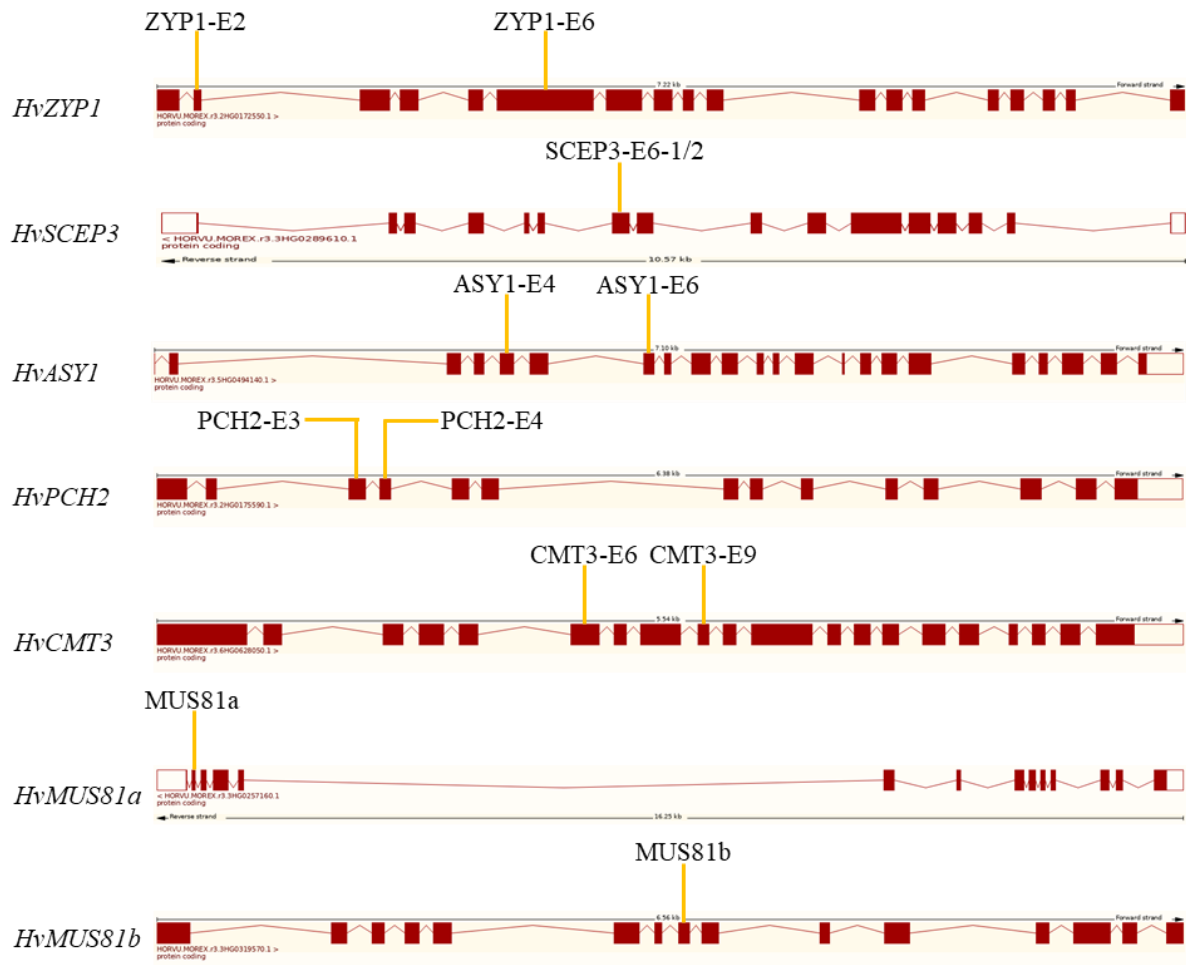


Figure 18: BSMVIGE targets within selected meiosis-related genes in barley.

Gene models predicted for seven putative meiosis-related genes. Selected BSMVIGE target sites, orange line; predicted exons, brown bar and predicted introns, brown line indicated.

4.3.2.1 Singleplex BSMVIGE

Using the established singleplex BSMVIGE approach (see section 4.2.2), *ZmUBI::Cas9* plants were infected with respective BSMVIGE virus sap targeting individual genomic sites within genes *ASY1*, *ZYP1*, *PCH2*, *CMT3*, *MUS81a* and *MUS81b*. Somatic editing at the respective target regions was assessed 5 wpi. The editing frequencies – defined as the percentage of M1 plants exhibiting somatic editing at the target sites – reached up to 46%. The mean mutation efficiency across targets ranged from 0% to 19%. Notably, single plants exhibiting the highest mutation efficiencies were identified for several targets: 74%, 94%, 89%, 51%, 31% and 76% for *ASY1-E4*, *ASY1-E6*, *ZYP1-E2*, *ZYP1-E6*, *PCH2-E3* and *MUS81a*, respectively. However, no detectable editing was observed for *PCH2-E4*, *CMT3-E6*, *CMT3-E9* and *MUS81b*. Together, in addition to the proof-of-principle target *CMF7*, BSMVIGE was successfully used to induce

targeted somatic mutations in meiosis-related genes. The absence of somatic editing at four out of 10 target sites, as assessed by Sanger analysis, in the BSMVIGE-inoculated progenies of *ZmUBI::Cas9* plants indicates potential issues such as the efficiency of the selected sgRNAs and/or reduced *SpCas9* expression due to transgene silencing in the subsequent generations.

Gene	Target site	Editing frequency	No. of plants infected	Mean mutation efficiency	Highest mutation efficiency in a single plant
<i>ASY1</i>	<i>ASY1-E4</i>	38%	8	18%	74%
	<i>ASY1-E6</i>	33%	12	14%	94%
<i>ZYP1</i>	<i>ZYP1-E2</i>	36%	11	11%	89%
	<i>ZYP1-E6</i>	46%	11	19%	51%
<i>PCH2</i>	<i>PCH2-E3</i>	9%	14	2%	31%
	<i>PCH2-E4</i>	0%	14	0%	0%
<i>CMT3</i>	<i>CMT3-E6</i>	0%	8	0%	0%
	<i>CMT3-E9</i>	0%	9	0%	0%
<i>MUS81a</i>	<i>MUS81a</i>	36%	11	17%	76%
<i>MUS81b</i>	<i>MUS81b</i>	0%	12	0%	0%

Table 1: Singleplex BSMVIGE-induced somatic editing in meiosis-related genes.

The mutation frequency and mean mutation efficiency at target sites within *ASY1*, *ZYP1*, *PCH2*, *CMT3*, *MUS81a* and *MUS81b* in offspring of *ZmUBI::Cas9*.

4.3.2.2 Multiplex BSMVIGE

To assess whether BSMVIGE can be used for multiplex TGE, a mixed *Agrobacterium* pool (MEA) strategy [141] was employed. This strategy targeted two independent target sites within different genes (*CMF7* and *ZYP1-E6*, MEA#1) to achieve multiplexed heritable editing at both loci, and two sites within different exons of the same gene (*ZYP1-E2* and *ZYP1-E6*, MEA#2) or two sites within the same exon of a gene (*SCEP3-E6-1* and *SCEP3-E6-2*, MEA#3) to identify whether larger deletions can be induced and/or mutant isolation frequency can be increased. For each combination, virus saps were produced by infecting *N. benthamiana* plants with *Agrobacterium* harboring BSMV- α , BSMV- β , two BSMV- γ plasmids containing each target guide (Target_1 and Target_2), following the MEA strategy. These virus saps were then used to inoculate *ZmUBI::Cas9* plants. Somatic editing at both target sites was assessed using Sanger reads analyzed via ICE Synthego 5 wpi.

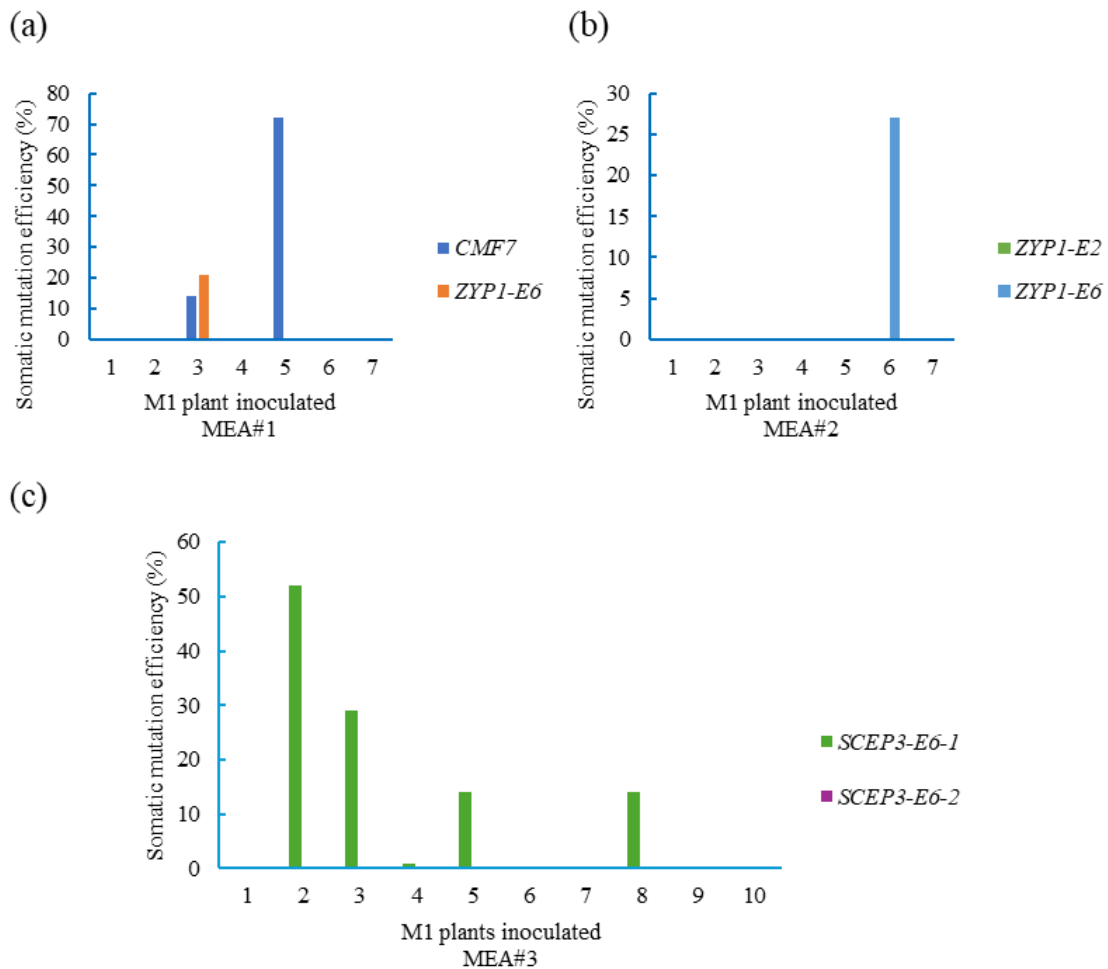


Figure 19: Multiplex BSMVIGE using mixed Agrobacterium pool strategy (MEA).

BSMVIGE-MEA at two target sites within different genes (MEA#1) (a) or a single gene (MEA#2 and MEA#3) (b, c). Somatic mutation frequencies at target sites for all inoculated M1 *ZmUBI::Cas9* plants.

For MEA#1, somatic editing at *CMF7* target site was observed in two out of seven plants, with a mean and a maximum mutation efficiency of 12 and 72%, respectively. At *ZYP1-E6*, only one plant exhibited editing, with a mutation efficiency of 21%, and the mean mutation efficiency being low with 3% (Fig. 20a). To determine whether multiplex BSMVIGE can induce heritable editing at two target sites simultaneously, M2 offspring plants of an M1 plant that showed editing at both target sites (14% for *CMF7* and 21% for *ZYP1-E6*) was analyzed for mutations at both target sites. Sanger analysis of 14 M2 plants revealed no detectable editing at either target site or both.

For MEA#2, no editing was detected at the *ZYP1-E2* target site in any inoculated plants 5 wpi. However, one plant exhibited editing at the *ZYP1-E6* target site with a mutation efficiency of 27%, and the mean efficiency for *ZYP1-E6* was low with 4% (Fig. 20b). Given that BSMVIGE-

induced heritable editing was found in segregating offspring plants from an individual that showed no editing at the *CMF7* target locus, heritable editing at both target loci, *ZYPI-E2* and *ZYPI-E6*, was assessed in 12 M2 offspring plants from the M1 plant exhibiting 27% mutation efficiency at the *ZYPI-E6* site but not at *ZYPI-E2* site. Unfortunately, no M2 plant showed editing at *ZYPI-E2*. However, a plant with homozygous editing at the *ZYPI-E6* target locus was identified but produced no grains. Further, 8 progenies were analyzed for editing at *ZYPI-E6* to isolate offspring plants with additional mutations. However, no editing was found among the progenies screened.

For MEA#3, no mutations were detected at the *SCEP3-E6-2* target site. However, four of 10 inoculated plants exhibited editing at *SCEP3-E6-1*, with one plant displaying the highest mutation efficiency (52%). The mean mutation efficiency at *SCEP3-E6-1* was 11% (Fig. 20c). To isolate M₂ offspring carrying inherited mutations, 18 and 20 M₂ offspring of M₁ plants exhibiting mutation efficiencies of 52% and 14%, respectively, were screened for mutations at both target sites. Two M₂ plants (one from each M₁ plant) were identified with mutations close to the *SCEP3-E6-1* target locus, as expected. These included a one-base pair insertion and a complex mutation involving both deletion and insertion (Fig. 21). This suggests that multiplexing BSMVIGE to target two or more sites simultaneously using the MEA strategy is less efficient in barley compared to targeting individual sites with BSMVIGE. Despite this, heritable editing can be achieved, albeit at a very low frequency, and isolating offspring with inherited (simultaneous) mutations at both target sites remains challenging.

ASY1-E4

HvASY1 CCCATGGATCCTGAATCCAGGAGGTTGATTG
hvasy1-1 CCCATGGAA**A**TCCCTGAATCCAGGAGGTTGATTG
hvasy1-2 CCCATG-ATCCTGAATCCAGGAGGTTGATTG
hvasy1-3 C-----GATTG
hvasy1-4 CCCATG-ATCCTGAATCCAGGAGGTTGATTG

ZYP1-E2

HvZYP1 CCTCGGTGAAGTCTGATCTAGAAATGGCGGT
hvyyp1-1 -----AAGTCTGATCTAGAAATGGCGGT
hvyyp1-2 CCTCGG-GAAGTCTGATCTAGAAATGGCGGT

SCEP3-E6-1

HvSCEP3 AGCAAGGAAGCTCCTCCAAGTGGGCCCTTGTAGAGTTAATATAATGT
hvscep3-1 AGCAAGGAAGCTCCTCCAAGTGTGGGCCCTTGTAGAGTTAATATAATGT
hvscep3-2 AGCAAGGAAGCTAATATAATGTCAAGGGAGAATAATAGCAGTGGGAGTTAATATAATGT

Figure 20: BSMV-induced heritable editing within putative meiotic axis- and SC-related genes in barley.

M2 offspring plants carrying inherited mutations at the target sites *ASY1-E4*, *ZYP1-E2* and *SCEP3-E6-1* are shown. Target regions in WT and mutant alleles are represented as nucleotide sequences on the DNA reverse strand. The PAM is highlighted in light blue; the 20-nt spCas9 target sequence is underlined. Insertions are shown as bold base(s), and deletions are represented hyphen(s).

4.3.3 Isolation of Putative Chromosome Axis and SC Mutants

In *A. thaliana*, chromosome axis-related component ASY1 is essential for coordinating DSB formation, interhomolog recombination and SC assembly. Loss-of-function *asy1* mutants exhibit profound meiotic defects, including incomplete homolog pairing, aberrant synapsis, and a significant reduction in fertility due to impaired CO formation [9]. In Arabidopsis, CO interference is significantly reduced in *asy1* carrying heterozygous mutations, leading to altered CO spacing and distribution [55]. The SC consists of various proteins, including ZYP1 [11] and SCEP1/2/3 [12, 13]. Notably, SC proteins are not only critical for meiotic recombination and synapsis, but they are also involved in implementing the number and chromosomal distribution of CO [189]. In Arabidopsis, the SC even seems to limit CO formation and to impose CO interference and heterochiasmy [12, 43, 81]. The orthologous SC genes in barley have not yet been functionally characterized. Understanding their roles is not only crucial for elucidating the molecular mechanisms of synapsis and homologous recombination in barley, but also to address whether they can be harnessed to alter the CO landscape in barley. Hence, this prompted the

isolation of axis-related (*asy1*) and SC (*zyp1*) mutants, following the successful isolation of two *scep3* mutants based on multiplex BSMVIGE.

Given the low heritable editing efficiency observed with the multiplex BSMVIGE approach and the absence of any heterozygous *zyp1* mutants, M2 offspring derived from M1 plants with editing at *ASY1* and *ZYP1* loci using the singleplex BSMVIGE approach were screened for heritable mutations. Sanger-ICE Synthego analysis was performed on M2 progeny from M1 plants that exhibited the highest somatic editing efficiencies of 74% at the target site *ASY1-E4* and 89% at *ZYP1-E2*. Of the 15 M2 offspring screened, four plants carried mutations at the target locus *ASY1-E4*, including three plants with diverse heterozygous mutations and one plant with a homozygous mutation (Fig. 21). For *ZYP1-E2*, three out of 11 M2 plants harbored edits at the target locus, comprising two plants with diverse heterozygous mutations and one plant with complex editing at the target locus (Fig. 21). This result demonstrates that the singleplex BSMVIGE enables the efficient generation and isolation of putative meiotic mutants in barley, supporting its use as a rapid and effective genome editing platform.

4.3.4 In barley, SC formation is required for CO formation

To determine whether barley plants carrying BSMVIGE-induced inherited mutations in putative meiosis-related genes encoding for SC central region proteins - ZYP1 (the TF protein) and SCEP3 (a CE protein of the SC recently identified in Arabidopsis) - lack the respective proteins, triple immunolocalization experiments of ASY1 (axis protein), ZYP1 and SCEP3 was performed in male meiotic nuclei from WT, *zyp1-1* and *scep3-2* plants. In WT meiocytes, ZYP1 and SCEP3 first appear after ASY1 is fully loaded along the chromosome axis. Initially, ZYP1 and SCEP3 are observed as scattered foci that progressively linearize as synapsis proceeds, while ASY1 signal diminishes from regions undergoing synapsis. In details, during early prophase I (leptotene), ASY1 appears as strong polarized linear signals emerging from one side of the nucleus, with weaker signals detected elsewhere. At this stage, ZYP1 and SCEP3 are visible as discrete foci. By early zygotene, ASY1 has formed continuous linear tracks throughout the nucleus. Concurrently, bright foci of ZYP1 and SCEP3 - presumed synapsis initiation sites - emerge from the same ASY1-enriched nuclear pole, reflecting a spatiotemporally asymmetric onset of synapsis [190].

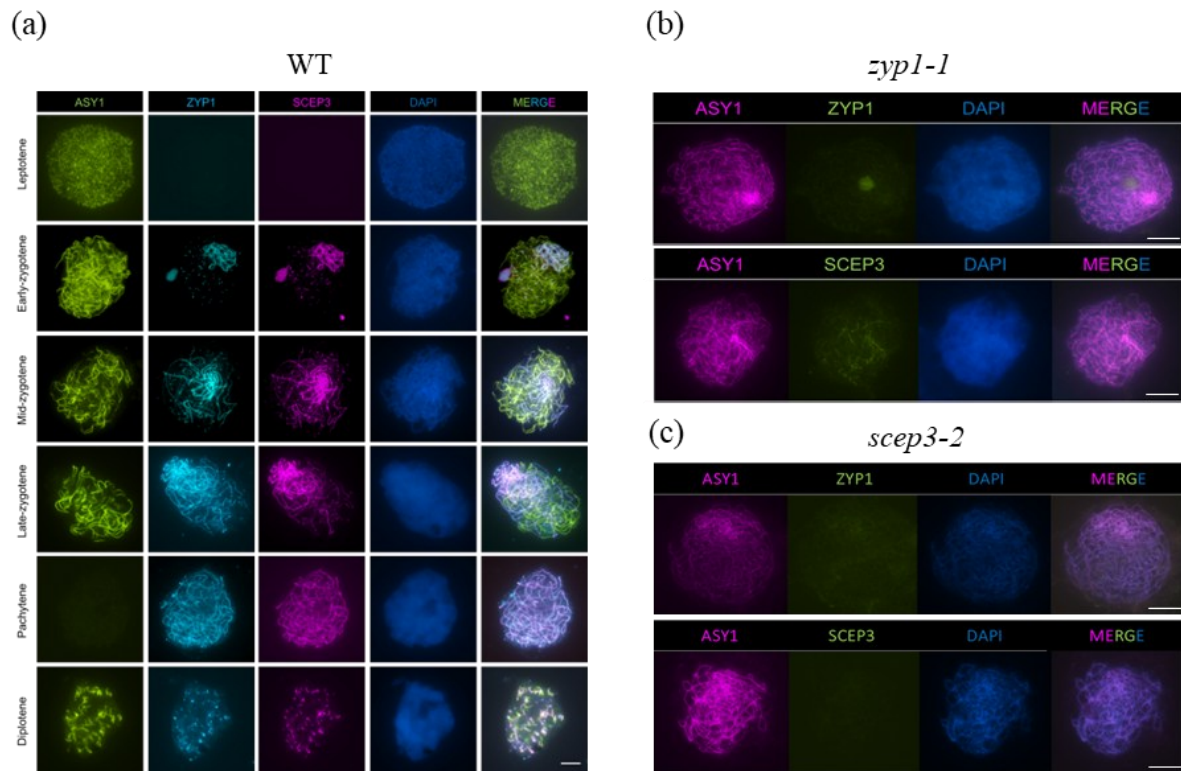


Figure 21: Immunolocalization of SC components in barley meiotic mutants.

(a) Male meiocytes in the WT immunostained for ASY1 (green), ZYP1 (turquoise) and SCEP3 (magenta) as well as in (b) *zyp1-1* and (c) *scep3-1* immunostained for ASY1 (pink) and ZYP1 (green; top panel) or SCEP3 (green; bottom panel). DAPI stained nuclei are in blue. Bar = 5 μm .

In mid-to-late zygotene, short ZYP1 stretches are apparent across the nucleus. During zygotene-pachytene, synapsis extends from multiple ZYP1/SCEP3-marked sites, while ASY1 fades in synapsed regions. By late pachytene, long ZYP1/SCEP3 threads span the nucleus, indicating synapsis completion, with only residual ASY1 signal colocalizing with the SC. During diplotene, ASY1, ZYP1, and SCEP3 display a characteristic "tinsel-like" structure, with ZYP1 and SCEP3 signals showing complete colocalization (Fig. 22a) [191]. Together, in the WT, ZYP1 and SCEP3 show full colocalization throughout meiosis with spatiotemporal dynamics reflecting their roles as SC proteins. However, the absence of ZYP1 in *zyp1-1* (Fig. 22b) and of SCEP3 in *scep3-2* (Fig. 22c) in late-zygotene to pachytene-like stages, suggests that in both mutants no full-length proteins are found and that SC assembly seems abolished.

Next, to investigate meiosis progression in *zyp1* and *scep3*, male meiotic chromosome spread analysis was performed in homozygous M3 offspring mutants (*zyp1-1*, *zyp1-2*, *scep3-1* and *scep3-2*), along with *ZmUBI::Cas9* plants, which served as WT control. In the WT, all seven

pairs of homologous chromosomes align and synapse during zygotene and pachytene. Until diakinesis, chromosomes condense resulting in homologous chromosome pairs being visible as bivalents connected by chiasmata, either rod- (at least one CO) or ring-shaped (at least two CO). At metaphase I, all seven bivalents are aligned on the metaphase I plate. During anaphase I, homologous chromosomes segregate to opposite poles, resulting in seven chromosomes per pole. At the end of meiosis II, tetrads form (Fig. 23a). However, in all four mutants, no thick pachytene chromosomes were found, indicating a lack of synapsis. This was further supported by the absence of SC assembly as revealed by immunolocalization studies.

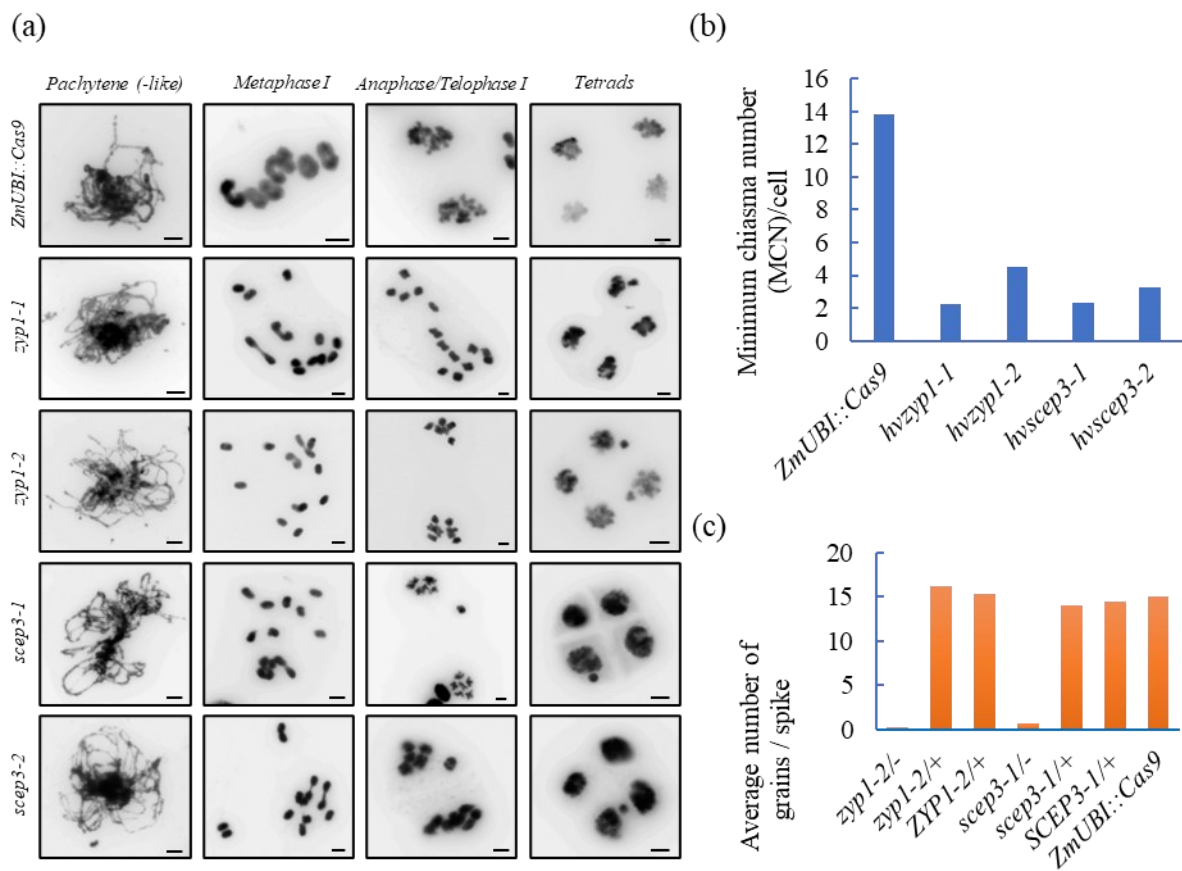


Figure 22: Meiosis in barley meiotic mutants.

(a) Male meiotic chromosome during pachytene(-like), metaphase I, anaphase/telophase I and tetrad stages (Bar 5 μm). **(b)** Minimum chiasma number (MCN) in *ZmUBI::Cas9*, *zyp1* and *scep3*. **(c)** Fertility based on the average number of grains per spike for plants homozygous, heterozygous or WT for *ZYP1* and *SCEP3*: *zyp1-2/-* (N = 5), *zyp1-2/+* (N = 30), *ZYP1-2+/+* (N = 5), *scep3-1/-* (N = 50), *scep3-1/+* (N = 50), *SCEP3-1+/+* (N = 47) and *ZmUBI::Cas9* (N = 25). N = number of spikes analysed.

Contrary to the WT, all mutants displayed a high frequency of univalent pairs (homologous chromosome pairs without physical chiasma connections) at metaphase I, suggesting a substantial reduction in chiasmata formation. Consequently, these mutants exhibited defects in faithful chromosome segregation during meiotic divisions, leading to micronuclei formation in tetrads (Fig. 23a). To quantify the number of chiasmata, the minimum chiasma number (MCN) was calculated from at least 50 cells per genotype. The MCN for *hvzyp1-1*, *hvzyp1-2*, *scep3-1* and *scep3-2* 2.28 ± 1.09 , 4.52 ± 2.26 , 2.36 ± 1.41 and 3.24 ± 1.44 , respectively, were strongly reduced when compared to WT (13.85 ± 0.44) (Fig. 23b). Together, in Arabidopsis, SC depletion results in an increase in CO frequency, with only a limited number of cells displaying 1-3 univalent pairs, ~10% in *zyp1* [43, 81] and ~50% in *scep3* [13], causing only mild fertility reduction. In contrast, SC depletion in barley leads to a drastic reduction in chiasmata and in fertility in both mutant lines (Fig. 23c).

4.3.5 BSMV-mediated Virus-Induced Gene Silencing (BSMVIGS) in barley

BSMVIGS has been successfully utilized to transiently knock-down target RNA transcripts for the rapid functional characterization of meiosis-related genes in wheat [86, 115, 192]. *RECQ4* is a DNA helicase belonging to the family RecQ, involved in DNA repair and homologous recombination [45, 193]. As *RECQ4* is expressed both in somatic and meiotic tissues and its depletion increases meiotic CO in hybrid *recq4* barley plants, assessed using the established multiplexed SPNG method, *RECQ4* was selected as a proof-of-principle target to test the BSMVIGS-based approach for alteration of the meiotic CO landscape in barley. To do so, si-Fi [168] was used to identify two potential siRNA-enriched regions within the *HvRECQ4* CDS. Subsequently, individual BSMVIGS constructs were generated, containing either a 114 bp (BSMVIGS-RECQ4-114), or 102 bp (BSMVIGS-RECQ4-102) fragment, expected to produce a high number of siRNAs, flanking the selected regions of the *HvRECQ4* CDS. To facilitate rapid BSMV inoculation into B x GP hybrid barley, *in vitro* transcripts (see materials and methods section 3.7.2) were employed instead of the traditional tobacco virus sap, ensuring an equivalent starting inoculum across different treatments. As negative controls, an empty BSMVIGS vector and a BSMVIGS vector carrying a 110-bp fragment of the *AvGFP* gene (BSMVIGS-YFP-110) - unrelated to the barley CDS - were used. CO rates were initially estimated using multiplex SNP-G, focusing on genetic intervals on chromosome 1 in F2 B x GP segregating populations heterozygous for 1bd, 1df, and 1bf. To account for potential variability in VIGS efficiency among anthers/spikes, two or three randomly selected spikes were pooled per biological replicate (a total of five F2 plants were used in each experiment). However, no

significant differences in CO rates were observed within the tested intervals among WT, control (empty BSMVIGS and BSMVIGS-YFP-110), and treated (BSMVIGS-RECQ4-114 and BSMVIGS-RECQ4-102) F2 plant populations (Fig. 24). This outcome suggests three possible explanations: *HvRECQ4* transcripts were not effectively degraded in reproductive cells (male meiocytes) following BSMVIGS application, the extent of *HvRECQ4* transcript downregulation was insufficient to induce an increase in CO rates, in contrast to the stable gene knockout approach, or the power of detection was insufficient to detect small variations in male CO rates. In addition, neither BSMVIGS nor BSMVIGS-YFP-110 influenced CO rates within the examined genetic intervals on chromosome 1 (Fig. 24; Table S), suggesting that these intervals are tightly regulated and resistant to CO rate alterations upon BSMV infection. However, further investigations are necessary to determine whether similar effects persist across other genomic regions or when BSMVIGS constructs carrying different homology sequences are used.

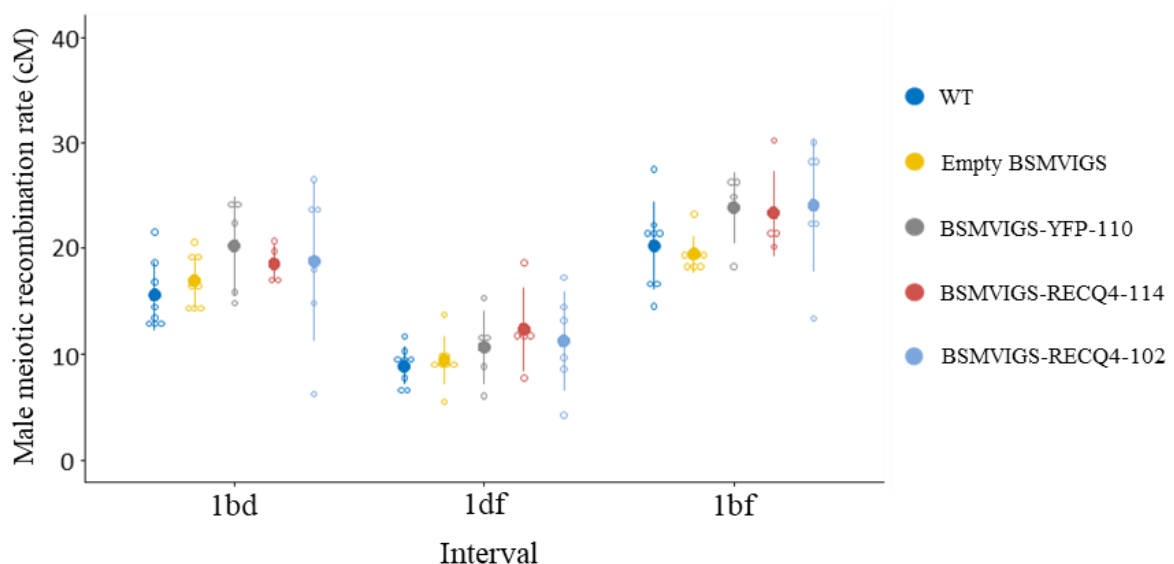


Figure 23: Male meiotic recombination rate measurements in BSMVIGS treated barley.

(a) CO rates in cM plotted for three tested intervals on chromosome 1 of barley hybrids, infected with BSMVIGS (empty), BSMVIGS-YFP-110, BSMVIGS-RECQ4-114 and BSMVIGS-RECQ4-102.

5 Discussion

5.1 Multiplex Crystal Digital PCR-based Single Pollen Nucleus Genotyping (Multiplex SPNG) for Male Meiotic Recombination Measurements in Barley

5.1.1 Barley Anther Storage Enables High-Throughput SPNG

In a previous dPCR-based SNP-G study, fresh barley anther materials were required to isolate pollen nuclei for male meiotic CO rate analysis [104]. This requirement limited the use of anther samples collected at different time points or from various locations. To address this, a freeze-storage method was explored in barley. However, pollen nuclei isolation efficiency using the conventional procedure [169] was reduced due to the altered ability of stored pollen to burst. To overcome this, bead-beating was employed on the pollen suspension, increasing the number of isolated nuclei up to fourfold compared to untreated or sonicated samples. However, the applicability of this established strategy to other barley genotypes or even to other plant species remains to be investigated. The current anther-storage strategy allowed employing anthers stored for at least 12 months in SNP-G experiments, thereby enabling high-throughput male CO rate analysis via multiplex SNP-G. Future research should assess whether pollen samples can be stored for extended periods beyond 12 months while remaining viable for single pollen nucleus isolation and downstream multiplex SNP-G applications. Additionally, alternative storage methods, such as wet storage, should be explored to further enhance preservation efficiency.

5.1.2 Multiplex SPNG: CO rate in Two Linked Genetic Intervals

The previously established dPCR-based male CO rate measurement approach, relying on a three-color dPCR instrument (Prism3), was restricted to measuring CO rates within a single interval per chamber, thereby limiting sample throughput [104]. The capability of the Prism6™ to measure six fluorescence channels allows for the genotyping of up to six polymorphic markers between barley cv. B and GP, therefore enabling the measurement of CO rate within two-linked genetic intervals in hybrid plants. The intervals selected on chromosomes 1 and 3 span diverse genomic regions, including distal, interstitial and (peri-)centromeric ones.

Using the established multiplex SPNG, CO rates were measured in barley F1 B x GP plants. The interval 1df, the largest interval among the selected intervals, on chromosome 1 spanning a large block of 331.3 Mbp (peri)centromere exhibited the lowest CO rate of approximately 7 cM, as expected since it resides in a region known to have a lower CO rate when compared to the chromosomal arms [64]. In contrast, the distal intervals on chromosomes 1 and 3 (1bd, 3gh,

and 3hi) displayed higher CO rates, ranging from approximately 10 to 27 cM, with the highest CO rate observed in 3gh. In the current dPCR setup, the nuclei input per chamber was increased by 1,000 compared to a previous study [104]. Increasing the number of nuclei input raises the likelihood of encapsulating two or more nuclei within a single droplet, which might result in false-positives. However, CO rate estimates did not differ significantly across all tested genetic intervals, regardless of whether droplets encapsulating multiple nuclei were considered. Therefore, these droplets were not excluded during the CO rate estimations in this study, unlike in previous analyses.

Whether CO rates determined using the multiplex SPNG approach in pollen nuclei (male CO) were similar to offspring rates (male and female CO combined) was addressed by genotyping segregating F2 populations. Slight differences in CO rates between pollen and offspring populations were found in intervals 1bd, 1df and 3hi, while a significant difference was found in other intervals. These discrepancies may be explained by heterochiasmy, a phenomenon observed in many species, including plants, where CO rates differ between sexes [43], or by post-meiotic distortion [91]. Nonetheless, the multiplex dPCR approach enables reliable measurement of male CO rates in pollen nuclei, circumventing segregation distortion issues and eliminating the need for segregating populations. Moreover, it allows for estimating CO events from large pollen populations even from individual plants, due to the high abundance of pollen from individual plants. As a result, this approach can be used for rapid and high-throughput analysis of CO rates; for example, in barley mutants or in plants subjected to varying growing/environmental conditions or chemical treatments.

5.1.3 CO Interference Strength in Barley Pollen Nuclei

CO distribution is non-random along a given chromosome with the probability of two CO occurring close together being lower than expected by chance due to CO interference. Its strength can be estimated through cytological methods [42] or genetic analysis. In *A. thaliana*, CO interference is also measured in pollen tetrads, or seeds using FTLs, which involves analyzing the segregation of three genetically-linked fluorescent markers along a chromosome [93, 94]. However, in crops like barley, methods to measure CO interference are limited to SNP arrays, sequencing methods, or cytology [59, 83, 84]. The multiplex SPNG approach enables the estimation of CO interference strength within two linked genetic intervals along a given chromosome. In barley, cytological analysis has shown that approximately 96% of homologous chromosome pairs form ring bivalents, indicating that at least one CO forms in each arm [40].

As expected, negative CO interference, more double CO than anticipated by chance, was observed within the tested intervals of chromosome 1, as these span both chromosome arms. Conversely, positive interference was observed for intervals located in close proximity on the distal region of chromosome 3, which is consistent with the notion that CO interference is stronger when the distance between intervals is smaller. Further, strong CO interference is observed in highly recombining distal chromosomal regions in cereals [36, 59]. Similar to the FTL system in *A. thaliana*, the multiplex SPNG approach enables measurement of CO interference strength across chromosomal intervals in barley, providing a new avenue to investigate CO interference in crop meiosis.

5.1.4 Multiplex SPNG Approach Detects Significant Increases in CO Rates of *recq4* Plants

The anti-CO protein RECQ4 limits class II CO formation in many plant species, including *A. thaliana*, pea, tomato, rice, and barley [45, 112, 194, 195]. Using the multiplex SPNG approach, an increased CO rate, up to a 4-fold, was observed in all six tested intervals of chromosomes 1 and 3 in barley. The strongest CO increase was found in distal chromosome regions. This finding is consistent with a previous study in barley using a SNP array-based method to assess CO rates, which reported up to a fivefold increase in genome-wide CO rates [112]. CO interference vanished in the close-proximity intervals of chromosome 3 in *recq4*, where strong interference is present in the WT. In *recq4*, additional CO are more frequently found in distal than interstitial chromosome regions [112]. Consequently, the two distal intervals on chromosome 3 likely experienced a higher number of simultaneous CO. Conversely, for chromosome 1, CO interference was observed in *recq4* compared to WT, where no CO interference was detected, suggesting that CO interference varies depending on the chromosomal position and/or context. In this study, the multiplex SPNG approach successfully detected significant changes in CO rates using a comparatively limited number of analyzed pollen nuclei, ranging from 983 to 2,480 across both two-color and three-color approaches. Additionally, reliable CO rate measurements were obtained from a small number of plants and spikes, with data collected from two to three spikes per six plants. However, the method's sensitivity in detecting slight to moderate differences in CO rates has yet to be fully evaluated. Increasing sample size, both in terms of pollen analyzed and biological replicates, may enhance the precision of CO rate estimations, enabling the detection of even subtle variations.

5.1.5 Consistent Male CO Rates in Anthers Developed Across Barley Tillers

In *A. thaliana*, CO frequency is influenced by factors such as plant development stage, age, sex, and growth conditions [93, 102]. Further, the average chiasma number varies with chromosome size and even among different chromosomal arms [196]. In barley, the development of each tiller occurs at different times. This timing can significantly influence the maturity of the plant, gamete development and the overall grain yield. Breeding programs strive to optimize tillering capacity to achieve higher grain yield [197]. In barley, anther differentiation occurs at varying time points across and within tillers. This temporal difference may reflect genetic or environmental factors affecting CO frequency in barley. Understanding these differences could inform breeding strategies to enhance genetic diversity and improve trait selection efficiency. However, male CO rate measurements using the multiplex SPNG approach indicated that there were no changes in CO rates among anthers developed from the first, second, and third emerging spikes. Further, variations in anther position within the first emerging spike had no impact on CO rates. This suggests that CO rates are tightly regulated and not influenced by tillering in the given barley hybrid within the tested genetic intervals under the experimental growth condition.

5.1.6 Improving the Efficiency of Multiplex SPNG

Treating pollen nuclei with restriction enzymes can improve SPNG efficiency [104]. Using a lower concentration of sheath buffer (0.5x PBS) improved the separation of positive and negative populations across any fluorescence channel [104]. Here, no specific treatments were applied to enhance the SPNG efficacy. However, it might be beneficial to explore the use of restriction enzyme treatment with the new setup to determine if genotyping efficiency can be further increased. Furthermore, testing even lower PBS concentrations (less than 0.5x) or alternative sheath buffers could be advantageous. Incorporating single-strand DNA binding proteins could also be considered, as it has been shown to improve PCR efficiency by enhancing DNA polymerase fidelity [198].

5.2 Barley Stripe Mosaic Virus-Induced Gene Editing (BSMVIGE) in barley

5.2.1 Utilizing BSMV for Targeted Genome Modifications in Crop Plants

Functional gene studies in barley, an important crop species, are hindered by the lack of easy and rapid genetic transformation methods, despite the availability of extensive (pan)genomic data [68, 199]. Only a few barley genotypes are amenable to genetic transformation, which

relies on tissue regeneration after *Agrobacterium*-mediated T-DNA transfer or particle-bombardment-mediated transgene introduction using immature embryos as explants. The isolation of immature embryos is a challenging process, and other explants, such as microspores and leaf tissue, are not widely used [200-203]. Alternative transgene delivery methods as in other species [204] such as nanoparticles, silicon carbide whisker, microinjection, or electroporation have not been established for rapid and high throughput isolation of barley transgenics.

The CRISPR/Cas system is primarily used among the existing programmable sequence-specific nucleases for targeted (epi)genome or RNA modifications in crops due to its simplicity and wide applicability [120, 123, 205, 206]. In recent years, plant viral vectors have shown promise in delivering nucleic acids into host plants to achieve targeted genome modifications [133, 207]. TGE was achieved via BSMV-mediated delivery of sgRNAs into wheat expressing *Cas9* constitutively [141, 142, 208]. This approach requires the generation of *Cas9*-expressing plants through a single genetic transformation procedure. Subsequently, using BSMVIGE, any gene can be targeted in this *Cas9*-expressing plant background. Therefore, it represents a rapid and easy-to-adopt plant genome editing approach. Since BSMV has been successfully used in barley as a VIGS vector [209, 210], this study focused on adopting BSMVIGE in barley.

5.2.2 Successful Implementation of BSMVIGE in Barley

The generation of *SpCas9*-expressing barley cv. GP (*ZmUBI::Cas9*), driven by the constitutive *ZmUBI* promoter, enabled BSMV-induced genome editing in barley. A strategy similar to that used by [141], was employed, involving Golden Gate-based cloning of a single gRNA into a generic BSMVIGE vector, followed by conventional tobacco leaf sap rub-inoculation of *ZmUBI::Cas9* plants. Somatic editing frequencies throughout infected plants were estimated using a Sanger sequencing-based method 5 wpi, which offers advantages over traditional NGS-based mutation detection approaches due to its simplicity, rapidity, and cost-effectiveness. As proof-of-principle target, *CMF7* (*ALBOSTRIANS*) was chosen [177]. Among first-generation (M1) BSMVIGE-inoculated *ZmUBI::Cas9* barley plants, a mean somatic mutation frequency of 57% and a mean mutation efficiency of 35%, ranging from zero to 94%, were observed. It involved a limited number of plants (in case of *CMF7*, n=14), contrasting with laborious conventional genetic transformation methods, which require the co-cultivation of a higher number of isolated immature embryos with *A. tumefaciens* carrying the desired transgene, followed by tissue regeneration [127].

5.2.3 Heritable Editing and BSMV Transmission in Progeny

Three M1 plants, confirmed for BSMV infection and exhibiting varied mutation efficiencies (0% (Null), 33% (Medium), and 94% (Highest)), were selected for heritable editing screening at the *CMF7* target site in their M2 progeny. This screening aimed to identify any correlation between the somatic mutation efficiency and heritable editing frequency in the first-generation BSMVIGE-*CMF7* inoculated *ZmUBI::Cas9* plants. Offspring from M1-Highest exhibited the highest heritable editing frequency of 76% while a moderate heritable editing frequency of 43% was found in M2 offspring from M1-Medium. Surprisingly, progenies screened from M1-Null exhibited a similar heritable editing frequency of 40% to that of M1-Medium. The unexpected presence of heritable editing observed in M1-null offspring raises two mutually non-exclusive possibilities: editing may have occurred in reproductive tissues, embryos, or offspring plants (due to the generative transmission of BSMV) but not in the somatic tissues examined, and/or the Sanger-based method used was not sensitive enough to detect low-frequency mutations. In any case, M1 plants, with comparatively high mutation frequencies, are obvious choices for screening for desired mutants in their offspring. Even within the M2 carrying BSMVIGE-induced mutations, albino or variegated plants were detected, indicating that the inherited mutations at the *CMF7* target site likely interfered with the *CMF7* protein translation, resulting in the complete loss of chloroplast activity. This mirrors the phenotype of mutants initially isolated through X-ray mutagenesis [211] and aligns with recent research identifying *CMF7* as the responsible gene in barley [177].

Germline transmission of BSMVIGE was found in barley at a higher frequency (63%) than in wheat (17%) [141]. This rate can vary depending on the stability of BSMV with the fused insert fragment [212], BSMV strain [213] and host genotype [214]. The effectiveness of barley grain treatments using acetic acid, hydrogen peroxide, hydrochloric acid, dry high temperature, sodium hypochlorite, ozone, UV, heated water, and antiviral drugs to eliminate seed-borne BSMV without impairing barley grain germination could be evaluated, as shown for other plant viruses [215]. Nevertheless, heritable editing was detected regardless of BSMV presence in both M2 and M3 generations. Hence, screening among M2 or M3 offspring for both inherited mutations and BSMV presence/absence can rapidly yield virus-free mutants as demonstrated here.

5.2.4 Rapid Isolation of Barley Mutants Using BSMVIGE

BSMVIGE enabled the isolation of plants defective for three meiosis-related genes, *ASY1*, *SCEP3*, and *ZYP1*. Somatic editing was achieved in M1 plants at frequencies of 38% (*ASY1-E4*), 33% (*ASY1-E6*), 36% (*ZYP1-E2*), and 45% (*ZYP1-E6*) across two independent target sites per gene. M1 plants with the highest somatic editing efficiency (74% for *ASY1-E4* and 89% for *ZYP1-E2*) were chosen to isolate M2 plants with inherited mutations at target sites. Four out of 15 (27%) and three out of 11 (27%) offspring plants exhibited diverse mutations at the target sites *ASY1-E4* and *ZYP1-E2*, respectively. Thus, it is possible to isolate offspring mutant plants with various editing events at target sites by screening a small number of plants, selected based on somatic mutation efficiency in M1 BSMVIGE-inoculated plants. An M2 plant with a homozygous mutation at *ASY1-E4* exhibited complete sterility. Hence, the likely phenotype caused by the inherited mutation is found already in the second generation, similar to the *CMF7* knockout using BSMVIGE in this study. However, a detailed characterization is required to decipher the phenotype of the corresponding mutant allele. Together, BSMVIGE is a reliable approach for achieving targeted gene knock-outs in barley, facilitating reverse genetic studies.

5.2.5 Insufficient BSMVIGE-Mediated Multiplexed Gene Editing Using MEA Strategy

Multiplexed TGE typically involves expressing various sgRNAs targeting different sites, assembled in tandem either with or without spacer elements such as tRNAs [216], or ribozyme sequences [217], that facilitate efficient cleavage of individual sgRNAs. These sgRNAs can be transcribed as a single transcriptional unit using one promoter-terminator combination or independently using individual promoters and terminators (polycistronic). Unlike TRV [218] or Potato virus X [219], expressing multiple sgRNAs in tandem within BSMV- γ might affect the stability of the virus, leading to the complete or partial loss of the inserted fragment [212, 220]. Therefore, an alternative approach, MEA, which had previously been demonstrated in wheat using BSMVIGE [141], was adopted in barley. Here, two sgRNAs targeting independent target sites, either in different genes (*CMF7* and *ZYP1-E6*) or within different exons of *ZYP1* gene (*ZYP1-E2* and *ZYP1-E6*) and the same exon of *HvSCEP3* gene (*SCEP3-E6-1* and *SCEP3-E6-2*), were expressed using two individual BSMV- γ components. In the first case, the mean editing frequencies were comparatively low, with 28% for *CMF7* and 14% for *ZYP1-E6*, compared to BSMVIGE targeting *CMF7* (57%) or *ZYP1-E6* (45%) individually. A single plant that exhibited editing at both target sites, with 14% mutation efficiency for *CMF7* and 21% mutation efficiency for *ZYP1-E6*, showed no heritable editing at either site among a limited number of progenies analyzed. On the other hand, targeting two sites within the same gene at different exons using BSMVIGE-MEA resulted in low mean editing frequencies (0% for *ZYP1-*

E2 and 14% for *ZYP1-E6*) in M1 plants while a higher mean somatic frequency of 36% was found with singleplex BSMVIGE at *ZYP1-E2*. Surprisingly, an M2 plant with a homozygous mutation at *ZYP1-E6* was isolated. However, no editing was detected in any of the analyzed progenies at the other *ZYP1* target site. In case of two targets within the same exon of *SCEP3*, low or no editing were observed (11% for *SCEP3-E6-1* and 0% for *SCEP3-E6-2*). However, two distinct *scep3* mutants were isolated. This indicates that BSMVIGE-mediated delivery of a single sgRNA targeting an individual site is more efficient in terms of both somatic editing efficiency/frequency and heritable editing rate compared to delivering two or more sgRNAs targeting different sites using the BSMVIGE-MEA strategy. However, plants carrying mutations at either of the targeted sites were still isolated.

In BSMVIGE-MEA, two infectious BSMV clones need to be generated, each containing a distinct BSMV- γ , by co-inoculating BSMV- α , BSMV- β , and the two BSMV- γ components in *N. benthamiana*. However, factors such as the super-exclusion of one BSMV clone over the other during systemic infection or recombination between the two BSMV- γ components cannot be ruled out. In this case, the presence of either one or both sgRNAs inserted into BSMV for induction of Cas9-mediated targeted DSBs at target sites may be limited, leading to inefficient editing. To tackle this, BSMV *in vitro* transcripts can be used to directly inoculate barley, bypassing the need for an intermediate host. This may increase the likelihood of multiple cognate sgRNAs being expressed through BSMVIGE before encountering recombination or super-exclusion issues, thereby facilitating editing at multiple targets [142, 208]. Alternatively, to stack multiple mutations in a given plant, BSMVIGE could be utilized to edit independent genes in already available mutant plants expressing *SpCas9*, which were isolated either through conventional transformation strategies or by BSMVIGE.

5.2.6 BSMVIGE: A Reliable Gene Editing Platform for Barley

BSMVIGE was also employed using *ZmUBI::Cas9* offspring, targeting six independent sites within five putative meiosis-related genes (*PCH2*, *CMT3a*, *CMT3b*, *MUS81a*, and *MUS81b*). Somatic editing frequencies ranging from 0 to 37% were found. Notably, somatic editing was achieved at only two target sites. The inefficiency of BSMVIGE in inducing TGE at certain targets may be due to the low efficiency of the selected sgRNAs, low *SpCas9* expression in offspring plants caused by transgene silencing, or a combination of both factors. Employing BSMVIGE with highly efficient sgRNAs, selected based on transient *in planta* cleavage assays in protoplasts isolated from *ZmUBI::Cas9* seedlings could address the first issue. However, for

BSMVIGE, the sgRNAs are expressed under the native γ b promoter instead of the more common pol III promoter used in traditional protoplast sgRNA cleavage assays [221]. Therefore, the protoplast assay should be adapted to accommodate the BSMVIGE-sgRNA delivery system or to select plants that express high levels of *SpCas9* before BSMVIGE-inoculation. In wheat, the efficiency of BSMVIGE was notably enhanced when a wheat transgenic line with high *SpCas9* expression was utilized [208]. Consequently, it is crucial to identify and isolate a high *SpCas9*-expressing line among the existing DH barley cv. GP lines that carry the *SpCas9* transgene. This investigation could significantly improve the efficacy of BSMVIGE in barley, similar to wheat. To further enhance the efficiency of the BSMVIGE approach in barley, different *Cas* variants, such as a highly efficient modified *Cas9* containing introns [222, 223], or the use of different promoters [224, 225], could be tested.

5.2.7 Enhancing the BSMVIGE Strategy in Barley and Other Crops: Further Insights

In *A. thaliana* [226] and *N. benthamiana* [218], fusing tRNAs or mobile RNA elements such as flowering locus T (FT) to gRNAs delivered by TRV was shown to increase heritable editing frequency. In contrast, no difference in editing was found between FT-fused and unmodified sgRNAs in cotton using a CLCrV vector [227]. Also, in wheat, the results varied, with reports indicating both increased and decreased heritability of induced mutations when RNA elements were fused to gRNAs in BSMV [142, 208]. These inconsistencies might be attributed to variations in the lengths and types of fusion RNAs used and the impact of adding tRNAs or FT sequences on viral stability. Additionally, the viral vector and the host or even the host genotype can influence the efficiency of (heritable) editing. In barley, at least five FT-like homologs [228] and multiple tRNA species, as commonly present in higher plants [229], are found. Future studies should explore whether adding tRNA or mobile RNA sequences to gRNAs can enhance BSMV-mediated (heritable) editing at target sites in barley cv GP.

Currently, the BSMVIGE approach is limited to barley cv. GP due to the availability of *Cas9* expressing transgenic lines. However, there are several ways to expand its application in barley. One option is to generate additional barley cultivars that stably express *Cas9*. Alternatively, the existing *Cas9* transgene could be introgressed into other cultivars of interest [142, 208]. Given the availability of haploid inducer barley lines [230], a novel strategy could be employed to induce mutations in cultivars of interest. This involves pollinating the desired cultivars with anthers isolated from donor *Cas9*-expressing haploid inducer barley lines that are infected with BSMV carrying the desired gRNA(s). This method could facilitate the isolation of *Cas9*-free

doubled-haploid recipient plants that possess BSMVIGE-induced mutations, thus expanding the potential for targeted genetic modifications.

Moreover, the transient delivery of complete genome editing reagents using BSMV could facilitate desired genome modifications in barley genotypes that are not amenable to genetic transformation, without integrating any foreign DNA. Unfortunately, the current BSMVIGE vector cannot deliver large gene fragments, such as the *SpCas9* gene. However, a reconstructed four-component BSMV system with increased cargo capacity, in which BSMV- γ was split into two components, has been utilized to deliver genes up to 2 kb in wheat [231]. This new BSMV vector has recently enabled transient somatic editing in cotton by delivering split *SpCas9*, although it did not achieve heritable editing [232]. It remains to be determined if a similar strategy can achieve reliable and frequent heritable editing in barley. Given the cargo capacity limitation of BSMV, smaller Cas variants, such as *Syntrophomonas palmitatica* Cas12f (497 aa) [233] and *Acidibacillus sulfuroxidans* Cas12f (422 aa) [234], can be tested using four-component BSMV to achieve efficient TGE in barley. In addition, the co-inoculation of two compatible viral vectors carrying distinct gene editing reagents can be explored in barley, as demonstrated in tobacco using PVX and TRV vectors [235]. For example, FoMV has been successfully used to deliver heterologous proteins up to 600 amino acids in wheat [236], and it is also capable of infecting barley [146]. Therefore, a FoMV-BSMV co-inoculation strategy can be tested to deliver split Cas9 and compatible sgRNA(s), aiming to achieve transgene-independent TGE in barley.

In addition to barley and wheat, BSMV is capable of infecting a variety of other cereal crops, including oat, maize, rice, rye, sorghum, and millet [149, 155, 237, 238]. Given that established genetic transformation protocols exist for these crops, such as for oats [239], maize [240], rice [241], rye [242], sorghum [243], and pearl millet [244], it is feasible to generate transgenic lines expressing Cas proteins in these species. Consequently, the BSMVIGE strategy can potentially be adapted and applied to these cereal crops for efficient genome editing.

5.3 Impaired Meiosis in SC Mutants

In most species - including flies, mice, worms, and *Sordaria* - the absence of the SC impairs CO formation [245]. In contrast, the SC appears to be dispensable for CO formation in some plant species, such as *A. thaliana* and rice [43, 81, 246]. Although the SC is structurally conserved across eukaryotes, its protein components show low sequence conservation [247].

Studies in *A. thaliana* using TF mutants (*zyp1a/b*) [43, 81]) and CE mutants (*scep1-3*) [12, 13] indicate that the SC itself is not essential for CO formation. Rather, it seems to regulate or even limit the number and distribution of CO. Specifically, SC formation seems to implement the obligate CO (ensuring at least one CO per homologous pair for proper segregation), CO interference, and heterochiasmy [43]. In rice, TF mutants (partial loss of function of *OsZEP1*) showed increased CO rates in specific chromosomal regions [109]. In contrast, RNAi-mediated knockdown of *ZYP1* in barley leads to reduced CO numbers, resembling the phenotype observed in *A. thaliana* upon RNAi-mediated *ZYP1* downregulation [11, 110]. These findings suggest that a partially formed or disrupted SC may hinder CO formation more severely than its complete absence, which may instead exhibit inhibitory effects on CO formation. To address that question, both *zyp1* and *scep3* knockout mutants in barley (no functional protein is detectable in any allele) were isolated. Importantly, immunolocalization studies of axis (*ASY1*) and SC components (*ZYP1* and *SCEP3*) showed that the barley WT SC is composed of similar components as in other plant species. Strikingly, depletion of *ZYP1* and *SCEP3* reveals that the complete absence of the SC (in both TF and CE mutants) results in a high frequency of univalents and only a few residual chiasmata. This suggests that, unlike in Arabidopsis and rice, the SC in barley is essential for CO formation rather than restricting it. These contrasting phenotypes highlight a fundamental difference in SC function between barley and other model plants. Further research is needed to elucidate the nature and distribution of residual CO/chiasmata in barley and to uncover the mechanisms underlying this divergence. Potential explanations include species-specific factors such as the spatiotemporal asymmetry of meiotic progression in barley, differences in genome size and chromosomal architecture, or variations in axis length and DSB density. These hypotheses warrant investigation in future studies.

5.4 BSMV-mediated Virus-Induced Gene Silencing (BSMVIGS) in Barley

In the case of stable genetic knockouts using CRISPR-Cas9, the target gene is completely disrupted, resulting in a loss of function. In contrast, VIGS leads to transient degradation of target transcripts, often causing variable phenotypic expression [248]. It was hypothesized that transient downregulation of *RECQ4* transcripts might lead to an increase in male CO rates within the tested intervals in barley, albeit to a lesser extent than the significant increase observed in *recq4* mutants. However, BSMVIGS targeting the anti-CO gene *RECQ4* resulted in no significant alteration in male CO rates within the tested genetic intervals on chromosome

1 among WT, control (empty or mock BSMV constructs), and BSMVIGS-treated F2 plant populations. This raises two key questions: (1) the efficacy of BSMVIGS in downregulating target transcripts in reproductive cells and (2) the potential haploinsufficiency of *RECQ4*. These questions can be addressed by assessing the effect of BSMVIGS-mediated *RECQ4* downregulation in barley *zmm* mutants, such as *msh4* or *hei10*, where class I CO are absent. If the downregulation of *RECQ4* restores fertility in these mutants, similar to observations in the stable knockout mutant [112], it would provide further insight into the efficacy of BSMVIGS in hybrid barley. Further, it is worthwhile to evaluate BSMVIGS-mediated downregulation of meiosis-specific genes known to be haploinsufficient or dosage-sensitive, such as *HEI10* and *ASY1*, in reproductive tissues, particularly in anthers, to assess the efficacy of the BSMVIGS approach.

6 Outlook

Based on the findings of the current work, in future, the following points should be addressed:

- Evaluate different treatments, such as enzymatic or chemical digestion of pollen nuclei, or employ vegetative or generative pollen nuclei separately, to possibly improve pollen nuclei accessibility and hence enhance the multiplex Single Pollen Nucleus Genotyping (SNPG) efficiency.
- Dissect crossover (CO) rate plasticity across different chromosomal regions in response to various influences such as genetic factors (meiosis-related genes or other (epi)genetic players), environmental cues, or abiotic/biotic stresses using multiplex SNPG.
- Implement the new Ruby™ crystal digital (d)PCR chips to achieve higher throughput and reduce the costs associated with multiplex SNPG.
- Adapt a rapid Barley Stripe Mosaic Virus (BSMV) screening method, such as Enzyme-Linked Immunosorbent Assay (ELISA), to test for BSMV presence/absence directly in grains. Further, investigate various grain treatments, including hydrogen peroxide, dry high temperature, sodium hypochlorite, Ultraviolet and heated water, to eliminate seed-borne BSMV.
- Test whether BSMV *in vitro* transcripts as starting inoculum improve the multiplex Barley Stripe Mosaic Virus-Induced Genome Editing (BSMVIGE) heritable editing frequency in barley. Isolate plants expressing either high *SpCas9* levels or different *Cas* variants (such as intron-optimised *Cas9*) and test whether BSMVIGE efficiency can be further improved in barley. Introduce the *SpCas9* transgene into other barley cultivars.
- Identify *pch2* and *mus81a* mutants by screening the progeny of M1 plants that showed the highest somatic editing efficiency.
- Dissect the origin and distribution of residual CO in barley SC mutants (*zyp1* and *scep3*) and uncover mechanisms behind differences in SC requirements for CO formation between barley and other plants, including potential species-specific factors such as meiotic progression timing, genome organization, axis length and Double-Strand Break (DSB) density.
- Assess the efficacy of Barley Stripe Mosaic Virus-Induced Gene Silencing (BSMVIGS) for targeted downregulation of meiotic transcripts, facilitating rapid reverse genetic studies of barley meiosis.

7 Summary

The tools developed and applied in this work - multiplex crystal digital PCR-based single nucleus pollen genotyping (multiplex SNP-G) and Barley stripe mosaic virus-induced genome editing (BSMVIGE) or gene silencing (BSMVIGS) - enable rapid studies of meiosis-related genes and their influence on crossover (CO) rates in barley. Hence, they enable to explore approaches to modify the barley meiotic recombination landscape. The key findings of the current research are summarized as follows:

- A multiplex SNP-G approach was established that enables to measure male CO rates, including CO interference strength, within two linked genetic intervals on chromosomes 1 and 3 in hybrid barley cv. Golden Promise (GP) x Barke (B) pollen, simultaneously.
- A freezing-based anther storage method, combined with efficient pollen nuclei isolation, facilitates multiplex SNP-G from plants grown at different times and locations.
- Using multiplex SNP-G, up to four-fold enhanced male CO rates in hybrids defective for the anti-CO gene *RECQ4*, were found. Additionally, CO rates were found to be consistent across anthers from different spikes and within individual spikes, suggesting tight CO rate regulation in barley and no impact on CO rates by the plant age or development.
- BSMVIGE was successfully implemented in barley cv. GP plants that express *SpCas9*. Somatic and heritable editing at the *ALBOSTRIANS* locus (*CMF7*) was demonstrated as a proof-of-concept. While germline transmission of BSMV was found, BSMVIGE-induced mutations were inherited independently of virus transmission in offspring.
- BSMVIGE was used to isolate barley plants defective for three meiosis-related genes, *ASY1*, *ZYP1* and *SCEP3*. Somatic editing was successfully achieved in several further putative meiosis-related genes, including *PCH2* and *MUS81a*.
- While depletion of the synaptonemal complex (SC) increases genetic CO frequency in Arabidopsis, in barley, SC depletion in *zyp1* and *scep3* drastically reduces chiasmata and severely impairs fertility, indicating the SC is required for CO formation in barley.
- Multiplex BSMVIGE targeting two sites in different or the same gene resulted in lower somatic and heritable editing frequencies compared to single plex BSMVIGE.
- BSMVIGS was employed for the transient downregulation of *RECQ4* transcripts, but CO rate measurements using multiplex SNP-G showed no change within the tested intervals in BSMVIGS-treated samples compared to controls.

8 Zusammenfassung

Die in dieser Arbeit entwickelten und angewandten Methoden - *multiplex crystal digital PCR*-basierende Einzelpollenzellkerngenotypisierung (*multiplex SNP*) und *Barley Stripe Mosaic Virus*-induzierte Genom-Editierung (*BSMVIGE*) oder *Gene Silencing* (*BSMVIGS*) - ermöglichen eine schnelle Analyse meiotischer Gene und deren Einfluss auf die meiotische Rekombinationsrate (*crossover*, CO) in der Gerste. Somit ermöglichen sie die Erforschung von Ansätzen zur Modifikation der meiotischen Rekombinationslandschaft der Gerste.

Die wesentlichen Erkenntnisse dieser Arbeit sind wie folgt zusammengefasst:

- Ein *multiplex SNP* Ansatz wurde etabliert, der es ermöglicht, männliche CO-Raten, einschließlich CO-Interferenzstärke, in zwei gekoppelten genetischen Intervallen auf den Chromosomen 1 und 3 in Hybridgerste (cv. Golden Promise x Barke) zu messen.
- Ein Gefrierspeicher-Verfahren für Antheren, kombiniert mit effizienter Pollenkernisolierung, ermöglicht *multiplex SNP* bei Pflanzen, die zu unterschiedlichen Zeiten oder an verschiedenen Orten gewachsen sind.
- Mittels *multiplex SNP* wurden um bis zu vierfach erhöhte männliche CO-Raten in Hybridgerste mit defektem anti-CO Gen *RECQ4* gefunden. Weiterhin waren CO-Raten in Antheren verschiedener Ähren und innerhalb einzelner Ähren vergleichbar, was auf eine strikte Regulation von CO-Raten in der Gerste ohne substantiellen Einfluss vom Pflanzenalter oder Entwicklung hinweist.
- *BSMVIGE* wurde erfolgreich in *SpCas9*-exprimierender Gerste (cv. Golden Promise) implementiert. Somatische und vererbare Editierungen am *ALBOSTRIANS*-Locus (*CMF7*) wurden als *Proof-of-Concept* demonstriert. Obwohl eine Übertragung von BSMV über die Keimbahn festgestellt wurde, erfolgte die Vererbung *BSMVIGE*-induzierter Mutationen unabhängig von der Virusübertragung.
- Mittels *BSMVIGE* wurden Gerstenpflanzen mit Mutationen in drei meiotischen Genen (*ASY1*, *ZYP1* und *SCEP3*) isoliert. Zudem wurden in mehreren weiteren potentiellen meiotischen Genen wie *PCH2* und *MUS81a* somatische Editierungen erzielt.
- Während das Fehlen des synaptonomalen Komplexes (SC) in Arabidopsis zu einer CO-Erhöhung führt, kommt es in der Gerste in den SC-Mutanten *zyp1* und *scep3* zu einer starken Chiasmata-Abnahme und einer schwerwiegenden Verminderung der Fertilität. Dies deutet darauf hin, dass der SC in der Gerste essenziell für die CO-Ausbildung ist.

- Die gleichzeitige Ansteuerung von zwei Stellen in einem Gen oder in unterschiedlichen Genen mittels BSMVIGE (*multiplex*) führte zu niedrigeren somatischen und vererbten Editierfrequenzen im Vergleich zu *singleplex* BSMVIGE.
- BSMVIGS wurde zur transienten *Downregulation* von *RECQ4*-Transkripten eingesetzt. Die resultierenden CO-Raten, gemessen mittels *multiplex SNP*, zeigten jedoch keine Änderung innerhalb der getesteten Intervalle in BSMVIGS-behandelten Proben im Vergleich zu Kontrollen.

9 References

1. Mercier, R., et al., *The molecular biology of meiosis in plants*. Annual Review of Plant Biology, 2015. 66: p. 297-327.
2. Ohkura, H., *Meiosis: An Overview of Key Differences from Mitosis*. Cold Spring Harbor Perspectives in Biology, 2015. 7(5): p. a015859.
3. Armstrong, S.J. and G.H. Jones, *Meiotic cytology and chromosome behaviour in wild-type Arabidopsis thaliana*. Journal of experimental botany, 2003. 54(380): p. 1-10.
4. Johnston, S.E., *Understanding the Genetic Basis of Variation in Meiotic Recombination: Past, Present, and Future*. Molecular Biology and Evolution, 2024. 41(7).
5. Lam, W.S., X. Yang, and C.A. Makaroff, *Characterization of Arabidopsis thaliana SMC1 and SMC3: evidence that AtSMC3 may function beyond chromosome cohesion*. Journal of cell science, 2005. 118(14): p. 3037-3048.
6. Bhatt, A.M., et al., *The DIF1 gene of Arabidopsis is required for meiotic chromosome segregation and belongs to the REC8/RAD21 cohesin gene family*. The Plant Journal, 1999. 19(4): p. 463-472.
7. Cai, X., et al., *The Arabidopsis SYN1 cohesin protein is required for sister chromatid arm cohesion and homologous chromosome pairing*. Journal of cell science, 2003. 116(14): p. 2999-3007.
8. Yoon, S.-W., et al., *Meiotic prophase roles of Rec8 in crossover recombination and chromosome structure*. Nucleic acids research, 2016. 44(19): p. 9296-9314.
9. Armstrong, S.J., et al., *Asy1, a protein required for meiotic chromosome synapsis, localizes to axis-associated chromatin in Arabidopsis and Brassica*. Journal of Cell Science, 2002. 115(18): p. 3645-3655.
10. Ferdous, M., et al., *Inter-homolog crossing-over and synapsis in Arabidopsis meiosis are dependent on the chromosome axis protein AtASY3*. PLoS genetics, 2012. 8(2): p. 1002507.
11. Higgins, J.D., et al., *The Arabidopsis synaptonemal complex protein ZYP1 is required for chromosome synapsis and normal fidelity of crossing over*. Genes & development, 2005. 19(20): p. 2488-2500.
12. Vrielynck, N., et al., *SCEP1 and SCEP2 are two new components of the synaptonemal complex central element*. Nature Plants, 2023. 9(12): p. 2016-2030.

13. Feng, C., et al., *The synaptonemal complex central element SCEP3 interlinks synapsis initiation and crossover formation in Arabidopsis thaliana*. *Nature Plants*, 2025: p. 1-14.
14. Grelon, M., et al., *AtSPO11-1 is necessary for efficient meiotic recombination in plants*. *The EMBO journal*, 2001. 20: p. 589-600.
15. Hartung, F., et al., *The catalytically active tyrosine residues of both SPO11-1 and SPO11-2 are required for meiotic double-strand break induction in Arabidopsis*. *The Plant Cell*, 2007. 19(10): p. 3090-3099.
16. Stacey, N.J., et al., *Arabidopsis SPO11-2 functions with SPO11-1 in meiotic recombination*. *The Plant Journal*, 2006. 48(2): p. 206-216.
17. Vrielynck, N., et al., *A DNA topoisomerase VI-like complex initiates meiotic recombination*. *Science*, 2016. 351(6276): p. 939-943.
18. De Muyt, A., et al., *AtPRD1 is required for meiotic double strand break formation in Arabidopsis thaliana*. *The EMBO journal*, 2007. 26(18): p. 4126-4137.
19. Lambing, C., et al., *Differentiated function and localisation of SPO11-1 and PRD3 on the chromosome axis during meiotic DSB formation in Arabidopsis thaliana*. *PLoS genetics*, 2022. 18(7): p. e1010298.
20. Zhang, C., et al., *The Arabidopsis thaliana DSB formation (AtDFO) gene is required for meiotic double-strand break formation*. *The Plant Journal*, 2012. 72(2): p. 271-281.
21. Vance, V. and Vaucheret, H., *RNA silencing in plants--defense and counterdefense*. *Science*, 2001. 292(5525), p. 2277-2280.
22. De Muyt, A., et al., *A high throughput genetic screen identifies new early meiotic recombination functions in Arabidopsis thaliana*. *PLoS genetics*, 2009. 5(9): p. 1000654.
23. Bleuyard, J.-Y., M.E. Gallego, and C.I. White, *Meiotic defects in the Arabidopsis rad50 mutant point to conservation of the MRX complex function in early stages of meiotic recombination*. *Chromosoma*, 2004. 113: p. 197-203.
24. Waterworth, W.M., et al., *NBS1 is involved in DNA repair and plays a synergistic role with ATM in mediating meiotic homologous recombination in plants*. *The Plant Journal*, 2007. 52(1): p. 41-52.
25. Puizina, J., et al., *Mre11 deficiency in Arabidopsis is associated with chromosomal instability in somatic cells and Spo11-dependent genome fragmentation during meiosis*. *The Plant Cell*, 2004. 16(8): p. 1968-1978.

26. Uanschou, C., et al., *A novel plant gene essential for meiosis is related to the human CtIP and the yeast COM1/SAE2 gene*. The EMBO Journal, 2007. 26(24): p. 5061-5070.
27. Aklilu, B.B., R.S. Soderquist, and K.M. Culligan, *Genetic analysis of the Replication Protein A large subunit family in Arabidopsis reveals unique and overlapping roles in DNA repair, meiosis and DNA replication*. Nucleic Acids Research, 2014. 42(5): p. 3104-3118.
28. Da Ines, O., et al., *Meiotic recombination in Arabidopsis is catalysed by DMC1, with RAD51 playing a supporting role*. PLoS genetics, 2013. 9(9): p. e1003787.
29. Doutriaux, M.-P., et al., *Isolation and characterisation of the RAD51 and DMC1 homologs from Arabidopsis thaliana*. Molecular and General Genetics MGG, 1998. 257: p. 283-291.
30. Singh, G., et al., *Analysis of the impact of the absence of RAD51 strand exchange activity in Arabidopsis meiosis*. PLoS One, 2017. 12(8): p. e0183006.
31. West, S.C., et al. *Resolution of recombination intermediates: mechanisms and regulation*. In Cold Spring Harbor symposia on quantitative biology, 2015. 80: p. 103-109.
32. Longhese, M.P., et al., *DNA double-strand breaks in meiosis: checking their formation, processing and repair*. DNA repair, 2009. 8(9): p. 1127-1138.
33. Chelysheva, L., et al., *The Arabidopsis HEI10 Is a New ZMM Protein Related to Zip3*. PLOS Genetics, 2012. 8(7): p. e1002799.
34. Pyatnitskaya, A., V. Borde, and A. De Muyt, *Crossing and zipping: molecular duties of the ZMM proteins in meiosis*. Chromosoma, 2019. 128(3): p. 181-198.
35. Ziolkowski, P.A., *Why do plants need the ZMM crossover pathway? A snapshot of meiotic recombination from the perspective of interhomolog polymorphism*. Plant Reproduction, 2023. 36(1): p. 43-54.
36. Wang, S., et al., *Meiotic crossover patterns: obligatory crossover, interference and homeostasis in a single process*. Cell cycle, 2015. 14(3): p. 305-314.
37. Sidhu, G.K., et al., *Recombination patterns in maize reveal limits to crossover homeostasis*. Proceedings of the National Academy of Sciences, 2015. 112(52): p. 15982-15987.
38. Berchowitz, L.E., et al., *The Role of AtMUS81 in Interference-Insensitive Crossovers in A. thaliana*. PLOS Genetics, 2007. 3(8): p. 132.
39. Kurzbauer, M.-T., et al., *Arabidopsis thaliana FANCD2 promotes meiotic crossover formation*. The Plant Cell, 2018. 30(2): p. 415-428.

40. Steckenborn, S., et al., *The meiotic topoisomerase VI B subunit (MTOPVIB) is essential for meiotic DNA double-strand break formation in barley (Hordeum vulgare L.)*. *Plant Reproduction*, 2023. 36(1): p. 1-15.
41. Fozard, J.A., C. Morgan, and M. Howard, *Coarsening dynamics can explain meiotic crossover patterning in both the presence and absence of the synaptonemal complex*. *Elife*, 2023. 12: p. 79408.
42. Morgan, C., et al., *Diffusion-mediated HEI10 coarsening can explain meiotic crossover positioning in Arabidopsis*. *Nature Communications*, 2021. 12(1): p. 4674.
43. Capilla-Pérez, L., et al., *The synaptonemal complex imposes crossover interference and heterochiasmy in Arabidopsis*. *Proceedings of the National Academy of Sciences*, 2021. 118(12): p. e2023613118.
44. Durand, S., et al., *Joint control of meiotic crossover patterning by the synaptonemal complex and HEI10 dosage*. *Nature communications*, 2022. 13(1): p. 5999.
45. Séguéla-Arnaud, M., et al., *Multiple mechanisms limit meiotic crossovers: TOP3α and two BLM homologs antagonize crossovers in parallel to FANCM*. *Proceedings of the National Academy of Sciences*, 2015. 112(15): p. 4713-4718.
46. Girard, C., et al., *AAA-ATPase FIDGETIN-LIKE 1 and Helicase FANCM Antagonize Meiotic Crossovers by Distinct Mechanisms*. *PLOS Genetics*, 2015. 11(7): p. e1005369.
47. Girard, C., et al., *FANCM-associated proteins MHF1 and MHF2, but not the other Fanconi anemia factors, limit meiotic crossovers*. *Nucleic Acids Research*, 2014. 42(14): p. 9087-9095.
48. Mieulet, D., et al., *Unleashing meiotic crossovers in crops*. *Nature Plants*, 2018. 4(12): p. 1010-1016.
49. Crismani, W., et al., *FANCM limits meiotic crossovers*. *Science*, 2012. 336(6088): p. 1588-1590.
50. Blary, A., et al., *FANCM Limits Meiotic Crossovers in Brassica Crops*. *Frontiers in Plant Science*, 2018. Volume 9 - 2018.
51. Li, Y., et al., *RECQ4 restricts non-interfering crossover formation to fine-tune meiotic recombination rates in rice*. *Plant Biotechnology Journal*, 2025.
52. Morgan, C., M. Howard, and I.R. Henderson, *HEI10 coarsening, chromatin and sequence polymorphism shape the plant meiotic recombination landscape*. *Current Opinion in Plant Biology*, 2024. 81: p. 102570.
53. Choi, K. and I.R. Henderson, *Meiotic recombination hotspots—a comparative view*. *The Plant Journal*, 2015. 83(1): p. 52-61.

54. Choi, K., et al., *Nucleosomes and DNA methylation shape meiotic DSB frequency in Arabidopsis thaliana transposons and gene regulatory regions*. Genome Research, 2018. 28(4): p. 532-546.
55. Lambing, C., et al., *ASY1 acts as a dosage-dependent antagonist of telomere-led recombination and mediates crossover interference in Arabidopsis*. Proceedings of the National Academy of Sciences, 2020. 117(24): p. 13647-13658.
56. Lambing, C., et al., *Interacting Genomic Landscapes of REC8-Cohesin, Chromatin, and Meiotic Recombination in Arabidopsis*. The Plant Cell, 2020. 32(4): p. 1218-1239.
57. Underwood, C.J., et al., *Epigenetic activation of meiotic recombination near Arabidopsis thaliana centromeres via loss of H3K9me2 and non-CG DNA methylation*. Genome Research, 2018. 28(4): p. 519-531.
58. Yelina, N.E., et al., *Epigenetic Remodeling of Meiotic Crossover Frequency in Arabidopsis thaliana DNA Methyltransferase Mutants*. PLOS Genetics, 2012. 8(8): p. e1002844.
59. Phillips, D., et al., *Quantitative high resolution mapping of HvMLH3 foci in barley pachytene nuclei reveals a strong distal bias and weak interference*. Journal of Experimental Botany, 2013. 64(8): p. 2139-2154.
60. Higgins, J.D., et al., *Factors underlying restricted crossover localization in barley meiosis*. Annual review of genetics, 2014. 48(1): p. 29-47.
61. Choulet, F., et al., *Structural and functional partitioning of bread wheat chromosome 3B*. Science, 2014. 345(6194): p. 1249721.
62. Darrier, B., et al., *High-resolution mapping of crossover events in the hexaploid wheat genome suggests a universal recombination mechanism*. Genetics, 2017. 206(3): p. 1373-1388.
63. Gardiner, L.-J., et al., *Analysis of the recombination landscape of hexaploid bread wheat reveals genes controlling recombination and gene conversion frequency*. Genome Biology, 2019. 20: p. 1-16.
64. Dreissig, S., M. Mascher, and S. Heckmann, *Variation in recombination rate is shaped by domestication and environmental conditions in barley*. Molecular biology and evolution, 2019. 36(9): p. 2029-2039.
65. Phillips, D., et al., *High Resolution Analysis of Meiotic Chromosome Structure and Behaviour in Barley (Hordeum vulgare L.)*. PLOS ONE, 2012. 7(6): p. e39539.
66. Lambing, C. and S. Heckmann, *Tackling Plant Meiosis: From Model Research to Crop Improvement*. Frontiers in Plant Science, 2018. 9.

67. Sreenivasulu, N., A. Graner, and U. Wobus, *Barley Genomics: An Overview*. International Journal of Plant Genomics, 2008. 2008: p. 1-13.
68. Jayakodi, M., et al., *The barley pan-genome reveals the hidden legacy of mutation breeding*. Nature, 2020. 588(7837): p. 284-289.
69. Choi, K., *Advances towards Controlling Meiotic Recombination for Plant Breeding*. Mol Cells, 2017. 40(11): p. 814-822.
70. Blary, A. and E. Jenczewski, *Manipulation of crossover frequency and distribution for plant breeding*. Theoretical and Applied Genetics, 2019. 132(3): p. 575-592.
71. Fayos, I., et al., *Manipulation of Meiotic Recombination to Hasten Crop Improvement*. Biology, 2022. 11(3): p. 369.
72. Epstein, R., et al., *Exploring impact of recombination landscapes on breeding outcomes*. Proceedings of the National Academy of Sciences, 2023. 120(14): p. 2205785119.
73. Dirks, R., et al., *Reverse breeding: a novel breeding approach based on engineered meiosis*. Plant Biotechnology Journal, 2009. 7(9): p. 837-845.
74. Kuo, P., O. Da Ines, and C. Lambing, *Rewiring meiosis for crop improvement*. Frontiers in Plant Science, 2021. 12: p. 708948.
75. d'Erfurth, I., et al., *Turning meiosis into mitosis*. PLoS biology, 2009. 7(6): p. 1000124.
76. De Storme, N. and D. Geelen, *The Arabidopsis mutant jason produces unreduced first division restitution male gametes through a parallel/fused spindle mechanism in meiosis II*. Plant physiology, 2011. 155(3): p. 1403-1415.
77. d'Erfurth, I., et al., *Mutations in AtPSI (Arabidopsis thaliana parallel spindle 1) lead to the production of diploid pollen grains*. PLoS genetics, 2008. 4(11): p. e1000274.
78. d'Erfurth, I., et al., *The cyclin-A CYCA1; 2/TAM is required for the meiosis I to meiosis II transition and cooperates with OSD1 for the prophase to first meiotic division transition*. PLoS genetics, 2010. 6(6): p. 1000989.
79. Mieulet, D., et al., *Turning rice meiosis into mitosis*. Cell Research, 2016. 26(11): p. 1242-1254.
80. Wang, Y., et al., *Harnessing clonal gametes in hybrid crops to engineer polyploid genomes*. Nature Genetics, 2024. 56(6): p. 1075-1079.
81. France, M.G., et al., *ZYP1 is required for obligate cross-over formation and cross-over interference in Arabidopsis*. Proceedings of the National Academy of Sciences, 2021. 118(14): p. 2021671118.

82. Cuacos, M., et al., *Meiotic chromosome axis remodelling is critical for meiotic recombination in Brassica rapa*. *Journal of Experimental Botany*, 2021. 72(8): p. 3012-3027.
83. Scheben, A., J. Batley, and D. Edwards, *Revolution in genotyping platforms for crop improvement*. *Plant Genetics and Molecular Biology*, 2018: p. 37-52.
84. Bayer, M.M., et al., *Development and evaluation of a barley 50k iSelect SNP array*. *Frontiers in plant science*, 2017. 8: p. 1792.
85. Abed, A., et al., *A high-resolution consensus linkage map for barley based on GBS-derived genotypes*. *Genome*, 2022. 65(2): p. 83-94.
86. Raz, A., et al., *Redistribution of meiotic crossovers along wheat chromosomes by virus-induced gene silencing*. *Frontiers in plant science*, 2021. 11: p. 635139.
87. Gardiner, L.J., et al., *Analysis of the recombination landscape of hexaploid bread wheat reveals genes controlling recombination and gene conversion frequency*. *Genome Biol*, 2019. 20(1): p. 69.
88. Lian, Q., et al., *The megabase-scale crossover landscape is largely independent of sequence divergence*. *Nature communications*, 2022. 13(1): p. 3828.
89. Sun, H., et al., *Linked-read sequencing of gametes allows efficient genome-wide analysis of meiotic recombination*. *Nature communications*, 2019. 10(1): p. 4310.
90. Dreissig, S., et al., *Measuring meiotic crossovers via multi-locus genotyping of single pollen grains in barley*. *PLoS One*, 2015. 10(9): p. e0137677.
91. Dreissig, S., et al., *Sequencing of single pollen nuclei reveals meiotic recombination events at megabase resolution and circumvents segregation distortion caused by postmeiotic processes*. *Frontiers in plant science*, 2017. 8: p. 1620.
92. Roy, B., G.P. Copenhaver, and A.G. von Arnim, *Fluorescence-Tagged Transgenic Lines Reveal Genetic Defects in Pollen Growth—Application to the Eif3 Complex*. *PLoS ONE*, 2011. 6(3).
93. Francis, K.E., et al., *Pollen tetrad-based visual assay for meiotic recombination in Arabidopsis*. *Proceedings of the national academy of sciences*, 2007. 104(10): p. 3913-3918.
94. Yelina, N.E., et al., *High-throughput analysis of meiotic crossover frequency and interference via flow cytometry of fluorescent pollen in Arabidopsis thaliana*. *Nature Protocols*, 2013. 8(11): p. 2119-2134.
95. Poethig, R.S., et al., *Short-interval traffic lines: versatile tools for genetic analysis in Arabidopsis thaliana*. *G3 Genes|Genomes|Genetics*, 2022. 12(10).

96. Melamed-Bessudo, C., et al., *A new seed-based assay for meiotic recombination in Arabidopsis thaliana*. The Plant Journal, 2005. 43(3): p. 458-466.
97. Lim, E.C., et al., *DeepTetrad: high-throughput image analysis of meiotic tetrads by deep learning in Arabidopsis thaliana*. The Plant Journal, 2020. 101(2): p. 473-483.
98. Kbiri, N., et al., *Quantifying Meiotic Crossover Recombination in Arabidopsis Lines Expressing Fluorescent Reporters in Seeds Using SeedScoring Pipeline for CellProfiler*. In Plant Gametogenesis: Methods and Protocols. 2022, Springer. p. 121-134.
99. Nageswaran, D.C., et al., *HIGH CROSSOVER RATE1 encodes PROTEIN PHOSPHATASE XI and restricts meiotic crossovers in Arabidopsis*. Nature plants, 2021. 7(4): p. 452-467.
100. Modliszewski, J.L., et al., *Elevated temperature increases meiotic crossover frequency via the interfering (Type I) pathway in Arabidopsis thaliana*. PLoS genetics, 2018. 14(5): p. 1007384.
101. Blackwell, A.R., et al., *MSH2 shapes the meiotic crossover landscape in relation to interhomolog polymorphism in Arabidopsis*. The EMBO Journal, 2020. 39(21): p. 104858.
102. Li, F., N. De Storme, and D. Geelen, *Dynamics of male meiotic recombination frequency during plant development using fluorescent tagged lines in Arabidopsis thaliana*. Scientific Reports, 2017. 7(1): p. 42535.
103. Gratiyas, A. and V. Geffroy, *Deciphering the Impact of a Bacterial Infection on Meiotic Recombination in Arabidopsis with Fluorescence Tagged Lines*. Genes, 2020. 11(7): p. 832.
104. Ahn, Y.-J., et al., *High-throughput measuring of meiotic recombination rates in barley pollen nuclei using Crystal Digital PCRTM*. The Plant Journal, 2021. 107(2): p. 649-661.
105. Basu, A.S., *Digital Assays Part I: Partitioning Statistics and Digital PCR*. SLAS TECHNOLOGY: Translating Life Sciences Innovation, 2017. 22(4): p. 369-386.
106. Quan, P.-L., M. Sauzade, and E. Brouzes, *dPCR: A Technology Review*. Sensors, 2018. 18(4): p. 1271.
107. Tan, L.L., et al., *Current commercial dPCR platforms: technology and market review*. Crit Rev Biotechnol, 2023. 43(3): p. 433-464.
108. Madic, J., et al., *Three-color crystal digital PCR*. Biomolecular Detection and Quantification, 2016. 10: p. 34-46.

109. Wang, K., et al., *Increasing the Genetic Recombination Frequency by Partial Loss of Function of the Synaptonemal Complex in Rice*. *Molecular Plant*, 2015. 8(8): p. 1295-1298.
110. Barakate, A., et al., *The Synaptonemal Complex Protein ZYP1 Is Required for Imposition of Meiotic Crossovers in Barley*. *The Plant Cell*, 2014. 26(2): p. 729-740.
111. Serra, H., et al., *Massive crossover elevation via combination of HEI10 and recq4a recq4b during Arabidopsis meiosis*. *Proceedings of the National Academy of Sciences*, 2018. 115(10): p. 2437-2442.
112. Arrieta, M., et al., *An induced mutation in HvRECQL4 increases the overall recombination and restores fertility in a barley HvMLH3 mutant background*. *Frontiers in plant science*, 2021. 12: p. 706560.
113. Bazile, J., et al., *TaRECQ4 contributes to maintain both homologous and homoeologous recombination during wheat meiosis*. *Frontiers in Plant Science*, 2024. 14: p. 1342976.
114. Zhang, P., et al., *The rice AAA-ATPase OsFIGNL1 is essential for male meiosis*. *Frontiers in Plant Science*, 2017. 8: p. 1639.
115. Desjardins, S.D., et al., *FANCM promotes class I interfering crossovers and suppresses class II non-interfering crossovers in wheat meiosis*. *Nature Communications*, 2022. 13(1): p. 3644.
116. Khandagale, K. and A. Nadaf, *Genome editing for targeted improvement of plants*. *Plant Biotechnology Reports*, 2016. 10: p. 327-343.
117. Van Vu, T., et al., *Genome editing and beyond: what does it mean for the future of plant breeding?* *Planta*, 2022. 255(6): p. 130.
118. Weeks, D.P., M.H. Spalding, and B. Yang, *Use of designer nucleases for targeted gene and genome editing in plants*. *Plant Biotechnology Journal*, 2016. 14(2): p. 483-495.
119. Till, B.J., et al., *High-throughput TILLING for functional genomics*. *Plant functional genomics*, 2003: p. 205-220.
120. Bao, A., et al., *The CRISPR/Cas9 system and its applications in crop genome editing*. *Critical Reviews in Biotechnology*, 2019. 39(3): p. 321-336.
121. Chen, K., et al., *CRISPR/Cas Genome Editing and Precision Plant Breeding in Agriculture*. *Annual Review of Plant Biology*, 2019. 70(1): p. 667-697.
122. Ran, F.A., et al., *Genome engineering using the CRISPR-Cas9 system*. *Nature Protocols*, 2013. 8(11): p. 2281-2308.
123. Song, G., et al., *CRISPR/Cas9: A powerful tool for crop genome editing*. *The Crop Journal*, 2016. 4(2): p. 75-82.

124. Xie, N., et al., *Novel Epigenetic Techniques Provided by the CRISPR/Cas9 System*. Stem Cells International, 2018. 2018: p. 7834175.
125. Doudna, J.A. and E. Charpentier, *The new frontier of genome engineering with CRISPR-Cas9*. Science, 2014. 346(6213): p. 1258096.
126. Anjanappa, R.B. and W. Gruissem, *Current progress and challenges in crop genetic transformation*. Journal of Plant Physiology, 2021. 261: p. 153411.
127. Marthe, C., J. Kumlehn, and G. Hensel, *Barley (Hordeum vulgare L.) Transformation Using Immature Embryos*. In Agrobacterium Protocols, 2015. 1: p. 71-83.
128. Hensel, G., *Genetic transformation of Triticeae cereals - Summary of almost three-decade's development*. Biotechnology Advances, 2020. 40: p. 107484.
129. Kumlehn, J., et al., *Genetic transformation of barley (Hordeum vulgare L.) via infection of androgenetic pollen cultures with Agrobacterium tumefaciens*. Plant Biotechnology Journal, 2006. 4(2): p. 251-261.
130. Holme, I.B., et al., *Transformation of barley (Hordeum vulgare L.) by Agrobacterium tumefaciens infection of in vitro cultured ovules*. Plant Cell Reports, 2006. 25: p. 1325-1335.
131. Cody, W.B. and H.B. Scholthof, *Plant Virus Vectors 3.0: Transitioning into Synthetic Genomics*. Annual Review of Phytopathology, 2019. 57(1): p. 211-230.
132. Varanda, C.M.R., et al., *Plant Viruses: From Targets to Tools for CRISPR*. Viruses, 2021. 13(1): p. 141.
133. Zaidi, S.S. and S. Mansoor, *Viral Vectors for Plant Genome Engineering*. Frontiers in Plant Science, 2017. 8: p. 539.
134. Zhang, C., et al., *Virus-induced gene editing and its applications in plants*. International Journal of Molecular Sciences, 2022. 23(18): p. 10202.
135. Oh, Y., H. Kim, and S.-G. Kim, *Virus-induced plant genome editing*. Current opinion in plant biology, 2021. 60: p. 101992.
136. Ali, Z., et al., *Efficient virus-mediated genome editing in plants using the CRISPR/Cas9 system*. Molecular plant, 2015. 8(8): p. 1288-1291.
137. Ali, Z., et al., *Pea early-browning virus-mediated genome editing via the CRISPR/Cas9 system in Nicotiana benthamiana and Arabidopsis*. Virus Research, 2018. 244: p. 333-337.
138. Mei, Y., et al., *Protein expression and gene editing in monocots using foxtail mosaic virus vectors*. Plant Direct, 2019. 3(11): p. 00181.

139. Hu, J., et al., *A barley stripe mosaic virus-based guide RNA delivery system for targeted mutagenesis in wheat and maize*. *Molecular Plant Pathology*, 2019. 20(10): p. 1463-1474.
140. Jackson, A.O., et al., *Hordeivirus replication, movement, and pathogenesis*. *Annual Review of Phytopathology*, 2009. 47: p. 385-422.
141. Li, T., et al., *Highly efficient heritable genome editing in wheat using an RNA virus and bypassing tissue culture*. *Molecular Plant*, 2021. 14(11): p. 1787-1798.
142. Chen, H., et al., *Development and optimization of a Barley stripe mosaic virus-mediated gene editing system to improve Fusarium head blight resistance in wheat*. *Plant Biotechnology Journal*, 2022. 20(6): p. 1018-1020.
143. Bekele, D., K. Tesfaye, and A. Fikre, *Applications of Virus Induced Gene Silencing (VIGS) in Plant Functional Genomics Studies*. *Journal of Plant Biochemistry & Physiology*, 2019. 07(01).
144. Burch-Smith, T.M., et al., *Applications and advantages of virus-induced gene silencing for gene function studies in plants*. *The Plant Journal: For Cell and Molecular Biology*, 2004. 39(5): p. 734-746.
145. Dommès, A.B., et al., *Virus-induced gene silencing: empowering genetics in non-model organisms*. *Journal of Experimental Botany*, 2019. 70(3): p. 757-770.
146. Liu, N., et al., *Foxtail Mosaic Virus-Induced Gene Silencing in Monocot Plants*. *Plant Physiology*, 2016. 171(3): p. 1801-1807.
147. Renner, T., et al., *Virus-induced gene silencing in the culinary ginger (Zingiber officinale): an effective mechanism for down-regulating gene expression in tropical monocots*. *Molecular Plant*, 2009. 2(5): p. 1084-1094.
148. Tavakol, E., *Virus-Induced Gene Silencing (VIGS) in Aegilops tauschii and Its Use in Functional Analysis of AetDREB2*. *Molecular Biotechnology*, 2018. 60(1): p. 41-48.
149. Yuan, C., et al., *A high throughput barley stripe mosaic virus vector for virus induced gene silencing in monocots and dicots*. *PLoS One*, 2011. 6(10): p. 26468.
150. Bennypaul, H.S., et al., *Virus-induced gene silencing (VIGS) of genes expressed in root, leaf, and meiotic tissues of wheat*. *Functional & Integrative Genomics*, 2012. 12(1): p. 143-156.
151. Buhrow, L.M., S.M. Clark, and M.C. Loewen, *Identification of an attenuated barley stripe mosaic virus for the virus-induced gene silencing of pathogenesis-related wheat genes*. *Plant Methods*, 2016. 12: p. 12.

152. Chen, G., et al., *TaEDS1 genes positively regulate resistance to powdery mildew in wheat*. *Plant Molecular Biology*, 2018. 96(6): p. 607-625.
153. Groszyk, J., et al., *Identification and VIGS-based characterization of Bx1 ortholog in rye (Secale cereale L.)*. *PloS One*, 2017. 12(2): p. e0171506.
154. Hein, I., et al., *Virus-Induced Gene Silencing-Based Functional Characterization of Genes Associated with Powdery Mildew Resistance in Barley*. *Plant Physiology*, 2005. 138(4): p. 2155-2164.
155. Holzberg, S., et al., *Barley stripe mosaic virus-induced gene silencing in a monocot plant*. *The Plant Journal*, 2002. 30(3): p. 315-327.
156. Gottwald, S., et al., *TILLING in the two-rowed barley cultivar 'Barke' reveals preferred sites of functional diversity in the gene HvHox1*. *BMC research notes*, 2009. 2: p. 1-14.
157. Ayoub, M.A.M., *Exploration of strategies to alter the meiotic recombination landscape in barley (Hordeum vulgare)*. 2023, Dissertation, Halle (Saale), Martin-Luther-Universität Halle-Wittenberg, 2023.
158. Ahn, Y.-J., et al., *In planta delivery of chemical compounds into barley meiocytes: EdU as compound example*. *Plant Meiosis: Methods and Protocols*, 2020: p. 381-402.
159. Werner, S., et al., *Fast track assembly of multigene constructs using Golden Gate cloning and the MoClo system*. *Bioengineered*, 2012. 3(1): p. 38-43.
160. Li, Y., et al., *HEIP1 regulates crossover formation during meiosis in rice*. *Proceedings of the National Academy of Sciences*, 2018. 115(42): p. 10810-10815.
161. Untergasser, A., et al., *Primer3Plus, an enhanced web interface to Primer3*. *Nucleic Acids Research*, 2007. 35: p. W71-4.
162. Madden, T., *The BLAST sequence analysis tool*. *The NCBI handbook*, 2013. 2(5): p. 425-436.
163. Haeussler, M., et al., *Evaluation of off-target and on-target scoring algorithms and integration into the guide RNA selection tool CRISPOR*. *Genome Biology*, 2016. 17(1): p. 148.
164. Schindele, P., F. Wolter, and H. Puchta, *CRISPR Guide RNA Design Guidelines for Efficient Genome Editing*, in *RNA Tagging: Methods and Protocols*, 2020. p. 331-342.
165. Hofacker, I.L., *Vienna RNA secondary structure server*. *Nucleic acids research*, 2003. 31(13): p. 3429-3431.
166. Conant, D., et al., *Inference of CRISPR Edits from Sanger Trace Data*. *The CRISPR Journal*, 2022. 5(1): p. 123-130.

167. Swift, M.L., *GraphPad prism, data analysis, and scientific graphing*. Journal of chemical information and computer sciences, 1997. 37(2): p. 411-412.
168. Luck, S., et al., *siRNA-Finder (si-Fi) Software for RNAi-Target Design and Off-Target Prediction*. Frontiers in Plant Sciences, 2019. 10: p. 1023.
169. Kron, P. and B.C. Husband, *Using flow cytometry to estimate pollen DNA content: improved methodology and applications*. Annals of Botany, 2012. 110(5): p. 1067-1078.
170. Galbraith, D.W., et al., *Rapid flow cytometric analysis of the cell cycle in intact plant tissues*. Science, 1983. 220(4601): p. 1049-1051.
171. Madic, J., et al., *6-Color Crystal Digital PCR™ for the High-Plex Detection of EGFR Mutations in Non-Small Cell Lung Cancer*. Lung Cancer: Methods and Protocols, 2021. p. 127-144.
172. Jayakodi, M., et al., *Structural variation in the pangenome of wild and domesticated barley*. Nature, 2024. p. 1-9.
173. Mascher, M., et al., *A chromosome conformation capture ordered sequence of the barley genome*. Nature, 2017. 544(7651): p. 427-433.
174. Beier, S., et al., *Construction of a map-based reference genome sequence for barley, *Hordeum vulgare* L.* Scientific Data, 2017. 4(1): p. 170044.
175. Phillips, D., et al., *The effect of temperature on the male and female recombination landscape of barley*. New Phytologist, 2015. 208(2): p. 421-429.
176. Hillers, K.J., *Crossover interference*. Current Biology, 2004. 14(24): p. 1036-1037.
177. Li, M., et al., *Leaf Variegation and Impaired Chloroplast Development Caused by a Truncated CCT Domain Gene in albobriars Barley*. Plant Cell, 2019. 31(7): p. 1430-1445.
178. Tamilselvan-Nattar-Amutha, S., et al., *Barley stripe mosaic virus-mediated somatic and heritable gene editing in barley (*Hordeum vulgare* L.)*. Frontiers in Plant Science, 2023. 14: p. 1201446.
179. Bradamante, G., O. Mittelsten Scheid, and M. Incarbone, *Under siege: virus control in plant meristems and progeny*. The Plant Cell, 2021. 33(8): p. 2523-2537.
180. Carroll, T.W., *Seed transmissibility of two strains of barley stripe mosaic virus*. Virology, 1972. 48(2): p. 323-336.
181. Lambing, C., et al., *Arabidopsis PCH2 Mediates Meiotic Chromosome Remodeling and Maturation of Crossovers*. PLOS Genetics, 2015. 11(7): p. 1005372.

182. Underwood, C.J., et al., *Epigenetic activation of meiotic recombination near Arabidopsis thaliana centromeres via loss of H3K9me2 and non-CG DNA methylation*. Genome Research, 2018. 28(4): p. 519-531.
183. Colas, I., et al., *A spontaneous mutation in MutL-Homolog 3 (HvMLH 3) affects synapsis and crossover resolution in the barley desynaptic mutant des10*. New Phytologist, 2016. 212(3): p. 693-707.
184. Pundir, S., et al., *UniProt tools*. Current protocols in bioinformatics, 2016. 53(1): p. 1-29.
185. Swarbreck, D., et al., *The Arabidopsis Information Resource (TAIR): gene structure and function annotation*. Nucleic acids research, 2007. p. 1009-1014.
186. Mascher, M., et al., *Long-read sequence assembly: a technical evaluation in barley*. The Plant Cell, 2021. 33(6): p. 1888-1906
187. Sym, M., J. Engebrecht, and G.S. Roeder, *ZIP1 is a synaptonemal complex protein required for meiotic chromosome synapsis*. Cell, 1993. 72(3): p. 365-378.
188. Hollingsworth, N.M., L. Goetsch, and B. Byers, *The HOP1 gene encodes a meiosis-specific component of yeast chromosomes*. Cell, 1990. 61(1): p. 73-84.
189. Hayashi, M., S. Mlynarczyk-Evans, and A.M. Villeneuve, *The Synaptonemal Complex Shapes the Crossover Landscape Through Cooperative Assembly, Crossover Promotion and Crossover Inhibition During Caenorhabditis elegans Meiosis*. Genetics, 2010. 186(1): p. 45-58.
190. Higgins, J.D., et al., *Spatiotemporal Asymmetry of the Meiotic Program Underlies the Predominantly Distal Distribution of Meiotic Crossovers in Barley*. The Plant Cell, 2012. 24(10): p. 4096-4109.
191. Colas, I., et al., *Observation of extensive chromosome axis remodeling during the “diffuse-phase” of meiosis in large genome cereals*. Frontiers in Plant Science, 2017. 8: p. 1235.
192. Osman, K., et al., *FIGL1 prevents aberrant chromosome associations and fragmentation and limits crossovers in polyploid wheat meiosis*. New Phytologist, 2024. 244(2): p. 528-541.
193. Li, H.Q., et al., *RecQ helicase enhances homologous recombination in plants*. FEBS Letters, 2004. 574(1-3): p. 151-5.
194. Fernandes, J.B., et al., *Unleashing meiotic crossovers in hybrid plants*. Proceedings of the National Academy of Sciences, 2018. 115(10): p. 2431-2436.

195. de Maagd, R.A., et al., *CRISPR/Cas inactivation of RECQ 4 increases homeologous crossovers in an interspecific tomato hybrid*. Plant Biotechnology Journal, 2020. 18(3): p. 805-813.
196. Sanchez-Moran, E., et al., *Variation in chiasma frequency among eight accessions of Arabidopsis thaliana*. Genetics, 2002. 162(3): p. 1415-1422.
197. Cannell, R., *The tillering pattern in barley varieties: I. Production, survival and contribution to yield by component tillers*. The Journal of Agricultural Science, 1969. 72(3): p. 405-422.
198. Perales, C., et al., *Enhancement of DNA, cDNA synthesis and fidelity at high temperatures by a dimeric single-stranded DNA-binding protein*. Nucleic acids research, 2003. 31(22): p. 6473-6480.
199. Milner, S.G., et al., *Genebank genomics highlights the diversity of a global barley collection*. Nature genetics, 2019. 51(2): p. 319-326.
200. Harwood, W., et al., *Barley transformation using Agrobacterium-mediated techniques*. Methods in molecular biology: Transgenic wheat, barley and oats: production and characterization protocols, 2009. p. 137-147.
201. Sood, P., A. Bhattacharya, and A. Sood, *Problems and possibilities of monocot transformation*. Biologia plantarum, 2011. 55(1): p. 1-15.
202. Hensel, G., *Genetic transformation of Triticeae cereals – Summary of almost three-decade's development*. Biotechnology Advances, 2019: p. 107484.
203. Bekalu, Z.E., et al., *Opportunities and Challenges of In Vitro Tissue Culture Systems in the Era of Crop Genome Editing*. International Journal of Molecular Sciences, 2023. 24(15): p. 11920.
204. Su, W., et al., *Technological Development and Application of Plant Genetic Transformation*. International Journal of Molecular Sciences, 2023. 24(13).
205. Xie, N., et al. *Novel Epigenetic Techniques Provided by the CRISPR/Cas9 System*. Stem Cells International, 2018. p. 7834175.
206. Nadakuduti, S.S. and F. Enciso-Rodríguez, *Advances in Genome Editing With CRISPR Systems and Transformation Technologies for Plant DNA Manipulation*. Frontiers in Plant Science, 2021. 11.
207. Shen, Y., et al., *Exploiting viral vectors to deliver genome editing reagents in plants*. aBIOTECH, 2024: p. 1-15.
208. Wang, W., et al., *Multiplexed promoter and gene editing in wheat using a virus-based guide RNA delivery system*. Plant Biotechnology Journal, 2022. 20(12): p. 2332-2341.

209. Holzberg, S., et al., *Barley stripe mosaic virus-induced gene silencing in a monocot plant*. *The Plant Journal*, 2002. 30(3): p. 315-327.
210. Yuan, C., et al., *A High Throughput Barley Stripe Mosaic Virus Vector for Virus Induced Gene Silencing in Monocots and Dicots*. *holzberg*, 2011. 6(10): p. e26468.
211. Hagemann, R. and F. Scholz, *A case of gene induced mutations of the plasmotype in barley*. *Theor. Appl. Genet*, 1962. 32: p. 50-59.
212. Bruun-Rasmussen, M., et al., *Stability of Barley stripe mosaic virus-Induced Gene Silencing in Barley*. *Molecular Plant-Microbe Interactions®*, 2007. 20(11): p. 1323-1331.
213. Edwards, M.C., *Mapping of the seed transmission determinants of barley stripe mosaic virus*. *Molecular plant-microbe interactions: MPMI*, 1995. 8(6): p. 906-915.
214. Edwards, M.C. and B.J. Steffenson, *Genetics and mapping of barley stripe mosaic virus resistance in barley*. *Phytopathology*, 1996. 86(2): p. 184-187.
215. Paylan, İ.C., et al., *Effects of different treatments on the inactivation of various seedborne viruses in some vegetables*. *Ozone: Science & Engineering*, 2014. 36(5): p. 422-426.
216. Xie, K., B. Minkenberg, and Y. Yang, *Boosting CRISPR/Cas9 multiplex editing capability with the endogenous tRNA-processing system*. *Proceedings of the National Academy of Sciences*, 2015. 112(11): p. 3570-3575.
217. He, Y., et al., *On improving CRISPR for editing plant genes: ribozyme-mediated guide RNA production and fluorescence-based technology for isolating transgene-free mutants generated by CRISPR*. *Progress in molecular biology and translational science*, 2017. 149: p. 151-166.
218. Ellison, E.E., et al., *Multiplexed heritable gene editing using RNA viruses and mobile single guide RNAs*. *Nature Plants*, 2020. 6(6): p. 620-624.
219. Uranga, M., et al., *Efficient Cas9 multiplex editing using unspaced sgRNA arrays engineering in a Potato virus X vector*. *The Plant Journal*, 2021. 106(2): p. 555-565.
220. Cakir, C. and M. Tör, *Factors influencing Barley Stripe Mosaic Virus-mediated gene silencing in wheat*. *Physiological and Molecular Plant Pathology*, 2010. 74(3): p. 246-253.
221. Gerasimova, S.V., et al., *Conversion of hulled into naked barley by Cas endonuclease-mediated knockout of the NUD gene*. *BMC Plant Biology*, 2020. 20(1): p. 255.
222. Grützner, R., et al., *Addition of Multiple Introns to a Cas9 Gene Results in Dramatic Improvement in Efficiency for Generation of Gene Knockouts in Plants*. *bioRxiv*. 2020.

223. Grützner, R., et al., *High-efficiency genome editing in plants mediated by a Cas9 gene containing multiple introns*. *Plant communications*, 2021. 2(2): p. 100135.
224. Feng, C., et al., *High-efficiency genome editing using a dmcl promoter-controlled CRISPR/Cas9 system in maize*. *Plant biotechnology journal*, 2018. 16(11): p. 1848-1857.
225. Wolter, F., J. Klemm, and H. Puchta, *Efficient in planta gene targeting in Arabidopsis using egg cell-specific expression of the Cas9 nuclease of Staphylococcus aureus*. *The Plant Journal*, 2018. 94(4): p. 735-746.
226. Nagalakshmi, U., et al., *High-efficiency multiplex biallelic heritable editing in Arabidopsis using an RNA virus*. *Plant Physiology*, 2022. 189(3): p. 1241-1245.
227. Lei, J., et al., *Efficient virus-mediated genome editing in cotton using the CRISPR/Cas9 system*. *Frontiers in Plant Science*, 2022. 13: p. 1032799.
228. Faure, S., et al., *The FLOWERING LOCUS T-Like Gene Family in Barley (Hordeum vulgare)*. *Genetics*, 2007. 176(1): p. 599-609.
229. Michaud, M., et al., *A global picture of tRNA genes in plant genomes*. *The Plant Journal*, 2011. 66(1): p. 80-93.
230. Tang, H., et al., *Development of a haploid inducer by editing HvMTL in barley*. *Journal of genetics and genomics*, 2023. 50(5): p. 366-369.
231. Cheuk, A. and M. Houde, *A New Barley Stripe Mosaic Virus Allows Large Protein Overexpression for Rapid Function Analysis*. *Plant Physiology*, 2018. 176(3): p. 1919-1931.
232. Chen, W., et al., *A new method for rapid subcellular localization and gene function analysis in cotton based on barley stripe mosaic virus*. *Plants*, 2022. 11(13): p. 1765.
233. Sukegawa, S., et al., *Genome editing in rice mediated by miniature size Cas nuclease SpCas12f*. *Frontiers in Genome Editing*, 2023. 5.
234. Ye, Z., et al., *Efficient genome editing in rice with miniature Cas12f variants*. *aBIOTECH*, 2024: p. 1-5.
235. Uranga, M., et al., *CRISPR-Cas12a genome editing at the whole-plant level using two compatible RNA virus vectors*. *The CRISPR Journal*, 2021. 4(5): p. 761-769.
236. Bouton, C., et al., *Foxtail mosaic virus: A Viral Vector for Protein Expression in Cereals*. *Plant Physiology*, 2018. 177(4): p. 1352-1367.
237. Zhang, K., et al., *Selection of reference genes for gene expression studies in virus-infected monocots using quantitative real-time PCR*. *Journal of Biotechnology*, 2013. 168(1): p. 7-14.

238. Pacak, A., et al., *Investigations of barley stripe mosaic virus as a gene silencing vector in barley roots and in Brachypodium distachyon and oat*. Plant Methods, 2010. 6(1): p. 26.
239. Zhang, S., et al., *Genetic transformation of commercial cultivars of oat (Avena sativa L.) and barley (Hordeum vulgare L.) using in vitro shoot meristematic cultures derived from germinated seedlings*. Plant Cell Reports, 1999. 18: p. 959-966.
240. Kausch, A.P., et al., *Maize transformation: history, progress, and perspectives*. Molecular Breeding, 2021. 41: p. 1-36.
241. Sahoo, K.K., et al., *An improved protocol for efficient transformation and regeneration of diverse indica rice cultivars*. Plant Methods, 2011. 7: p. 1-11.
242. Popelka, J.C. and F. Altpeter, *Agrobacterium tumefaciens-mediated genetic transformation of rye (Secale cereale L.)*. Molecular Breeding, 2003. 11: p. 203-211.
243. Liu, G. and I.D. Godwin, *Highly efficient sorghum transformation*. Plant Cell Reports, 2012. 31: p. 999-1007.
244. Sood, P., R.K. Singh, and M. Prasad, *An efficient Agrobacterium-mediated genetic transformation method for foxtail millet (Setaria italica L.)*. Plant Cell Reports, 2020. 39(4): p. 511-525.
245. Zickler, D. and N. Kleckner, *Recombination, pairing, and synapsis of homologs during meiosis*. Cold Spring Harbor perspectives in biology, 2015. 7(6): p. 016626.
246. Wang, M., et al., *The central element protein ZEP1 of the synaptonemal complex regulates the number of crossovers during meiosis in rice*. The Plant Cell, 2010. 22(2): p. 417-430.
247. Kursel, L.E., H.D. Cope, and O. Rog, *Unconventional conservation reveals structure-function relationships in the synaptonemal complex*. Elife, 2021. 10: p. 72061.
248. Ma, M., et al., *Virus-induced gene-silencing in wheat spikes and grains and its application in functional analysis of HMW-GS-encoding genes*. BMC plant biology, 2012. 12: p. 1-13.

Curriculum Vitae

Name Suriya Tamilselvan Nattar Amutha
ORCID <https://orcid.org/0000-0002-2940-4354>

Education	Martin Luther University Halle-Wittenberg Ph.D. candidate	Halle, Germany (Jan 2020 - Present)
	Justus Liebig University Master of Science (M.Sc) in Agrobiotechnology	Giessen, Germany (Oct 2016 - Jan 2020)
	Government College of Technology Bachelor of Technology (B.Tech) in Industrial Biotechnology	Coimbatore, India (May 2011 - May 2015)
Professional Experience	Leibniz Institute of Plant Genetics and Crop Plant Research (IPK) Developed Virus- and Digital PCR-based tools to dissect crop meiosis. Experience in genome editing and single pollen nucleus genotyping.	Gatersleben, Germany (Jan 2020 – June 2024)
	Leibniz Institute of Plant Genetics and Crop Plant Research (IPK) Screening of chemical compounds altering epigenetic marks in plant meristematic tissues. Experience in immunohistochemistry.	Gatersleben, Germany (May 2019 – July 2019)
	Justus Liebig University Established Long read sequencing-based Structural variations detection strategy in polyploid crop species. Experience in Next generation sequencing and Genomics.	Giessen, Germany (Aug 2018 – Nov 2020)
	Government College of Technology Developed a Silica-based Methylene blue kit to detect the presence of bacteria in milk. Experience in microbial characterisation and nanofilm spraying strategy	Coimbatore, India (Dec 2014 – Mar 2015)
	Bioline Laboratory, Coimbatore, India Underwent In-plant training on Clinical Microbiology, Serology and Biochemistry.	Coimbatore, India (Dec 2012 – Jan 2013)
	Teaching Experience IPK Gatersleben Supervised one Master and one Ph.D exchange student	
	IPK Gatersleben Instructed practical course module on Crystal Digital PCR assays	

Justus Liebig University

Instructed practical course module on Oxford Nanopore Sequencing

Publications	<p>Tamilselvan-Nattar-Amutha S, Fuchs J, Ayoub MA, Cuacos M, Torres Mendoza MA, Hartmann F, Lorenz J, Stein N, Hensel G, Kumlehn J and Heckmann S (2025) Meiotic Recombination and Crossover Interference Rate Variation Assessed by Multiplex Crystal Digital PCR™ Genotyping of Single Pollen Nuclei in Barley (<i>Hordeum vulgare L.</i>) (In preparation).</p> <p>Suriya Tamilselvan-Nattar-Amutha S, Fuchs J and Heckmann S (2025) Crystal Digital PCR™-based single nucleus pollen genotyping in barley (<i>Hordeum vulgare L.</i>) to measure meiotic crossover rates in defined chromosomal intervals. <i>Methods in Molecular Biology</i>, doi:10.1007/978-1-0716-4767-7_6.</p> <p>Dhandapani V, Santharam MA, Tamilselvan-Nattar-Amutha S, and Purushothama CRA (2025) On-Site Diagnostic Techniques for Fungal Pathogens. In <i>Molecular Approaches for the Detection of Fungal Phytopathogens</i>, pp. 216-232. CRC Press.</p> <p>Tamilselvan-Nattar-Amutha S, Hiekel S, Hartmann F, Lorenz J, Dabhi RV, Dreissig S, Hensel G, Kumlehn J and Heckmann S (2023) Barley stripe mosaic virus mediated somatic and heritable gene editing in barley (<i>Hordeum vulgare L.</i>). <i>Frontiers in Plant Science</i>, doi: 10.3389/fpls.2023.1201446.</p> <p>Chawla HS, Lee H, Gabur I, Vollrath P, Tamilselvan-Nattar-Amutha S, Obermeier C, Schiessl SV, Song JM, Liu K, Guo L, Parkin IAP and Snowdon RJ (2021) Long-read sequencing reveals widespread intragenic structural variants in a recent allopolyploid crop plant. <i>Plant Biotechnology Journal</i>, doi:10.1111/pbi.13456.</p>				
Selected talks/ presentations (during PhD)	<p>Presented my doctoral research work on crystal digital PCR-based single nucleus genotyping technology and virus-induced genome editing strategy for studying barley meiosis at the following conferences:</p> <p>Plant and Animal Genome Conference in San Diego, USA (2023).</p> <p>Cytogenetic Meeting in Brno, Czech Republic (2023)</p> <p>Hutton-IPK Symposium in Dundee, Scotland (2023).</p> <p>Cytogenetic Meeting in Goerlitz, Germany (2021).</p>				
Skills	<table><tr><td>Lab</td><td>Nucleic acid isolation, cloning, genome editing, plant virus delivery, handling & maintaining S2 biosafety level laboratory equipment & protocols, plant tissue culture, NGS, western blot, immunostaining, microscopy and barley & oilseed rape handling</td></tr><tr><td>Bioinformatics</td><td>Command line BLAST tool, long read & short read sequence alignment, NGS data analysis, mutation detection & variant analysis, oligonucleotide design and gRNA design.</td></tr></table>	Lab	Nucleic acid isolation, cloning, genome editing, plant virus delivery, handling & maintaining S2 biosafety level laboratory equipment & protocols, plant tissue culture, NGS, western blot, immunostaining, microscopy and barley & oilseed rape handling	Bioinformatics	Command line BLAST tool, long read & short read sequence alignment, NGS data analysis, mutation detection & variant analysis, oligonucleotide design and gRNA design.
Lab	Nucleic acid isolation, cloning, genome editing, plant virus delivery, handling & maintaining S2 biosafety level laboratory equipment & protocols, plant tissue culture, NGS, western blot, immunostaining, microscopy and barley & oilseed rape handling				
Bioinformatics	Command line BLAST tool, long read & short read sequence alignment, NGS data analysis, mutation detection & variant analysis, oligonucleotide design and gRNA design.				

Software and Scripting, visualisation & data analysis using python & R, Linux
computer skills environments for command-line operations and microsoft office suite.

References

Dr. Stefan Heckmann
Group leader of the Meiosis lab,
IPK Gatersleben,
Gatersleben 06466, Germany.
+49 (0)39482 608
heckmann@ipk-gatersleben.de

Prof. Dr. Andreas Houben
Group leader of the CSF lab,
IPK Gatersleben,
Gatersleben 06466, Germany.
+49 (0)39482 5486
houben@ipk-gatersleben.de

Prof. Dr. Rod Snowdon
Professor and Chair of Plant Breeding,
Justus Liebig University,
Giessen 35392 Germany
+49 (641) 99 37420 / 37421
Rod.Snowdon@agrar.uni-giessen.de

Eidesstattliche Erklärung / Declaration under Oath

Ich erkläre an Eides statt, dass ich die vorliegende Arbeit selbstständig und ohne unerlaubte Hilfe angefertigt habe. Es wurden ausschließlich die von mir angegebenen Quellen und Hilfsmittel verwendet. Alle Stellen, die aus anderen Werken wörtlich oder sinngemäß übernommen wurden, sind als solche kenntlich gemacht.

I hereby declare, under penalty of perjury, that this thesis is entirely my own work and has been completed without any unauthorized assistance. I have used only the sources cited, and all references - whether quoted directly or paraphrased - have been properly acknowledged in both wording and content.

Datum / Date

Unterschrift des Antragstellers / Signature of the applicant

Appendix

Table S1. Primers used in this study

Name	Sequence (5' to 3')	Purpose
b_F	CCTTGCCAAGAGATGGATAC	Amplification of flanking region of Locus b
b_R	ACAACAAGTAAACATTGACTGC	
d_F	CATTCCAACAATGCGTATCA	Amplification of flanking region of Locus d
d_R	AAAGTGATGGCAGTCGAAT	
f_F	CTGACAGTTTCCTGGTGTT	Amplification of flanking region of Locus f
f_R	AGACACAATGTACAGATCCTTC	
g_F	CCGTTCCCTAACAAATAGAGGA	Amplification of flanking region of Locus g
g_R	TTTGATGCAAGTTTCTGTTGAA	
h_F	GGAGCTGCAGTGCAAATTTAT	Amplification of flanking region of Locus h
h_R	CTGCACAAGCGAAGAAGATG	
i_F	TCATATAAAAATATTGATGTGGCACT	Amplification of flanking region of Locus i
i_R	AAATCTTCACGCTTGTTTACACT	
1H-Zygoty-F	AGGGCCGTCCAAAAGAAA	Confirming the zygoty at Chromosome 1 of BxGP hybrid plants
1H-Zygoty-R	ATGTGGGATGGGGAGAGAG	
3H-Zygoty-F	CCCGAGGTAGCCCTCCA	Confirming the zygoty at Chromosome 3 of BxGP hybrid plants
3H-Zygoty-R	CATAGAGATGTTTCGGTCTGT	
MA-57	CCACTTGGTCAGTAGCATCA	Isolation of <i>recq4-1</i>
MA-58	GGTAGGTGCTTCCATCCATA	
Bie475	TTTAGCCCTGCCTTCATACG	Confirmation of transgene presence
GH-zCas9-R1	TTAATCATGTGGGCCAGAGC	
MA-365	CCAGTGTATCGCTTTGCTGA	Together with MA-57, isolation of <i>recq4-2</i>
MA-225	CCATTCGTATCATAAACTGCGATC	Genotyping for <i>recq4-1</i>
MA-227	TGCAGTGCACATCTAAATAA	
MA-437	TGGATGATGACGAGATTCTGG	Genotyping for <i>RECQ4</i>
MA-438	TTGAGGACTGAGTTCCCA	
MA-440	TGGATGATGACGAGATTCGC	Genotyping for <i>recq4-2</i>
MA-441	ACCATCAAGAAGTTTATTGG	
sgTarget_Primer_1	GTAANNNNNNNNNNNNNNNNNNNNGTTT	'N' and 'n' represent 20 bp target complementary sequence on the forward and reverse DNA strand, respectively
sgTarget_Primer_2	TCTAAAACnnnnnnnnnnnnnnnnnn	
sgHvCMF7_Primer_1	GTA ACTCAAGGCGTGGTATGACAGGTTT	Cloning of sgHvCMF7 into BSMV- γ -sg
sgHvCMF7_Primer_2	TCTAAAACCTGTCATACCACGCCTTGAG	
Sanger_HvCMF7_F	GATGTGATGCCCTGTTTTCC	Sanger sequencing of the <i>CMF7</i> target region
Sanger_HvCMF7_R	GGAGCTCGACTTTGAGGATG	
sgHvASY1_Primer_1	GTA ACTCCTGGATTCAGGATCCATGTTT	Cloning of sgHvASY1 into BSMV- γ -sg
sgHvASY1_Primer_2	TCTAAAACATGGATCCTGAATCCAGGAG	
Sanger_HvASY1_F	CTGTTCCGGCACTAGGTCAG	Sanger sequencing of the <i>ASY1</i> target region
Sanger_HvASY1_R	TGCCTTCACTTTATGAGGCCA	

sgHvMUS81_Primer_1	GTAAGCAGACGTTGCGGTAGGCGTGTTT	Cloning of sgHvMUS81 into BSMV- γ -sg
sgHvMUS81_Primer_2	TCTAAAACACGCCTACCGCAACGTCTGC	
Sanger_HvMUS81_F	GATTCCAAGTGCTTATTC	Sanger sequencing of the <i>MUS81</i> target region
Sanger_HvMUS81_R	AATAAAATCCTCCCTTTATC	
sgHvZYP1_Primer_1	GTAATTCTAGATCAGACTTCACCGGTTT	Cloning of sgHvZYP1 into BSMV- γ -sg
sgHvZYP1_Primer_2	TCTAAAACCGGTGAAGTCTGATCTAGAA	
Sanger_HvZYP1_F	CTCGATGGGTTCCGATCTCT	Sanger sequencing of the <i>ZYP1</i> target region
Sanger_HvZYP1_R	ACATGCAGCCCCAGAATAAC	
sgHvSCEP3_primer_1	GTAATTAACTCTACAAGGGCCACGTTT	Cloning of sgHvSCEP3 into BSMV- γ -sg
sgHvSCEP3_primer_2	TCTAAAACGTGGGCCCTGTAGAGTTAA	
Sanger_HvSCEP3_F	AGTCATCTAACGACATGC	Sanger sequencing of the <i>SCEP3</i> target region
Sanger_HvSCEP3_R	TTAGGTCACAAACAAGTAAAC	
sgHvPCH2_primer_1	GTAATGAATTGTCAGGAGGTATCGTTT	Cloning of sgHvPCH2 into BSMV- γ -sg
sgHvPCH2_primer_2	TCTAAAACGATACCTCTGACAATTCAT	
Sanger_HvPCH2_F	ACTCACCAAAGCAATGCCAG	Sanger sequencing of the <i>PCH2</i> target region
Sanger_HvPCH2_R	CAAAACACCAGCACCTCAGC	
sgHvCMT3_primer_1	GTAAAACCAGAATACAGATCAAGGGTTT	Cloning of sgHvPCH2 into BSMV- γ -sg
sgHvCMT3_primer_2	TCTAAAACCTTGATCTGTATTCTGGTT	
Sanger_HvCMT3_F	CAGTTCTTTGCAAGGGGTGT	Sanger sequencing of the <i>PCH2</i> target region
Sanger_HvCMT3_R	CTCAACAGGTTCTGCTGCAT	
RBSMV-RECQ4-1-1	AAGGAAGTTTAACCAAGCATCACACTATCATGGT	Cloning of 114 bp fragment of <i>RECQ4</i> CDS into BSMVIGS- γ b
RBSMV-RECQ4-1-2	AACCACCACCACCGTCCCATCCCAAATGCAACTGT	
RBSMV-RECQ4-2-1	AAGGAAGTTTAAGACGTGCTGGTAGAGATGGA	Cloning of 102 bp fragment of <i>RECQ4</i> CDS into BSMVIGS- γ b
RBSMV-RECQ4-2-2	AACCACCACCACCGTGCTCTGCAGATCCTTGTGTA	
RBSMV-YFP-1	AAGGAAGTTTAATATATCATGGCCGACAAGCA	Cloning of 110 bp fragment of <i>YFP</i> into BSMVIGS- γ b
RBSMV-YFP-2	AACCACCACCACCGTGGGTGTTCTGCTGGTAGTGG	
BSMV- α _F	GTACGGCGCAACATCTCCTC	Verification of BSMV- α plasmid in agrotransformation
BSMV- α _R	CACCCGCATTCACCTCACCTG	
BSMV- β _F	ACCACTTCACAGTATGCCGAAC	Verification of BSMV- β plasmid in agrotransformation
BSMV- β _R	TCAACAGCAGGTACAGCTTC	
BSMV- γ _F	TGGCTAAGCTTGAAAGTGAGG	Verification of insert presence in BSMV- γ -sg plasmid
BSMV- γ _R	TAAAGTGTGACGCAGCTACC	
ZmUBI::cas9_F	GGCGATCATCTCCTCACAT	Confirmation of <i>spcas9</i> expression
ZmUBI::cas9_R	CCCTGAAGTCAAAGCTCGTC	
spcas9_F	TTTAGCCCTGCCTTCATACG	Confirmation of transgenicity
spcas9_R	TTAATCATGTGGGCCAGAGC	

Table S2. Oligonucleotides used in this study

Name	Sequence (5' to 3')	5' modification (Fluorophore)	3' modification	Final concentration used	Purpose
------	---------------------	-------------------------------	-----------------	--------------------------	---------

			(Quencher)	in the Crystal dPCR mix	
b-B-550	TTGTTGTGTCAGCACCAAGCG T	ATTO550/FAM	BHQ2/ BHQ1	0.3 µM	Probe distinguishing polymorphism at b in Barke genome
b-GP-700	TGAACGGGTGCTGAGTGCTG A	ATTO700/HEX	BHQ3/ BHQ1	0.3 µM	Probe distinguishing polymorphism at b in Golden Promise genome
d-B-FAM	TACTACTACGTCTCGCTTTTA TTTATGCA	FAM	BHQ1/ BHQ1	0.3 µM	Probe distinguishing polymorphism at d in Barke genome
d-GP-CY5	TACTACTACGTCAATGTTGCA CATTTC	CY5/HEX	BHQ2/ BHQ1	0.3 µM	Probe distinguishing polymorphism at d in Golden Promise genome
f-B-YY	AGAGCAGCAATTATTCGGCA AGCTT	YAKIMA YELLOW/FAM	BHQ1/ BHQ1	0.3 µM	Probe distinguishing polymorphism at f in Barke genome
f-GP-ROX	TATTCGGCGACAATGACCAGC T	ROX/HEX	BHQ2/ BHQ1	0.3 µM	Probe distinguishing polymorphism at f in Golden Promise genome
g-B-YY	TTTGGTCGGTACTAGCTGATA CCCAA	YAKIMA YELLOW	BHQ1	0.6 µM	Probe distinguishing polymorphism at g in Barke genome
g-GP-ROX	TTGGTCGATACCCAAAACATC GCG	ROX	BHQ2	0.3 µM	Probe distinguishing polymorphism at g in Golden Promise genome
h-B-FAM	TGGTGGCTCTATTACGATGTT ATAATATGGA	FAM	BHQ1	0.3 µM	Probe distinguishing polymorphism at h in Barke genome
h-GP-CY5	GGTGGTCGTAGTACAATGTTA TAATATGATG	CY5	BHQ2	0.3 µM	Probe distinguishing polymorphism at h in Golden Promise genome
i-B-550	TGGGTGAAAAAGATTATCCG AGATACTCG	ATTO550	BHQ2	0.3 µM	Probe distinguishing polymorphism at i in Barke genome
i-GP-700	TGGGTGAAAAAGATTATCCG AGCGTG	ATTO700	BHQ3	0.3 µM	Probe distinguishing polymorphism at i in Golden Promise genome

Table S3. Analysis configuration file setup for quantifying different genotype combinations for CO rate analysis using Crystal Miner software

	Interval	Genotype (Gen) at b-d-f or g-h-i		Fluorescence channel					
				Blue	Teal	Green	Yellow	Red	Infra-red
Three-color approach	1bd, 1df, 1bf, 3gh, 3hi, or 3gi	Non-recombinants	B-B-B	Positive	Positive	Positive	Negative	Negative	Negative
			GP-GP-GP	Negative	Negative	Negative	Positive	Positive	Positive
		Recombinants	B-GP-GP	Negative	Negative	Positive	Positive	Positive	Negative
			GP-B-B	Positive	Positive	Negative	Negative	Negative	Positive
			B-B-GP	Positive	Negative	Positive	Positive	Negative	Negative
			GP-GP-B	Negative	Positive	Negative	Negative	Positive	Positive
			B-GP-B	Negative	Positive	Positive	Negative	Positive	Negative
GP-B-GP	Positive	Negative	Negative	Positive	Negative	Positive			
Two-color approach	1bd, or 3gh	Non-recombinants	B-B-*	Positive	Undefined	Positive	Undefined	Negative	Negative
			GP-GP-*	Negative	Undefined	Negative	Undefined	Positive	Positive
		Recombinants	B-GP-*	Negative	Undefined	Positive	Undefined	Positive	Negative
			GP-B-*	Positive	Undefined	Negative	Undefined	Negative	Positive
	1df, or 3hi	Non-recombinants	*-B-B	Positive	Positive	Undefined	Negative	Negative	Undefined
			*-GP-GP	Negative	Negative	Undefined	Positive	Positive	Undefined
		Recombinants	*-B-GP	Positive	Negative	Undefined	Positive	Negative	Undefined

			*-GP-B	Negative	Positive	Undefined	Negative	Positive	Undefined
	1bf, or 3gi	Non-recombinants	B-*-B	Undefined	Positive	Positive	Negative	Undefined	Negative
			GP-*-GP	Undefined	Negative	Negative	Positive	Undefined	Positive
		Recombinants	B-*-GP	Undefined	Negative	Positive	Positive	Undefined	Negative
			GP-*-B	Undefined	Positive	Negative	Negative	Undefined	Positive

* denotes any possible allele at the specified locus

Table S4. Efficacy of different pollen-bursting strategies for haploid pollen nuclei isolation from stored anthers

Treatment	Total no. of events detected within the selected gate	Average no. of events detected within the selected gate	Total no. of haploid pollen nuclei sorted	Efficiency of haploid pollen nuclei sorted among total number of events (%)
None	11356	11022.20	286	3.04
	10660		303	
	9117		293	
	10831		342	
	13147		459	
Bead beating using TissueLyser (30 Hz/s for 1 min)	19872	17001.40	2051	11.74
	10728		1127	
	17469		2202	
	19306		2267	
	17632		2381	
Bead beating using TissueLyser (30 Hz/s for 30 sec)	12980	14732.60	979	8.90
	12737		979	
	10993		950	
	15015		1817	
	21938		1875	
Sonication (1 min)	4231	7081.00	62	1.97
	9125		162	
	8269		148	
	6341		145	
	7439		187	
Sonication (3 min)	9449	7041.00	270	2.25
	6111		123	
	6463		96	
	6227		181	
	6955		137	

Table S5. Selected genetic intervals on barley chromosomes for CO rate measurement using the multiplex SPNG approach

Chromosome	Locus name	InDel breakpoint at physical position based on Morex v3 (bp)	InDel (bp)	Recombination rate based on POPSEQ of the Morex x Barke population (cM) *
1H	b	16530084	4 bp Deletion in Barke	25.48
	d	56167285	13 bp Deletion in Barke	44.25
	f	387546447	9 bp Deletion in Barke	47.86

3H	g	585924946	10 bp Deletion in Golden Promise	71.7
	h	605255566	3 bp Deletion in Golden Promise	84.88
	i	617944121	6 bp Deletion in Golden Promise	93.53

* Recombination rate based on the closest marker

Table S6. CO rate analysis based on the three-color approach using multiplex SPNG approach

Population	Replicate	No. plants per replicate	Total genotyping call	No. of chambers	Total number of positive droplets												Expected Double crossover frequency	Observed Double crossover frequency	I-Co C [*]
					Interval-1 (1bd or 3gh)			Interval-2 (1df or 3hi)			Interval-1+2 (1bf or 3gi)								
					Non-recombinants	Recombinants	Recombination rate (cM)	Non-recombinants	Recombinants	Recombination rate (cM)	Non-recombinants	Recombinants	Recombination rate (cM)						
1H																			
Wild type F1 hybrid (Greenhouse condition)	A		444	3	189	185	70	15.77	208	205	31	6.98	180	175	89	20.05	0.01	0.01	-0.01
	B		752	8	317	334	101	13.43	351	360	41	5.45	303	325	124	16.49	0.01	0.01	-0.39
	C		764	4	317	340	107	14.01	344	366	54	7.07	305	320	139	18.19	0.01	0.01	-0.22
	Cumulative	18	1960	15	823	859	278	14.18	903	931	126	6.43	788	820	352	17.96	0.01	0.01	-0.45
Wildtype F1 hybrid_recq4-1 x recq4-2 (Greenhouse condition)	A		215	3	93	90	32	14.88	110	96	9	4.19	93	85	37	17.21	0.01	0.01	-0.26
	B		352	4	129	169	54	15.34	148	182	22	6.25	122	166	64	18.18	0.01	0.01	-0.48
	C		416	4	162	192	62	14.90	189	206	21	5.05	157	184	75	18.03	0.01	0.01	-0.07
	Cumulative	6	983	11	384	451	148	15.06	447	484	52	5.29	372	435	176	17.90	0.01	0.01	-0.53
Mutant F1 hybrid_recq4-1 x recq4-2 (Greenhouse condition)	A		454	3	139	132	183	40.31	176	162	116	25.55	136	117	201	44.27	0.10	0.07	0.32
	B		529	3	161	154	214	40.45	222	193	114	21.55	149	138	242	45.75	0.09	0.05	0.39
	C		296	3	101	92	103	34.80	118	109	69	23.31	84	78	134	45.27	0.08	0.04	0.48
	Cumulative	6	1279	9	401	378	500	39.09	516	464	299	23.38	369	333	577	45.11	0.09	0.09	0.05
Wild type F1 hybrid 1° off-centre (Controlled growth chamber)	A		609	3	250	268	91	14.94	270	299	40	6.57	240	258	111	18.23	0.01	0.01	-0.40
	B		164	3	60	77	27	16.46	74	80	10	6.10	59	72	33	20.12	0.01	0.01	0.00
	C		56	3	24	21	11	19.64	26	26	4	7.14	22	21	13	23.21	0.01	0.01	-0.02
	Cumulative	15	829	9	334	366	129	15.56	370	405	54	6.51	321	351	157	18.94	0.01	0.01	-0.28
Wild type F1 hybrid 1° centre (Controlled growth chamber)	A		239	4	104	92	43	17.99	118	106	15	6.28	96	87	56	23.43	0.01	0.00	0.70
	B		216	3	87	94	35	16.20	90	106	20	9.26	84	89	43	19.91	0.02	0.02	-0.51
	C		448	3	178	199	71	15.85	204	220	24	5.36	172	191	85	18.97	0.01	0.01	-0.09
	Cumulative	15	903	10	369	385	149	16.50	412	432	59	6.53	352	367	184	20.38	0.01	0.01	-0.01
Wild type F1 hybrid	A		217	3	84	95	38	17.51	97	107	13	5.99	79	91	47	21.66	0.01	0.01	0.28

2° centre (Controlled growth chamber)	B		366	3	154	159	53	14.48	169	168	29	7.92	142	146	78	21.31	0.01	0.00	0.61
	C		527	3	211	241	75	14.23	240	263	24	4.55	207	235	85	16.13	0.01	0.01	0.74
	Cumulative	15	1110	9	449	495	166	14.95	506	538	66	5.95	428	472	210	18.92	0.01	0.01	0.07
Wild type F1 hybrid 3° centre (Controlled growth chamber)	A		585	3	247	238	100	17.09	274	269	42	7.18	238	233	114	19.49	0.01	0.02	0.60
	B		455	3	193	187	75	16.48	218	214	23	5.05	187	184	84	18.46	0.01	0.01	0.54
	C		540	3	231	214	95	17.59	265	240	35	6.48	224	208	108	20.00	0.01	0.02	0.46
	Cumulative	15	1580	9	671	639	270	17.09	757	723	100	6.33	649	625	306	19.37	0.01	0.02	0.54
3H																			
Wild type F1 hybrid (Greenhouse condition)	A		435	4	180	153	102	23.45	208	175	52	11.95	160	133	142	32.64	0.03	0.01	0.63
	B		603	9	214	234	155	25.70	251	290	62	10.28	186	212	205	34.00	0.03	0.01	0.72
	C		754	4	260	283	211	27.98	319	363	72	9.55	239	252	263	34.88	0.03	0.01	0.64
	Cumulative	18	1792	17	654	670	468	26.12	778	828	186	10.38	585	597	610	34.04	0.03	0.01	0.55
Wildtype F1 hybrid_recq4-1 x recq4-2 (Greenhouse condition)	A		263	3	89	109	65	24.71	105	134	24	9.13	80	106	77	29.28	0.02	0.02	0.23
	B		425	5	162	157	106	24.94	195	180	50	11.76	146	143	136	32.00	0.03	0.02	0.40
	C		375	4	146	137	92	24.53	176	173	26	6.93	136	127	112	29.87	0.02	0.01	0.64
	Cumulative	6	1063	12	397	403	263	24.74	476	487	100	9.41	362	376	325	30.57	0.02	0.02	0.23
Mutant F1 hybrid_recq4-1 x recq4-2 (Greenhouse condition)	A		425	3	96	103	226	53.18	109	119	197	46.35	106	114	205	48.24	0.25	0.15	0.40
	B		493	3	119	132	242	49.09	121	145	227	46.04	113	127	253	51.32	0.23	0.13	0.44
	C		250	3	67	64	119	47.60	77	76	97	38.80	64	60	126	50.40	0.18	0.11	0.42
	Cumulative	6	1168	9	282	299	587	50.26	307	340	521	44.61	283	301	584	50.00	0.22	0.22	0.00
Wild type F1 hybrid 1° off-centre (Controlled growth chamber)	A		401	3	148	150	103	25.69	184	170	47	11.72	135	136	130	32.42	0.03	0.02	0.39
	B		188	3	76	59	53	28.19	96	75	17	9.04	75	51	62	32.98	0.03	0.02	0.38
	C		145	3	54	55	36	24.83	60	67	18	12.41	48	49	48	33.10	0.03	0.02	0.50
	Cumulative	15	734	9	278	264	192	26.16	340	312	82	11.17	258	236	240	32.70	0.03	0.02	0.41
Wild type F1 hybrid 1° centre (Controlled growth chamber)	A		220	4	80	73	67	30.45	100	100	20	9.09	74	67	79	35.91	0.03	0.01	0.52
	B		216	3	94	79	43	19.91	105	92	19	8.80	86	72	58	26.85	0.02	0.01	0.59
	C		277	3	104	119	54	19.49	117	123	37	13.36	94	100	83	29.96	0.03	0.01	0.58
	Cumulative	15	713	10	278	271	164	23.00	322	315	76	10.66	254	239	220	30.86	0.02	0.01	0.57
Wild type F1 hybrid 2° centre (Controlled growth chamber)	A		207	3	91	69	47	22.71	102	87	18	8.70	83	63	61	29.47	0.02	0.01	0.62
	B		378	3	143	145	90	23.81	172	167	39	10.32	124	135	119	31.48	0.02	0.01	0.59
	C		544	3	190	202	152	27.94	248	244	52	9.56	170	176	198	36.40	0.03	0.00	0.85
	Cumulative	15	1129	9	424	416	289	25.60	522	498	109	9.65	377	374	378	33.48	0.02	0.01	0.73
Wild type F1 hybrid 3° centre (Controlled growth chamber)	A		497	3	186	175	136	27.36	226	230	41	8.25	166	164	167	33.60	0.02	0.01	0.67
	B		443	3	152	169	122	27.54	194	205	44	9.93	141	150	152	34.31	0.03	0.01	0.57
	C		295	2	113	111	71	24.07	133	140	22	7.46	105	105	85	28.81	0.02	0.01	0.42

	Cumulative	15	1235	8	451	455	329	26.64	553	575	107	8.66	412	419	404	32.71	0.02	0.01	0.58
--	------------	----	------	---	-----	-----	-----	-------	-----	-----	-----	------	-----	-----	-----	-------	------	------	------

* CoC value = Expected double crossover frequency / Observed crossover frequency

Table S7. CO rate analysis based on the two-color approach using multiplex SPNG approach

Population	Replicate	No. plants per replicate	1bd						1df						1bf						
			Total no. of positive droplets				Recombination rate (cM)	Total genotyping call	Total no. of positive droplets				Recombination rate (cM)	Total genotyping call	Total no. of positive droplets				Recombination rate (cM)	Total genotyping call	No. of chambers
			Non-recombinants		Recombinants				Non-recombinants		Recombinants				Non-recombinants		Recombinants				
Wild type F1 hybrid (Greenhouse condition)	A	6	240	246	45	52	16.64	583	301	293	21	24	7.04	639	158	163	47	45	22.28	413	3
	B	6	388	426	69	78	15.30	961	579	591	32	27	4.80	1229	511	507	131	106	18.88	1255	8
	C	6	434	450	90	74	15.65	1048	534	548	49	56	8.85	1187	426	412	88	109	19.03	1035	4
	Cumulative	18	1062	1122	204	204	15.74	2592	1414	1432	102	107	6.84	3055	1095	1082	266	260	19.46	2703	15

Wildtype F1 hybrid_rec q4-1 x recq4-2 (Greenhouse condition)	A	2	151	140	23	28	14.91	342	208	196	4	10	3.35	418	171	168	37	42	18.90	418	3
	B	2	203	244	42	49	16.91	538	266	298	29	16	7.39	609	221	246	49	61	19.06	577	4
	C	2	277	317	50	64	16.10	708	339	372	20	28	6.32	759	309	323	66	70	17.71	768	4
	Cumulative	6	631	701	115	141	16.12	1588	813	866	53	54	5.99	1786	701	737	152	173	18.43	1763	11

Mutant F1 hybrid_rec q4-1 x recq4-2 (Greenhouse condition)	A	2	249	232	150	165	39.57	796	288	296	83	99	23.76	766	212	201	156	154	42.88	723	3
	B	2	192	188	126	137	40.90	643	336	314	91	92	21.97	833	211	208	177	185	46.35	781	3
	C	2	133	128	79	85	38.59	425	176	167	48	46	21.51	437	131	131	113	104	45.30	479	3
	Cumulative	6	574	548	355	387	39.81	1864	800	777	222	237	22.54	2036	554	540	446	443	44.83	1983	9

Wild type F1 hybrid 1° off-centre (Controlled growth chamber)	A	5	414	435	85	77	16.02	1011	479	506	34	31	6.19	1050	433	435	105	93	18.57	1066	3
	B	5	144	170	22	35	15.36	371	147	150	6	9	4.81	312	124	142	28	40	20.36	334	3
	C	5	73	77	19	14	18.03	183	75	71	4	6	6.41	156	54	71	23	13	22.36	161	3
	Cumulative	15	631	682	126	126	16.10	1565	701	727	44	46	5.93	1518	611	648	156	146	19.35	1561	9

Wild type F1 hybrid 1° centre (Controlled growth chamber)	A	5	203	197	43	35	16.32	478	236	223	21	6	5.56	486	175	171	51	43	21.36	440	4
	B	5	183	200	43	29	15.82	455	206	203	16	7	5.32	432	174	167	46	39	19.95	426	3
	C	5	298	288	50	61	15.93	697	379	419	19	27	5.45	844	320	347	76	87	19.64	830	3
	Cumulative	15	684	685	136	125	16.01	1630	821	845	56	40	5.45	1762	669	685	173	169	20.17	1696	10

Wild type F1 hybrid 2° centre (Controlled growth chamber)	A	5	161	163	32	37	17.56	393	169	190	13	11	6.27	383	162	175	40	40	19.18	417	3
	B	5	218	226	46	45	17.01	535	269	271	22	25	8.01	587	231	220	60	57	20.60	568	3
	C	5	337	344	51	59	13.91	791	364	378	18	21	4.99	781	329	354	70	75	17.51	828	3
	Cumulative	15	716	733	129	141	15.71	1719	802	839	53	57	6.28	1751	722	749	170	172	18.86	1813	9

Wild type F1 hybrid 3° centre (Controlled growth chamber)	A		312	303	74	66	18.54	755	371	379	29	27	6.95	806	324	328	76	87	20.00	815	3
	B		306	312	61	66	17.05	745	322	323	19	16	5.15	680	300	284	67	72	19.23	723	3
	C		323	328	78	70	18.52	799	374	354	31	25	7.14	784	315	317	91	100	23.21	823	3
	Cumulative	15	941	943	213	202	18.05	2299	1067	1056	79	68	6.48	2270	939	929	234	259	20.88	2361	9

Population	Replicate	No. plants per replicate	3gh						3hi						3gi						
			Total no. of positive droplets				Recombination rate (cM)	Total genotyping call	Total no. of positive droplets				Recombination rate (cM)	Total genotyping call	Total no. of positive droplets				Recombination rate (cM)	Total genotyping call	No. of chambers
			Non-recombinants		Recombinants				Non-recombinants		Recombinants				Non-recombinants		Recombinants				
Wild type F1 hybrid (Greenhouse condition)	A	6	225	218	68	72	24.01	583	320	316	35	37	10.17	708	199	194	111	97	34.61	601	4
	B	6	317	364	124	131	27.24	936	451	509	50	56	9.94	1066	281	287	138	154	33.95	860	9
	C	6	355	381	129	161	28.27	1026	674	711	84	76	10.36	1545	332	340	175	182	34.69	1029	4
	Cumulative	18	897	963	321	364	26.92	2545	1445	1536	169	169	10.18	3319	812	821	424	433	34.42	2490	17

Wildtype F1 hybrid_rec q4-1 x req4-2 (Greenhouse condition)	A	2	162	173	54	59	25.22	448	252	262	24	37	10.61	575	137	161	65	65	30.37	428	3
	B	2	219	212	81	74	26.45	586	431	445	55	58	11.43	989	206	217	103	104	32.86	630	5
	C	2	227	210	67	67	23.47	571	401	434	34	47	8.84	916	193	175	88	83	31.73	539	4
	Cumulative	6	608	595	202	200	25.05	1605	1084	1141	113	142	10.28	2480	536	553	256	252	31.81	1597	12

Mutant F1 hybrid_rec q4-1 x req4-2 (Greenhouse condition)	A	2	164	167	194	178	52.92	703	231	242	184	191	44.22	848	173	160	157	158	48.61	648	3
	B	2	175	185	166	178	48.86	704	224	239	200	188	45.59	851	151	161	160	165	51.02	637	3
	C	2	92	84	85	87	49.43	348	145	153	97	86	38.05	481	85	83	74	83	48.31	325	3
	Cumulative	6	431	436	445	443	50.60	1755	600	634	481	465	43.39	2180	409	404	391	406	49.50	1610	9

Wild type F1 hybrid 1° off-centre (Controlled growth chamber)	A	5	256	265	96	85	25.78	702	420	431	55	43	10.33	949	212	218	109	84	30.98	623	3
	B	5	137	123	52	57	29.54	369	265	277	43	28	11.58	613	126	106	69	49	33.71	350	3
	C	5	108	107	37	43	27.12	295	202	215	30	30	12.58	477	96	87	45	50	34.17	278	3
	Cumulative	15	501	495	185	185	27.09	1366	887	923	128	101	11.23	2039	434	411	223	183	32.45	1251	9

Wild type F1 hybrid 1° centre (Controlled growth chamber)	A	5	147	135	56	69	30.71	407	246	243	33	25	10.60	547	115	105	60	66	36.42	346	4
	B	5	145	131	43	38	22.69	357	225	218	25	28	10.69	496	129	122	51	48	28.29	350	3
	C	5	182	194	55	55	22.63	486	275	279	43	35	12.34	632	148	136	70	58	31.07	412	3
	Cumulative	15	474	460	154	162	25.28	1250	746	740	101	88	11.28	1675	392	363	181	172	31.86	1108	9

Wild type F1 hybrid 2° centre (Controlled growth chamber)	A	5	128	118	35	46	24.77	327	294	304	29	27	8.56	654	122	107	49	52	30.61	330	3
	B	5	234	215	84	66	25.04	599	321	339	36	41	10.45	737	190	175	95	77	32.03	537	3
	C	5	278	284	102	100	26.44	764	467	484	63	58	11.29	1072	222	227	142	123	37.11	714	3
	Cumulative	15	640	617	221	212	25.62	1690	1082	1127	128	126	10.31	2463	534	509	286	252	34.03	1581	9

Wild type F1 hybrid 3° centre (Controlled growth chamber)	A		261	250	98	96	27.52	705	353	362	36	38	9.38	789	220	207	103	118	34.10	648	3
	B		220	246	87	88	27.30	641	395	398	54	45	11.10	892	197	209	106	103	33.98	615	3
	C		151	167	48	54	24.29	420	250	234	15	29	8.33	528	136	131	58	66	31.71	391	2
	Cumulative	15	632	663	233	238	26.67	1766	998	994	105	112	9.82	2209	553	547	267	287	33.49	1654	8

Table S8. Pairwise comparisons of cumulative CO rate measurements using the two-color approach analyzed with Welch's t-test

Pairwise comparisons of measured cumulative male meiotic recombination rate	p-value (Welch's t-test; $\alpha = 0.05$)					
	1bd	1df	1bf	3gh	3hi	3gi
WT vs WT- <i>recq4</i>	0.8861	0.5241	0.3324	0.4150	0.8761	0.0675
WT vs MUT- <i>recq4</i>	0.0001	0.0014	0.0005	0.0009	0.0051	0.0035
WT- <i>recq4</i> vs MUT- <i>recq4</i>	0.0001	0.0012	0.0018	0.0005	0.0057	0.0006
1° Off-center vs 1° Center	0.6395	0.5502	0.9342	0.5380	0.7614	0.7296
1° Off-center vs 2° Center	0.8380	0.5821	0.4149	0.2318	0.2707	0.9055
1° Off-center vs 3° Center	0.1950	0.5051	0.8300	0.5169	0.1654	0.8220
1° Center vs 2° Center	0.9160	0.3804	0.3247	0.9810	0.3421	0.6979
1° Center vs 3° Center	0.0599	0.2677	0.7445	0.7555	0.2016	0.6475
2° Center vs 3° Center	0.2690	0.9932	0.3384	0.4987	0.6930	0.9956

Table S9. Comparison of CO rates after and before exclusion of droplets encapsulating double nuclei in BxGP F1 WT plants

	Chamber ID	1bd						1df						1bf						
		Total no. of positive droplets		Recombination rate (cM)	Total genotyping call	Total no. of positive droplets		Recombination rate (cM)	Total genotyping call	Total no. of positive droplets		Recombination rate (cM)	Total genotyping call	Total no. of positive droplets		Recombination rate (cM)	Total genotyping call			
		Non-recombinants	Recombinants			Non-recombinants	Recombinants			Non-recombinants	Recombinants			Non-recombinants	Recombinants					
Before exclusion	1	96	88	20	23	18.94	227	122	110	9	7	6.45	248	109	95	27	26	20.62	257	
	2	134	146	24	27	15.41	331	169	176	11	16	7.26	372	151	157	46	42	22.22	396	
	3	75	87	10	16	13.83	188	115	119	6	3	3.70	243	100	95	20	22	17.72	237	
	4	73	74	14	13	15.52	174	127	119	6	4	3.91	256	104	101	29	18	18.65	252	
	5	37	33	7	8	17.65	85	39	29	4	5	11.69	77	53	51	14	13	20.61	131	
	Cumulative	415	428	75	87	16.12	1005	572	553	36	35	5.94	1196	517	499	136	121	20.19	1273	
After exclusion	1	96	88	20	22	18.58	226	122	110	9	6	6.07	247	109	95	27	26	20.62	257	
	2	134	146	24	27	15.41	331	169	176	11	15	7.01	371	151	157	46	42	22.22	396	
	3	75	87	10	15	13.37	187	115	119	6	3	3.70	243	100	95	20	22	17.72	237	
	4	73	74	13	13	15.03	173	127	119	6	4	3.91	256	104	101	29	18	18.65	252	
	5	37	33	7	8	17.65	85	39	29	4	5	11.69	77	53	51	14	13	20.61	131	
	Cumulative	415	428	74	85	15.87	1002	572	553	36	33	5.78	1194	517	499	136	121	20.19	1273	
Before exclusion	Chamber ID	3gh						3hi						3gi						
		Total no. of positive droplets		Recombination rate (cM)	Total genotyping call	Total no. of positive droplets		Recombination rate (cM)	Total genotyping call	Total no. of positive droplets		Recombination rate (cM)	Total genotyping call	Total no. of positive droplets		Recombination rate (cM)	Total genotyping call			
		Non-recombinants	Recombinants			Non-recombinants	Recombinants			Non-recombinants	Recombinants			Non-recombinants	Recombinants					
		1	110	112	32	34	22.92	288	151	146	16	18	10.27	331	102	93	57	50	35.43	302
		2	91	84	28	32	25.53	235	130	115	15	13	10.26	273	83	83	42	36	31.97	244
		3	16	15	6	6	27.91	43	27	31	4	3	10.77	65	9	12	10	9.00	47.5	40
		4	34	31	16	14	31.58	95	40	38	4	5	10.34	87	29	22	13	18	37.80	82
5	67	65	27	23	27.47	182	113	111	11	19	11.81	254	64	59	40	38	38.81	201		
Cumulative	318	307	109	109	25.86	843	461	441	50	58	10.69	1010	287	269	162	151	36.02	869		
1	110	112	32	34	22.92	288	130	115	15	13	10.26	273	102	93	57	50	35.43	302		

After exclusion	2	91	84	28	31	25.21	234	27	31	4	3	10.77	65	83	83	42	36	31.97	244
	3	16	15	6	6	27.91	43	52	58	4	7	9.09	121	9	12	9	9	46.15	39
	4	34	31	12	14	28.57	91	40	38	3	5	9.30	86	29	22	13	18	37.80	82
	5	67	65	27	23	27.47	182	113	111	11	17	11.11	252	64	59	40	38	38.81	201
	Cumulative	318	307	105	108	25.42	838	362	353	37	45	10.29	797	287	269	161	151	35.94	868

Table S10. CO rate analysis in WT and BSMVIGS-inoculated plants based on the two-color approach using multiplex SPNG

Population	Replicate	1bd				1df				1bf										
		Total no. of positive droplets		Recombination rate (cM)	Total genotyping call	Total no. of positive droplets		Recombination rate (cM)	Total genotyping call	Total no. of positive droplets		Recombination rate (cM)	Total genotyping call	No. of chambers						
		Non-recombinants	Recombinants			Non-recombinants	Recombinants			Non-recombinants	Recombinants									
Wild type F2 (Controlled growth chamber)	A	75	78	15	9	13.56	177	83	75	9	12	11.73	179	69	69	21	17	21.59	176	2
	B	135	148	42	23	18.68	348	190	184	12	15	6.73	401	150	157	48	37	21.68	392	2
	C	256	261	50	38	14.55	605	232	259	24	33	10.40	548	201	213	68	51	22.33	533	2
	D	161	166	48	42	21.58	417	174	182	21	16	9.41	393	140	144	62	46	27.55	392	2
	E	208	240	52	39	16.88	539	246	265	24	31	9.72	566	211	219	54	62	21.25	546	2
	F	227	300	34	42	12.60	603	271	327	32	30	9.39	660	275	264	46	61	16.56	646	2
	G	303	348	50	50	13.32	751	338	351	25	24	6.64	738	336	313	62	69	16.79	780	2
	F	171	236	32	31	13.40	470	181	242	22	14	7.84	459	211	205	45	26	14.58	487	2
Cumulative	1536	1777	323	274	15.27	3910	1715	1885	169	175	8.72	3944	1593	1584	406	369	19.61	3952	16	
Empty BSMVI GS F2 (Controlled growth chamber)	A	63	64	16	17	20.63	160	64	76	8	8	10.26	156	67	81	22	23	23.32	193	2
	B	51	41	9	6	14.02	107	56	48	5	6	9.57	115	55	54	18	6	18.05	133	2
	C	130	129	32	31	19.57	322	142	157	23	25	13.83	347	156	160	40	32	18.56	388	2
	D	209	212	42	40	16.30	503	201	199	25	16	9.30	441	195	184	44	46	19.19	469	2
	E	182	198	39	25	14.41	444	193	196	9	14	5.58	412	185	192	42	41	18.04	460	2
	F	143	156	30	40	18.97	369	154	145	13	19	9.67	331	130	135	30	35	19.70	330	2
	G	161	166	30	27	14.84	384	155	160	17	14	8.96	346	150	148	42	31	19.68	371	2
	F	94	101	18	21	16.67	234	90	108	9	10	8.76	217	87	97	23	21	19.30	228	2
Cumulative	1033	1067	216	207	16.77	2523	1055	1089	109	112	9.34	2365	1025	1051	261	235	19.28	2572	16	
BSMVI GS-YFP-110 F2 (Controlled growth chamber)	A	122	146	43	44	24.51	355	146	167	19	21	11.33	353	156	156	46	51	23.72	409	2
	B	112	137	35	37	22.43	321	131	150	15	23	11.91	319	139	134	44	55	26.61	372	2
	C	47	58	21	12	23.91	138	70	83	11	4	8.93	168	77	88	33	25	26.01	223	2
	D	92	114	24	15	15.92	245	127	137	13	35	15.38	312	123	118	38	42	24.92	321	2
	E	76	67	11	14	14.88	168	100	98	4	9	6.16	211	88	77	14	23	18.32	202	2
	Cumulative	449	522	134	122	20.86	1227	574	635	62	92	11.30	1363	583	573	175	196	24.30	1527	10
BSMVI GS-RECQ4-114 F2 (Controlled growth chamber)	A	96	104	19	22	17.01	241	105	118	11	8	7.85	242	95	90	23	24	20.26	232	2
	B	68	82	17	14	17.13	181	64	95	10	12	12.15	181	78	77	22	21	21.72	198	2
	C	91	96	22	24	19.74	233	118	138	14	19	11.42	289	92	106	24	37	23.55	259	2
	D	40	59	15	11	20.80	125	52	65	9	7	12.03	133	42	47	5	19	21.24	113	2
	E	65	77	18	14	18.39	174	86	97	17	25	18.67	225	76	79	32	35	30.18	222	2
	Cumulative	360	418	91	85	18.45	954	425	513	61	71	12.34	1070	383	399	106	136	23.63	1024	10
BSMVI GS-RECQ4-114 F2 (Controlled growth chamber)	A	114	121	18	23	14.86	276	123	120	5	6	4.33	254	102	117	34	30	22.61	283	2
	B	62	76	23	20	23.76	181	89	74	9	16	13.30	188	70	70	31	29	30.00	200	2
	C	54	54	21	18	26.53	147	51	49	7	14	17.36	121	56	60	20	26	28.40	162	2
	D	64	68	19	10	18.01	161	101	93	14	19	14.54	227	88	71	16	29	22.06	204	2
	E	66	73	27	16	23.63	182	99	112	15	5	8.66	231	79	93	34	33	28.03	239	2
	Cumulative	360	392	108	87	20.59	947	463	448	50	60	10.77	1021	395	411	135	147	25.92	1088	10

Pairwise comparisons of measured cumulative male meiotic recombination rate	p-value (Welch's t-test; $\alpha = 0.05$)		
	1bd	1df	1bf
WT vs Empty BSMVIGS	0.3626	0.6251	0.62
WT vs BSMVIGS-YFP-110	0.08462	0.34	0.1124
BSMVIGS-YFP-110 vs BSMVIGS-RECQ4-114	0.466	0.4914	0.8263
BSMVIGS-YFP-110 vs BSMVIGS-RECQ4-110	0.7372	0.756	0.3255